VILNIUS GEDIMINAS TECHNICAL UNIVERSITY

Gediminas GAIDULIS

NUMERICAL MODELING OF TRANSAPICAL MITRAL VALVE REPAIR

DOCTORAL DISSERTATION

TECHNOLOGICAL SCIENCES,
MECHANICAL ENGINEERING (T 009)

VGTU
LEIDYKLA
TECHNIKA
Vilnius 2019

Doctoral dissertation was prepared at Vilnius Gediminas Technical University in 2014–2019.

Supervisor

Prof. Dr Habil. Rimantas KAČIANAUSKAS (Vilnius Gediminas Technical University, Mechanical Engineering – T 009).

Consultant

Prof. Dr Audrius AIDIETIS (Vilnius University, Medicine – M 001).

The Dissertation Defense Council of Scientific Field of Mechanical Engineering of Vilnius Gediminas Technical University:

Chairman

Prof. Dr Dalius MAŽEIKA (Vilnius Gediminas Technical University, Mechanical Engineering – T 009).

Members:

Assoc. Prof. Dr Sergejus BORODINAS (Vilnius Gediminas Technical University, Mechanical Engineering – T 009),
Dr Habil. Jolanta PAUK (Bialystok University of Technology, Poland, Mechanical Engineering – T 009),
Prof. Dr Vytautas TURLA (Vilnius Gediminas Technical University, Mechanical Engineering – T 009),
Prof. Dr Janina TUTKUVIENĖ (Vilnius University, Medicine – M 001).

The dissertation will be defended at the public meeting of the Dissertation Defense Council of Mechanical Engineering in the Senate Hall of Vilnius Gediminas Technical University at **2 p. m. on 28 August 2019**.

Address: Saulėtekio al. 11, LT-10223 Vilnius, Lithuania.
Tel.: +370 5 274 4956; fax: +370 5 270 0112; e-mail: doktor@vgtu.lt

A notification on the intend defending of the dissertation was sent on 26 July 2019.

A copy of the doctoral dissertation is available for review at VGTU repository http://dspace.vgtu.lt and at the Library of Vilnius Gediminas Technical University (Saulėtekio al. 14, LT-10223 Vilnius, Lithuania).

VGTU leidyklos TECHNIKA 2019-031-M mokslo literatūros knyga

ISBN 978-609-476-188-1

gediminas.gaidulis@vgtu.lt

VILNIAUS GEDIMINO TECHNIKOS UNIVERSITETAS

Gediminas GAIDULIS

TRANSAPIKALINĖS MITRALINIO VOŽTUVO KOREKCIJOS SKAITINIS MODELIAVIMAS

DAKTARO DISERTACIJA

TECHNOLOGIJOS MOKSLAI,
MECHANIKOS INŽINERIJA (T 009)

VGTU
LEIDYKLA
Vilnius TECHNIKA 2019

Disertacija rengta 2014–2019 metais Vilniaus Gedimino technikos universitete.

Vadovas

prof. habil. dr. Rimantas KAČIANAUSKAS (Vilniaus Gedimino technikos universitetas, mechanikos inžinerija – T 009).

Konsultantas

prof. dr. Audrius AIDIETIS (Vilniaus universitetas, medicina – M 001).

Vilniaus Gedimino technikos universiteto Mechanikos inžinerijos mokslo krypties disertacijos gynimo taryba:

Pirmininkas

prof. dr. Dalius MAŽEIKA (Vilniaus Gedimino technikos universitetas, mechanikos inžinerija – T 009).

Nariai:

doc. dr. Sergejus BORODINAS (Vilniaus Gedimino technikos universitetas, mechanikos inžinerija – T 009),
habil. dr. Jolanta PAUK (Balstogės technologijos universitetas, Lenkija, mechanikos inžinerija – T 009),
prof. dr. Vytautas TURLA (Vilniaus Gedimino technikos universitetas, mechanikos inžinerija – T 009),
prof. dr. Janina TUTKUVIENĖ (Vilniaus universitetas, medicina – M 001).

Disertacija bus ginama viešame Mechanikos inžinerijos mokslo krypties disertacijos gynimo tarybos posėdyje **2019 m. rugpjūčio 28 d. 14 val.** Vilniaus Gedimino technikos universiteto senato posėdžių salėje.

Adresas: Saulėtekio al. 11, LT-10223 Vilnius, Lietuva.
Tel.: (8 5) 274 4956; faksas: (8 5) 270 0112; el. paštas: doktor@vgtu.lt

Pranešimai apie numatomą ginti disertaciją išsiųsti 2019 m. liepos 26 d.

Disertaciją galima peržiūrėti VGTU talpykloje http://dspace.vgtu.lt ir Vilniaus Gedimino technikos universiteto bibliotekoje (Saulėtekio al. 14, LT-10223 Vilnius, Lietuva).

Abstract

This dissertation presents the numerical modeling approach for the simulation of transapical mitral valve (MV) repair procedure. The main object of the research is the development of the finite element (FE) model of the MV with ruptured chordae tendineae and its application for modeling of MV repair with neochordae implantation through the transapical approach. The dissertation aims to develop and implement a numerical model of the MV for quantitative evaluation of transapical MV repair surgical procedure and its effect on post-operative MV function.

The work presents five tasks. Firstly, studies describing computational models used for investigation of MV biomechanical functions and evaluation of novel MV repair surgical techniques are reviewed. Next, the modeling strategy for the numerical simulation of virtual transapical MV repair procedure is developed. Patient-specific echocardiographic image data are obtained for the reconstruction of MV geometry and creation of structural FE model with MV prolapse. Virtual repair using different neochordal lengths is performed and the systolic function of the MV model is simulated. Finally, the outcomes of virtual transapical MV repair are evaluated and the eligibility of numerical modeling strategy is considered.

The present thesis consists of an introduction, three main chapters, general conclusions, references, a list of publications by the author on the topic of the dissertation and a summary in Lithuanian.

The introduction presents the research problem, the relevance of the thesis, the object of the research, formulates the aim and the tasks of the work, describes the research methodology and scientific novelty, considers the practical significance of the results and the defensive statements. Chapter 1 discusses the problem of MV prolapse from both medical and mechanical point of view. In the medical part, the anatomy and physiology of the human heart are described and thorough analysis of the MV structure is presented. In the mechanical part, an overview of studies describing computational MV models is provided and the models analyzing different MV repair techniques are distinguished. Chapter 2 introduces the modeling strategy applied for virtual transapical MV repair and its mathematical formulation. Chapter 3 presents the systolic function simulations of virtual repair procedures using two sets of patient-specific data and evaluates the parameters calculated during these simulations before and after virtual repair.

The results of this dissertation were published in 4 scientific papers: two articles in journals with impact factor indexed in Clarivate Analytics Web of Science database, one article in a journal indexed in other international databases and one paper in international conference proceedings. These results were presented at 7 international conferences.

Reziumė

Disertacijoje pristatomas transapikalinės mitralinio vožtuvo (MV) korekcijos skaitinis modeliavimas. Šio tyrimo objektas – vožtuvo su nutrūkusiomis chordomis baigtinių elementų modelio kūrimas ir jo taikymas modeliuojant transapikalinę MV korekciją. Pagrindinis tyrimo tikslas – sukurti MV skaitinį modelį, kiekybiškai įvertinantį transapikalinės MV korekcijos chirurginę procedūrą ir jos poveikį pooperacinei MV funkcijai.

Disertacijoje iškelti penki uždaviniai. Pirmiausia, apžvelgti tyrimai, kuriuose aprašomi skaitiniai modeliai, naudoti MV biomechaninėms funkcijoms tirti ir naujiems MV chirurginės korekcijos būdams vertinti. Toliau, sudaryta virtualios transapikalinės MV korekcijos skaitinės simuliacijos modeliavimo strategija. Surinkti ultragarsinio tyrimo metu gauti duomenys, kurie panaudoti MV geometrijos rekonstrukcijai bei struktūrinio nesandaraus MV baigtinių elementų modelio kūrimui. Atlikta virtuali korekcija naudojant skirtingo ilgio neochordas ir MV modelio sistolinės funkcijos simuliacija. Galiausiai, įvertinti virtualios MV transapikalinės korekcijos rezultatai ir skaitinio modeliavimo strategijos tinkamumas.

Disertaciją sudaro įvadas, trys pagrindiniai skyriai, bendrosios išvados, literatūros sąrašas, autoriaus publikacijų sąrašas disertacijos tema ir santrauka lietuvių kalba.

Įvade pristatoma tyrimo problema, tyrimo aktualumas, tyrimo objektas, suformuluojamas darbo tikslas ir uždaviniai, aprašoma tyrimo metodika ir mokslinis naujumas, įvertinama rezultatų praktinė vertė ir pateikiami ginamieji teiginiai. Pirmajame skyriuje MV nesandarumo problema aptariama medicininiu ir mechaniniu požiūriu. Medicininėje dalyje aprašoma žmogaus širdies anatomija ir fiziologija bei pristatoma išsami MV struktūros analizė. Mechaninėje dalyje apžvelgiami tyrimai, aprašantys skaitinius MV modelius, ir išskiriami modeliai, analizuojantys skirtingus MV korekcijos būdus. Antrajame skyriuje pristatoma virtualios transapikalinės MV korekcijos modeliavimo strategija ir jos matematinio modelio sudarymas. Trečiajame skyriuje aprašomos virtualios korekcijos sistolinės funkcijos simuliacijos, atliktos naudojant dviejų pacientų ultragarsinių duomenų rinkinius, ir įvertinami parametrai, apskaičiuoti šių simuliacijų metu prieš ir po virtualios korekcijos.

Tyrimo rezultatai paskelbti keturiose mokslinėse publikacijose: du straipsniai išspausdinti žurnaluose, įtrauktuose į „Clarivate Analytics Web of Science“ duomenų bazę, vienas straipsnis – žurnale, indeksuotame kitose tarptautinėse duomenų bazėse, ir viena publikacija – tarptautinės konferencijos pranešimų medžiagoje. Tyrimų rezultatai pristatyti septyniose tarptautinėse konferencijose Lietuvoje ir užsienyje.

Notations

Symbols

a_0, c_0 – Fourier constant terms;
a_k, c_k – Fourier cosine coefficients;
B – strain-displacement matrix;
b_k, d_k – Fourier sine coefficients;
C – damping matrix (page 36) or right Cauchy-Green strain tensor (page 39);
$c_{i,ij}$ – material parameter characterizing deformation of the material;
D_i – material parameter that controls bulk compressibility of the material;
F – deformation gradient tensor;
F – force;
I – internal force vector;
I_i – invariant of the right Cauchy-Green strain tensor;
J – volume ratio;
K – stiffness matrix;
k_i – material parameter related to the stored energy in fibers;
L – distance;
M – mass matrix;
N – shape function (page 38) or unit vector identifying the direction of fibers (page 39);
P – applied load vector;
p – pressure;

S – surface area;
S_1 – maximum principal stress;
t – time;
$\mathbf{u}$ – displacement vector;
$\dot{\mathbf{u}}$ – velocity vector;
$\ddot{\mathbf{u}}$ – acceleration vector;
u_x, u_y, u_z – displacements along x-, y- and z-axes;
V – volume;
$\mathbf{x}_{i,j}$ – position vector;
z – axial position in the cylindrical coordinate system;
β – material parameter related to the level of material anisotropy;
ε – strain;
θ_x, θ_y, θ_z – rotations about x-, y- and z-axes;
κ – dispersion parameter used to describe fiber orientation;
$\lambda_{i,ij}$ – stretch ratio;
ρ – radial position in the cylindrical coordinate system;
$\boldsymbol{\sigma}$ – Cauchy stress tensor;
σ – stress;
φ – angular position in the cylindrical coordinate system;
Ψ – strain energy density;
ω – eigenvalue of the system.

Abbreviations

A1, P1 – lateral segments;
A2, P2 – middle segments;
A2D – annular 2D area;
A2L, P2L – middle-lateral segments;
A2M, P2M – middle-medial segments;
A3, P3 – medial segments;
AH – annular height;
AL – anterior leaflet;
ALP – prolapse of the anterior leaflet;
Al-Pm – commissural diameter;
ALVR – virtual repair with neochordae implantation into the anterior leaflet;
A-P – anteroposterior diameter;
ASH – anterior saddle horn;
C1, C2 – commissures;
C3D – annular 3D circumference;
CFD – computational fluid dynamics;
cMRI – cardiovascular magnetic resonance imaging;
CoA – coaptation area;

CoL – coaptation length;
ePTFE – expanded polytetrafluoroethylene;
FE – finite element;
FEM – finite element method;
FSI – fluid-structure interaction;
LA – left atrium;
LV – left ventricle;
micro-CT – micro-computed tomography;
MR – mitral regurgitation;
MV – mitral valve;
MVP – mitral valve with prolapse;
PL – posterior leaflet;
PLP – prolapse of the posterior leaflet;
PLVR – virtual repair with neochordae implantation into the posterior leaflet;
PM – papillary muscle;
PSH – posterior saddle horn;
TEE – transesophageal echocardiography;
TTE – transthoracic echocardiography;
VolDICOM – volumetric medical image;
VUMAT – vectorized user-defined material;
VR0, VR5, VR10, VR15 – virtual repair with different neochordal length.

Contents

[1] The annexes are supplied in the enclosed compact disc

Introduction

Problem Formulation

Numerical methods, particularly the finite element method (FEM), successfully applied for the structural analysis, lately have started to be used for modeling of biological objects. Mechanical behavior of the human body, including the human heart, became an object of interest for the investigations using finite element (FE) analysis. Such analysis can be a powerful tool to quantify the alterations in diseased heart mechanics, to explore its physiology and pathology, and to investigate the impacts of novel treatment strategies.

Cardiovascular diseases are the leading cause of death in the world. There are many types of such diseases, including valvular disorders, characterized by damage to or defect in one of the heart valves. Accordingly, mitral valve (MV) prolapse with mitral regurgitation (MR) is the most common valvular disease, affecting 2–3% of the world population. This disorder usually appears due to disruption of the valve restraining force structures, such as rupture of the diseased chordae tendineae, which occurs when the strain forces exceed the stretching threshold of the chordae.

Transapical MV repair with neochordae implantation is a novel surgical technique, allowing beating-heart correction of MR caused by chordae tendineae rupture through a minimally-invasive approach. While transapical MV repair shows

promising clinical results, there are some concerns regarding this surgical technique. Few aspects of the procedure, such as exact positioning or length adjustment of the neochordae to eliminate prolapse while preventing additional restriction of the leaflet, can only be assumed at this moment and requires additional experience and further research. To investigate such aspects, numerical modeling of MV structure and its transapical repair procedure using FEM is presented in this study.

Relevance of the Thesis

During the last three decades, the numerical simulation studies concerning different MV repair surgical techniques have proven to be useful while quantifying the biomechanical aspects of such procedures. However, only several studies on the modeling of MV repair with neochordae implantation were published. Moreover, none of them had addressed the problem of transapical MV repair.

In the present study, the modeling strategy used for virtual transapical MV repair application is elaborated and patient-specific highly nonlinear finite element model of the MV is developed. The main challenge related to transapical MV repair is the evaluation of the mechanical state of the implanted neochordae and correct adjustment of their length. There is a risk of residual prolapse or tearing of the repaired leaflet if either too short or too long neochordae are implanted. Since transapical MV repair relies solely on the echocardiographic determination of proper neochordal length, there was no convenient way to estimate this length in the computational models. Therefore, in this thesis, the effect of the neochordal length on the function of the prolapsing MV is evaluated, and the method to determine the required neochordal length is suggested and applied to investigate transapical MV repair surgical procedure outcomes using FEM.

The Object of Research

The object of the present study is the mitral valve affected by prolapse and regurgitation due to ruptured chordae tendineae, and numerical modeling of its repair with neochordae implantation through transapical approach.

The Aim of the Thesis

The main aim of the thesis is to determine the biomechanical parameters of mitral valve after transapical repair surgical procedure and to evaluate the effect of such procedure on post-operative mitral valve function.

The Tasks of the Thesis

To achieve the aim of this thesis, the following tasks have to be performed:

1. To review studies describing computational models used for investigation of mitral valve biomechanical functions and to investigate their eligibility for the evaluation of novel mitral valve repair surgical techniques.
2. To develop modeling strategy applied for the numerical simulation of virtual transapical mitral valve repair procedure.
3. To reconstruct the geometry of patient-specific mitral valve using echocardiographic image data and kinematic parameters of mitral valve motion, and to create structural finite element model of the mitral valve with prolapse based on the reconstructed geometry.
4. To apply the created model for the implementation of virtual transapical mitral valve repair followed by the simulation of mitral valve systolic function, and to investigate the effect of neochordal length on post-repair mitral valve functioning.
5. To evaluate the outcomes of virtual transapical mitral valve repair and to consider the eligibility of the developed numerical modeling strategy.

Research Methodology

In the present study, methods of literature and comparative analysis were used to investigate the research object and to review its modeling methods, as well as to validate the obtained computational results. Patient-specific data of MV structure and its movement in early systole was obtained using echocardiographic imaging technique. Calculations regarding the structural analysis of the MV and its transapical repair procedure were made using FEM in Abaqus (Dassault Systèmes, Inc.).

Scientific Novelty of the Thesis

The following novelties regarding numerical modeling of transapical MV repair surgical technique were presented:

1. The development of the modeling strategy applied for virtual repair, during which the echocardiographic image data is converted to a computational model followed by virtual transapical repair and dynamic FE simulation of the MV systolic function.
2. The evaluation of the effect of the neochordal length on the function of the prolapsing MV and the development of the method to determine this length for the application in virtual transapical MV repair.
3. The computation of the biomechanical parameters, describing MV deformations, tension forces in chordae and neochordae, reaction forces on papillary muscles and left ventricle apex, and stress distribution on the leaflets after virtual transapical MV repair.

Practical Value of the Research Findings

In the present study, personalized computational modeling strategy for transapical MV repair application allowed to determine quantitative information about the effect of such surgical procedure and the contribution of neochordal implantation to the MV function improvement. Virtual models are suitable for the investigation of MV deformations, acting forces and stress distribution, and can be used to predict post-operative MV morphology and coaptation of the leaflets as the main indicators of MV prolapse elimination. Since the presented modeling strategy provides detailed quantification of MV biomechanics, it shows the potential to have practical value in scenarios of clinical relevance.

The Defended Statements

1. From the mechanical perspective, MV can be considered as a mechanical system, thus its structure can be analyzed using numerical modeling methods.
2. Transapical MV repair eliminates prolapse, improves leaflet coaptation, decreases chordal tension forces and reduces excessive leaflet stress.
3. Proper neochordal length reduces the risk of residual prolapse or tearing of the repaired leaflet.

4. Virtual transapical MV repair helps to predict post-operative MV morphology and coaptation of the leaflets.

Approval of the Research Findings

The main results of this thesis were published in 4 scientific papers: two articles in journals with impact factor indexed in Clarivate Analytics Web of Science database (Gaidulis *et al.* 2018a; 2019), one article in journal indexed in other international databases (Gaidulis *et al.* 2018b) and one paper in international conference proceedings (Romashov *et al.* 2016). These results were presented at 7 international conferences:

- 40th International Conference "SOLMECH 2016", held in Warsaw (Poland) on August 29 – September 2, 2016.
- 5th International Conference "Nonlinear Dynamics 2016", held in Kharkov (Ukraine) on September 27–30, 2016.
- 11th International Conference "BIOMDLORE 2016", held in Druskininkai (Lithuania) on October 20–22, 2016.
- 13th International Conference "Mechatronic Systems and Materials (MSM 2017)", held in Vilnius (Lithuania) on July 3–5, 2017.
- 12th International Conference "BIOMDLORE 2018", held in Białystok (Poland) on June 28–30, 2018.
- 41st International Conference "SOLMECH 2018", held in Warsaw (Poland) on August 27–31, 2018.
- 55th International Conference "SES 2018", held in Madrid (Spain) on October 10–12, 2018.

Structure of the Dissertation

The dissertation consists of an introduction, three main chapters, general conclusions, references, a list of publications by the author on the topic of the dissertation and a summary in Lithuanian. The volume of this thesis is 104 pages (without annexes), including 34 pictures, 6 tables and 46 numbered equations. A total of 124 references were used when writing the thesis.

1

Literature Review of Mitral Valve Modeling

In the present chapter, the problem of MV prolapse resulting in MR is introduced and analyzed from both medical and mechanical points of view. In the medical part, the anatomy and physiology of the human heart are described, and thorough analysis of the MV structure is presented. The dysfunction of the MV, leading to prolapse and regurgitation, is explained, and the techniques for diagnostic imaging and surgical repair in the presence of such condition are introduced. In the mechanical part, an overview of studies describing structural and fluid-structure interaction computational models is provided, and the models analyzing different MV repair techniques are distinguished. Material models characterizing the mechanical behavior of the MV structure are introduced.

Parts of this chapter are published in Gaidulis *et al.* (2018a; 2018b; 2019) and Romashov *et al.* (2016).

1.1. Review of Mitral Valve Medical Background

1.1.1. Principles of Functional Anatomy of Heart and Mitral Valve

The heart is a muscular organ located inside the thoracic cavity, medial to the lungs and posterior to the sternum. It is the central organ of the circulatory system, which pumps blood into the blood vessels of the whole cardiovascular system (Fig. 1.1).

The heart is divided into four chambers: two atria (left and right) placed above two ventricles (left and right). The two sides are separated by the internal wall of fibrous and muscular tissue called the septum. Each side can be seen as a separate pump placed in series with the adjacent one. The distinction between both sides of the heart depends on the characteristics of the pumped blood: the left side pumps arterial blood rich in oxygen, while the right side pumps venous blood, which is oxygen-poor.

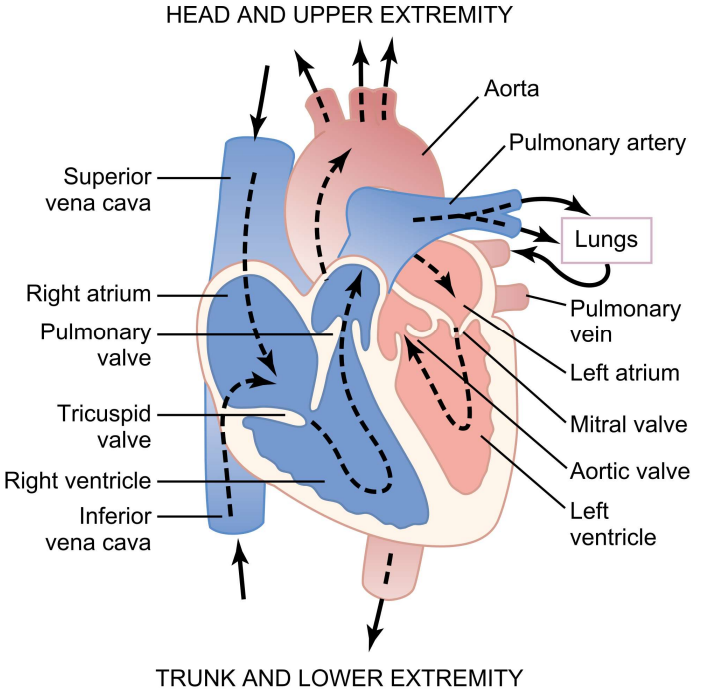

Fig. 1.1. Structure of the heart and direction of the blood flow through the heart chambers and heart valves (Hall 2015)

The unidirectional blood flow in the heart is controlled by the presence of four valves. There are two atrioventricular valves (mitral in the left side of the heart and tricuspid in the right side) that allow blood to flow from atria to ventricles, and two semilunar valves (aortic and pulmonary in the left and right sides, respectively) that allow blood to flow into the arteries. Each atrioventricular valve has a complex structure and consists of two (left side) or three (right side) asymmetrical leaflets. Semilunar valves, on the other hand, have a simpler configuration, both consisting of three half-moon-shaped leaflets (Zhu 2015).

Cardiac activity is composed of electrical activation phase and mechanical phase, responsible for the action of pumping blood. The electrical activity involves conduction of a stimulus starting from the sinoatrial node that allows contraction of the muscular tissue of the heart, called myocardium. The mechanical activity consists of a cyclic repetition of contraction and relaxation, or systole and diastole. Both sides of the heart act in sync, though contraction of atria starts earlier than that of ventricles. The whole cardiac cycle consists of both those phases that occur from the beginning of a heartbeat to the beginning of the next one (Fig. 1.2). Considering a normal heart rate, the cardiac cycle has a duration of approximately 0.8–0.9 s (Fukuta and Little 2008).

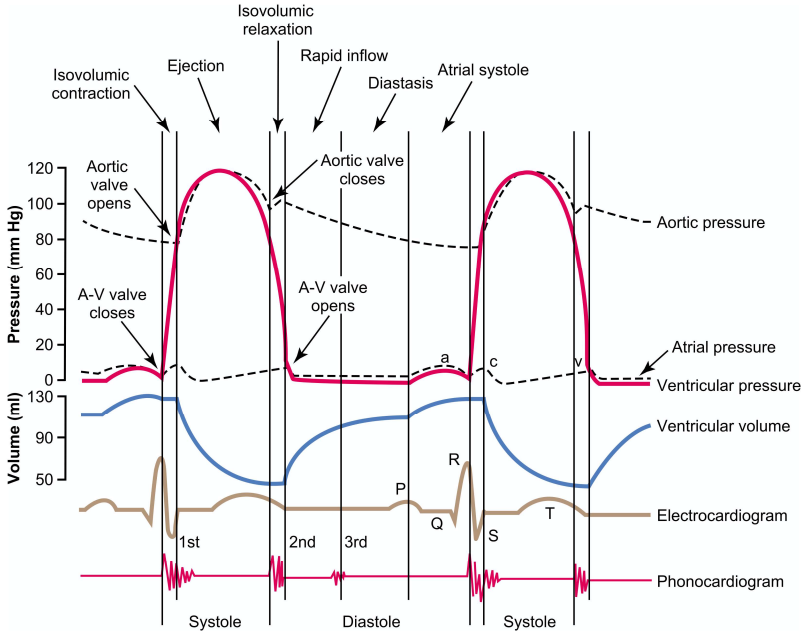

Fig. 1.2. Phases of the cardiac cycle showing changes in pressure, ventricular volume, electrocardiogram and phonocardiogram (Hall 2015)

The cardiac cycle, therefore, proceeds in four stages (Hall 2015):

1. Atrial systole. At the beginning of this stage, atrioventricular valves are opened. Both atria contract and allow blood to be pushed through valves into ventricles.
2. Ventricular systole. Both ventricles begin to contract, causing an increase in blood pressure. When pressure increases to the point that it is higher than the one present in atria, atrioventricular valves close. Increasing pressure eventually exceeds the one present in the arteries, semilunar valves open and blood starts to flow into the vessels. When the maximum pressure peak is reached, which is normally around 120 mmHg (or 16 kPa), blood flow begins to reduce and pressure decreases. When pressure becomes lower than that in the arteries, semilunar valves close and systole phase ends.
3. Atrial diastole. Ventricular pressure reduces to a value around 0 mmHg. Since pressure is now higher in atria, this induces the opening of atrioventricular valves and allows blood to flow from atria to ventricles, aided by the aspiration due to the relaxation of ventricular walls.
4. Ventricular diastole. Blood continues to flow from atria to ventricles, but with less speed due to the reducing pressure difference between the chambers.

The mitral valve, also called bicuspid, is located between the left atrium (LA) and the left ventricle (LV). It consists of two leaflets, anterior (AL) and posterior (PL), attached to the mitral annulus and anchored to the papillary muscles (PMs) by a group of thread-like branched fibrous tendons, called the chordae tendineae. The main role of the MV is to ensure unidirectional blood flow from the LA to the LV and to prevent its backflow. Therefore, cardiac function highly depends on correct and synchronous functioning of all MV elements (Zhu 2015).

The mitral annulus is a flexible structure of fibrous and muscular tissue, divided to anterior and posterior sections, into which the corresponding MV leaflets are directly inserted. Both sections are separated by two anatomical landmarks, called commissures. If observed from the LA, the annulus has an ellipsoidal shape with a greater transverse diameter compared to a longitudinal one. Its dimensions are not the same in different individuals and, moreover, they are not constant throughout the cardiac cycle, changing based on the stage of the cycle.

Furthermore, the annulus has a non-planar profile, naturally conforming a saddle shape, as first reported by Levine *et al.* (1987). The highest point of the saddle, which is the most distant point from the LV apex, is called anterior saddle horn and is located in the anterior section of the annulus. The second peak of the saddle is in the opposite side, in the central region of the posterior annular section,

and is called posterior saddle horn. The lowest points of the saddle correspond to two commissures, indicated as anterolateral and posteromedial.

During diastole, the annulus relaxes and reaches its maximum size, appearing almost circular, if observed from the LA. With the beginning of systole, the annulus begins to contract, becoming shortened and flexed. This movement of the annulus is induced by the contraction and subsequent relaxation of the surrounding myocardium. Consequently, alterations of the annulus shape and dimensions in healthy MV result in optimal leaflet coaptation and valve function (Jimenez *et al.* 2003)

The MV consists of two thin, asymmetrical leaflets (AL and PL) attached to the annulus and conjoined at the commissures. Both leaflets have a hinge type motion with respect to the annulus. The proper closure of the leaflets ensures the optimal function of the MV and prevents backflow of blood into the LA.

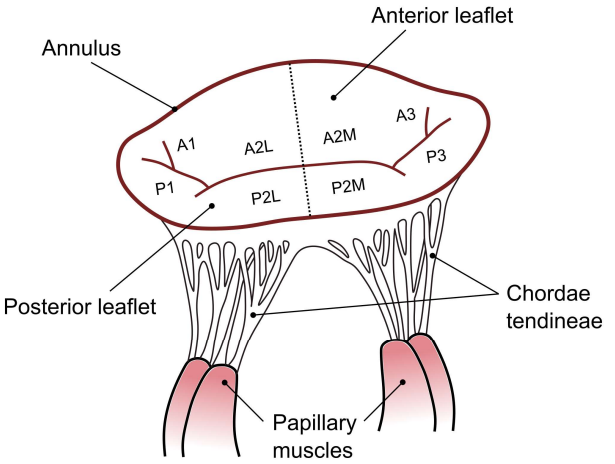

Fig. 1.3. Anatomy of the mitral valve at peak systole. Anterior and posterior leaflets are divided into the segments based on the modified Carpentier classification

MV leaflets are remarkably different in structure. The AL is typically larger in area and is extended more in the vertical direction. It has a semicircular or triangular shape and narrower attachment to the annulus. The PL has a quadrangular shape and is extended more in the transverse direction. It also has two indentations on the free margin, which generally split leaflet into three segments, called lateral (P1), middle (P2) and medial (P3), as proposed by Carpentier (1983) and widely used. Of those segments, the middle one has the largest dimensions and is the one into which the greater number of the chordae tendineae are inserted. Each of the

segments of the PL is matched by corresponding areas on the AL, called A1, A2 and A3.

However, in the present study, the modified Carpentier classification (Shah 2010) is used characterized by the division of A2 and P2 segments in halves, namely middle-lateral (A2L, P2L) and middle-medial (A2M, P2M) segments (Fig. 1.3). This approach allows a more precise description of the location of the valve dysfunction.

The ventricular surface and the free margin of the leaflets are connected to the PMs by the branched network of the chordae tendineae. The chordae tendineae are thread-like branched tendons of fibrous and cartilaginous tissue. Starting from the PMs, from which they originate, a single main branch can be identified, subdivided into two or more secondary chordae, which have a large number of branches. The chordae attached to the commissural sections are called commissural chordae, whereas the chordae inserted into the leaflets are referred to as the leaflet chordae (Gunnal *et al.* 2015). Based on their insertion point, the leaflet chordae can be divided into two categories:

1. First order chordae are the thinnest. They originate from the PMs and, progressively dividing, are inserted into the free margin of the leaflets, thus often called marginal chordae (Liao and Vesely 2003).
2. Second order or basal chordae are inserted into the ventricular surface of the leaflets closer to the annulus (Degandt *et al.* 2007). Among these, four chordae (two inserted into the AL, and two into the PL) are particularly thick and strong, named as strut chordae (Gunnal *et al.* 2015).

There are two PMs arising from the LV wall, each having one or multiple heads with the chordae attached (Madu and D'Cruz 1997). The lateral half of the leaflets is anchored by the chordae to the anterolateral PM, while the medial half has chordal attachments to the posteromedial PM. Both muscles contract simultaneously, and the contraction is synchronized with that of the ventricular myocardium. During systole, the PMs contract and the chordae are put in tension, holding the MV leaflets below the annular plane. During diastole, they relax and recover initial position.

1.1.2. Mitral Valve Function and Dysfunction

The MV opens and closes mainly because of pressure differences between the LA and the LV, opening when there is higher pressure in the LA, and closing when pressure is higher in the LV. During diastole, blood fills the LA, thus increasing pressure and opening the MV. Blood begins to flow through the valve, increasing pressure in the LV and forcing the MV to close. Since pressure in the LA becomes

much lower than in the LV, the leaflets attempt to evert to the lower pressure region. This eversion is called MV prolapse (Hall 2015).

The chordae tendineae play an important role in the MV function (Fig. 1.4). During ventricular systole, the chordae tendineae transmit tension generated by the contraction of the PMs to the leaflets avoiding their eversion into the LA due to pressure. Specifically, basal and strut chordae provide only basic structural support and are more involved in the LV function, whereas marginal chordae prevent prolapse of the leaflet margin (Obadia *et al.* 1997).

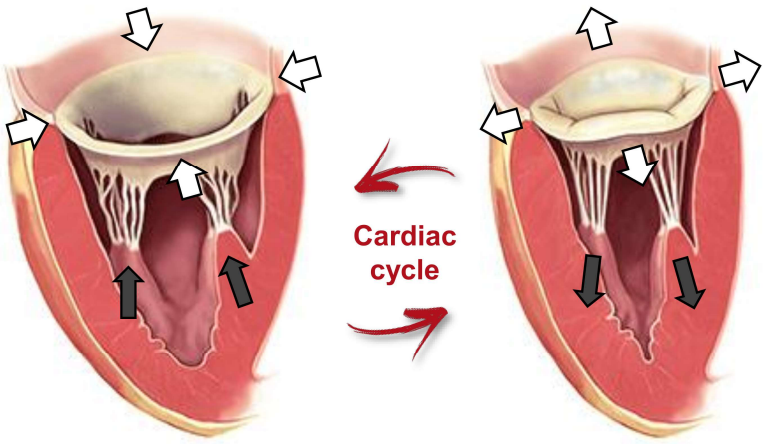

Fig. 1.4. Function of the mitral valve during the cardiac cycle pointing out changes in annular dimensions (white arrows) and transmission of chordal tension (grey arrows). Adapted from (Carpentier 2010)

MV prolapse usually appears due to disruption of the valve restraining force structures, such as rupture of the chordae tendineae. In some cases, the prolapsed MV lets a small amount of blood flow backward from the LV into the LA. This disorder is called mitral regurgitation. If mild, MR may not cause problems, however, severe MR can lead to a life-threatening emergency, including pulmonary congestion and heart failure. The severity of MR generally depends on the number and location of the ruptured chordae. A single ruptured chorda may lead to mild MR, which requires no treatment, while the multiple chordae ruptured simultaneously can cause severe MR (Gabbay and Yosefy 2010). Moreover, ruptured basal and strut chordae might not compromise the coaptation of the leaflets, however, rupture of the marginal chordae almost always results in loss of normal coaptation and valvular leakage (Dal-Bianco *et al.* 2014).

The underlying causes of chordae tendineae rupture include subacute endocarditis, rheumatic heart disease, myxomatous degeneration, and other heart and valvular diseases (Gabbay and Yosefy 2010). Mechanical properties of the diseased chordae are significantly different from those of the intact ones (Barber *et al.* 2001), therefore, the rupture occurs when the strain forces exceed the stretching threshold of the chordae damaged by the disease (Gabbay and Yosefy 2010).

1.1.3. Diagnostic Imaging of Mitral Regurgitation

Mitral regurgitation is the most common heart valvular disease (El Sabbaqh *et al.* 2018), affecting 2–3% of the world population (Han *et al.* 2018). This disease cannot be treated with medications, so it is necessary to use clinical parameters, especially those obtained from diagnostic images, to decide when and how the surgeon has to intervene.

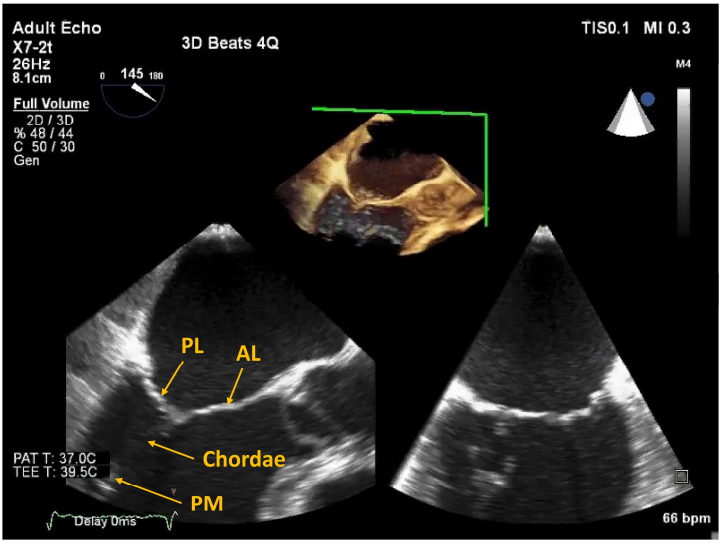

Fig. 1.5. Echocardiographic image of healthy mitral valve at peak systole. The main components of the valve structure can be seen: anterior (AL) and posterior (PL) leaflets, posteromedial papillary muscle (PM) and chordae tendineae

The easiest to detect symptom of MR is a heart murmur heard with a stethoscope. Other symptoms can also include shortness of breath, dizziness, chest pain, swelling in the ankles and feet, extreme tiredness and weakness (Enriquez-Sarano *et al.* 2009). Of course, having these symptoms does not necessarily indicate the

presence of MR. Further examination should be done, including the use of diagnostic imaging, to assess the condition. The most common imaging techniques for the diagnosis of MR are (Durst and Gilon 2015):

1. Chest X-ray. It works on the principle that different materials absorb dissimilar amounts of radiation. However, in case of MR, X-ray can only be used to detect non-specific data concerning the disease, such as enlargement of the LV, which can be related to MR (Anderson *et al.* 2008).
2. Angiography. The trace of blood in the circulatory system can be observed using X-ray based techniques, such as fluoroscopy, after the injection of a contrast fluid into the vessels. By placing this fluid in the LV, the presence of MR can be checked, observing the presence or absence of contrast material in the LA (Apostolakis and Baikoussis 2009).
3. Cardiovascular magnetic resonance imaging (cMRI) is the most accurate technique for visualizing the severity of the valve condition and assess the size and function of the LV. cMRI does not involve exposure to ionizing radiation, but the patient must not be a carrier of metal prostheses or pacemakers in order to perform the examination (Uretsky *et al.* 2018).
4. Echocardiography (Fig. 1.5). This ultrasound-based imaging technique has become routinely used in the diagnosis, management and follow-up of patients with MR. Echocardiography provides real-time images of the heart chambers, thus allowing to observe presence and severity of MR. Different types of echocardiography can be performed (Zeng *et al.* 2014):
    - Transthoracic echocardiography (TTE) is the most common type of ultrasound diagnostic technique for the assessment of morphology and geometry of the MV, which provides accurate quantification of valvular dysfunction. During TTE, the ultrasound transducer is placed on the chest of the subject to get various real-time views of the heart.
    - Transesophageal echocardiography (TEE). During TEE, the ultrasound transducer is placed into the esophagus of the subject to get various real-time views of the cardiac structures. The resulting images are much sharper than that provided by the TTE because ultrasound needs to cross only a few millimeters from the esophagus before reaching the heart.
    - Doppler echocardiography can be used during either TTE or TEE examinations to determine the velocity and direction of the blood flow. Therefore, color flow Doppler is able to reveal the backflow of blood from the LV to the LA during systole. However, while not evaluating the actual flow, but only its velocity, it is subject to errors and provides only a semi-quantitative estimation of MR severity.

1.1.4. Mitral Valve Surgical Repair Techniques

MV repair is a preferred surgical treatment for MR and has significant advantages over MV replacement with an artificial valve, such as preservation of postoperative LV function, reduction of the risk of valve-related complications and improved long-term survival rate (Mick *et al.* 2015). However, there is no standard surgical repair technique for MR, it can depend on individual patient anatomy, pathology and even surgeon preference (Morgan *et al.* 2016). The surgical techniques that today are part of the clinical standard include leaflet resection, chordal transposition, edge-to-edge procedure and annuloplasty using a prosthetic ring (Pozzoli *et al.* 2016). Still, the use of artificial neochordae for the MV repair has become the most common method, and currently over 40 different surgical techniques for applying neochordae to MV repair is used (Ibrahim *et al.* 2012). Expanded polytetrafluoroethylene (ePTFE), also known as Gore-Tex, sutures are typically used to form neochordae (Ibrahim *et al.* 2014). These sutures appear to be a good material for the chordae replacement because of their biomechanical properties, similar to those of the natural chordae (Salvador *et al.* 2008).

The most common technique for replacing the ruptured chordae with the neochordae is called the loop technique. This technique uses a set of premade ePTFE suture loops, which are anchored to the PM (Fig. 1.6 a) and then used to resuspend the prolapsing segment of the leaflet. It involves the following steps: (1) measurement of the required neochordal length; (2) making a loop set of the premeasured length; (3) anchoring the loop set to the PM; (4) implanting anchored neochordae to the prolapsing leaflet; (5) if necessary, adjusting the neochordal length (Shibata *et al.* 2015).

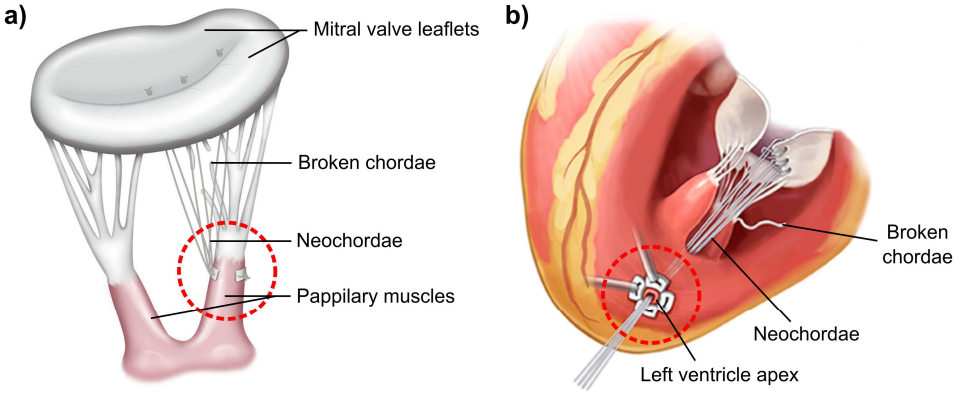

Fig. 1.6. Neochordal anchoring site (marked with circle) in different mitral valve repair surgical techniques: a) loop technique; b) transapical implantation of neochordae. Adapted from (NeoChord 2016)

The main disadvantage of loop technique is that during such surgery the heart is stopped, and the cardiopulmonary bypass pump takes over the work of the heart and the lungs. Another disadvantage is that estimation of the proper neochordal length can be challenging (Hysi *et al.* 2017) and is often obtained by a process of trial and error during the surgery, therefore, the heart may have to be stopped and restarted few times (Ibrahim *et al.* 2012).

Recently, a new technique for neochordae implantation was introduced. NeoChord DS1000 device enables off-pump (also called "beating-heart") transapical implantation of the neochordae through a minimally-invasive approach (Fig. 1.6 b). It is a single-use, hand-held device designed to replace ruptured chordae tendineae with the artificial neochordae made of ePTFE sutures (NeoChord 2016). This device can be used in cases of MV pathologies that lead to more or less severe MR. It has three essential features: (1) a gripper-like tip with expandable jaws used to catch the prolapsing segment of the leaflet; (2) four optical sensors with a device monitor allowing to confirm proper leaflet capture; (3) a semi-dull needle used to implant the neochordae to the leaflet.

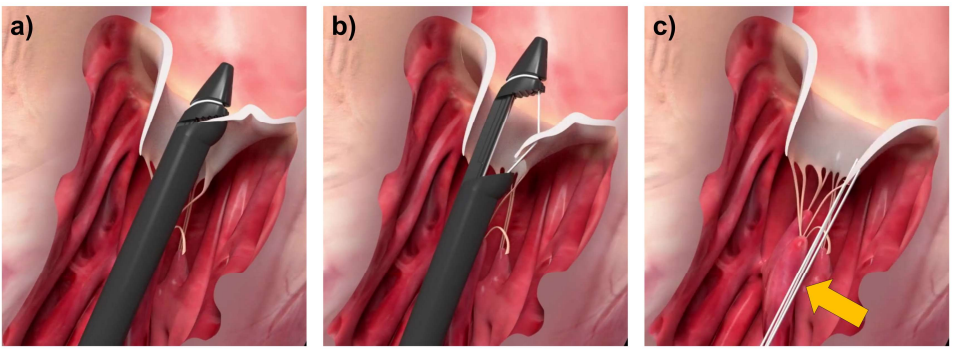

Fig. 1.7. NeoChord DS1000 device during surgery: a) prolapsing segment of the mitral valve leaflet captured by the grasping mechanism of the device; b) insertion of the suture; c) neochordae anchored to the prolapsing leaflet (NeoChord 2016)

During surgery, a small incision of about 6 cm is made on the right side of the chest. The device is passed into the beating heart through this incision and advanced through the MV into the LA under TEE guidance. A grasping mechanism of the device is used to capture and control the prolapsing leaflet (Fig 1.7 a). Effective leaflet capture is confirmed by observing the device monitor of the optical sensors. The leaflet is then penetrated with the semi-dull needle (Fig. 1.7 b) and the neochorda is anchored to the prolapsing segment (Fig. 1.7 c). Since usually three to six neochordae are implanted (Colli *et al.* 2018), the procedure is

repeated for each suture. The implantation procedure and results are controlled with echocardiography. After successful implantation is confirmed, all neochordae are secured under proper tension to the LV apex with additional felt pledgets, used to distribute pressure of the suture knots (Merk *et al.* 2015). The neochordae implanted in such way usually have a length of 50 to 70 mm and are formed using CV-4 type sutures with a diameter of 0.307 mm (NeoChord 2016).

Transapical MV repair approach was introduced in 2009, and at first the animal studies were performed (Bajona *et al.* 2009), before enrolling patients in the clinical trial soon after (Seeburger *et al.* 2010). The first results regarding the use of this technique on subjects suffering from MR were published by surgeons from Vilnius University Hospital Santaros Klinikos (Rucinskas *et al.* 2014), reviewing 13 cases of transapical MV repair. It was observed that more than 90% of patients actually experienced a reduction in MR six months after the surgery. Later published studies on larger patient populations only confirmed this rate of success (Colli *et al.* 2016; 2018). In general, it can be stated that it is possible to obtain satisfactory clinical results even in most critical cases, such as high-risk patients or patients in old age.

However, some aspects of this technique, such as exact positioning of the neochordae to the prolapsing segment or the length adjustment of the neochordae to eliminate prolapse while preventing additional restriction of the leaflet, can only be assumed (Seeburger *et al.* 2012) and require additional experience and further studies.

Transapical MV repair with neochordae implantation is performed under 2D and 3D echocardiographic guidance. TEE is used, which allows to obtain various real-time views of the heart after placing the ultrasound transducer into the esophagus of the subject. TEE guidance plays an important role while the following phases of the surgical procedure are executed:

- pre-operative identification and evaluation of MV prolapse;
- insertion of NeoChord DS1000 device into the heart;
- grasping of the prolapsing leaflet and assessment of the leaflet capture;
- proper tension adjustment of the implanted neochordae;
- post-operative evaluation of the surgical procedure and its results (Demetrio *et al.* 2015).

Color flow Doppler is usually used during 2D echocardiography to identify the presence of MR before and after the procedure by showing the existence or absence of the blood backflow from the LV to the LA during systole. Still, the use of 3D TEE is mandatory to perform transapical MV repair, as it provides more accurate information than two-dimensional TEE for the device guidance to the target segment of the leaflet and the implantation of the neochordae.

For the numerical simulation studies, investigating the MV function and evaluating novel MV surgical repair techniques, echocardiography contributes image data that can be used to reconstruct the geometry of the valvular structure. This imaging technique has some advantages among others, providing real-time views of the cardiac structure without exposing a patient to hazardous ionizing radiation, thus pre-, intra- and post-operative image data can be safely recorded.

1.2. Review of Mitral Valve Computational Models

During the last three decades, a number of numerical simulation studies have shown promising outcomes while investigating the MV function (Kunzelman *et al.* 1993; Votta *et al.* 2008a; Toma *et al.* 2016) and evaluating novel MV surgical repair techniques (Reimink *et al.* 1995; Votta *et al.* 2007; Morgan *et al.* 2016). Two categories of the computational models can be distinguished. Structural models use FEM to simulate the MV function without directly considering the blood flow. Whereas fluid-structure interaction (FSI) models study the interactions between the MV and the blood flow using computational fluid dynamics (Gao *et al.* 2017).

1.2.1. Structural Mitral Valve Models

Structural FE models are often used for the MV modeling to study dynamics, stress-strain behavior and deformations in scenarios of clinical relevance. These models are suitable for the investigation of both physiological and pathological behavior and for the analysis of specific surgical treatment. Basically, they are aimed at quantifying the biomechanical aspects of pathologies and surgical techniques. However, the FE models involve calculation times of several hours on parallel computing systems, and therefore these models are not yet used as the clinical analysis tool.

Early FE models of the MV published in the literature were defined on the basis of animal or ex vivo measurements with an idealized geometry, representing an average case of a certain condition without accurate anatomical details. Large mammalian animal measurement data (most often porcine or ovine) was usually chosen, as it can be held the most physiologically and clinically relevant to the human heart (Camacho *et al.* 2016).

The first structural FE model of the MV was developed in the University of Washington (United States) by Kunzelman *et al.* (1993). The data for this model was obtained from ex vivo porcine valves, which were used to define the geometry of the MV at end-diastole, making the assumption that at this point in time the MV is approximately unloaded. This model was used to simulate the systolic

function of the physiological MV and to calculate stresses acting on the leaflets. The main limitations of this work were the anatomical simplification of the leaflets and chordae tendineae geometry, for example, the annular profile was hypothesized to be planar and kept fixed throughout the simulation. In terms of chordae tendineae, only marginal chordae without branches were modeled. Moreover, the MV tissue was described as a linear elastic material.

In the later studies, the researchers from the University of Washington adapted this approach to investigate the functions of the pathological MV (Kunzelman *et al.* 1997; 1998) and to evaluate surgical techniques for MV repair (Reimink *et al.* 1995; Kunzelman *et al.* 1996).

A similar approach was used by the research group from the Politecnico di Milano (Italy). A simplified anatomical model with planar and static annular profile was created to investigate MV pathologies (Votta *et al.* 2003). The profile of the leaflets was obtained from ex vivo data of MV measurements, published by Kunzelman *et al.* (1994). Stress distribution across the leaflets was calculated for pathological and virtually repaired MV models.

A different approach was taken in the Nanyang Technological University (Singapore) by Lim *et al.* (2005) to investigate stress distribution profiles on the MV leaflets. Their model had a saddle shape profile created from in vivo measurements of the ovine MV. The annular geometry was created after positioning 12 transceiver crystals on the MV and tracing their positions at different time points using sonomicrometer. Still, some simplifications were taken into account. The leaflets were modeled as a single membrane of a constant length without the commissures and described as a linear isotropic material. As in the previously described studies, the simplified geometry of the chordae tendineae with linear elastic mechanical behavior was created.

Nonlinear mechanical response of the MV was first considered in the model developed by Dal Pan *et al.* (2005) from the University of Brescia (Italy). The hyperelastic behavior of the leaflets, created based on medical literature and direct observations, was described using the reduced polynomial model. The developed MV model was used to investigate structural and functional effects of the edge-to-edge surgical technique for MV repair. However, no actual chordae tendineae were included in the model, and the effect of the chordae was simulated by imposing displacement to the free margin nodes.

The more complete model of the MV structure was created by the researchers from the Norwegian University of Science and Technology (Fig. 1.8). In their studies (Prot *et al.* 2007; 2009a; 2009b; 2010), the MV model with simplified geometry created from ex vivo porcine data, with the flat annulus and marginal chordae attached to the free margin of the leaflets, was used to investigate the behavior of healthy and pathological MV. For the leaflets, transversely isotropic mechanical response was considered, characterized using hyperelastic strain

energy density function, proposed by May-Newman and Yin (1998) from Johns Hopkins School of Medicine (United States) (see paragraph 1.2.4).

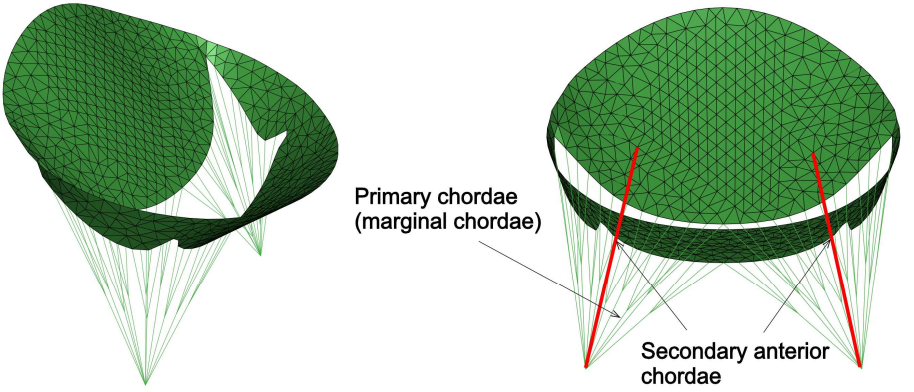

Fig. 1.8. Mitral valve model with simplified geometry created from ex vivo porcine data by Prot *et al.* (2007)

All the models presented so far used idealized geometry of the MV with some geometrical simplifications. In a structure such as the MV, geometry is crucial to the structural response, so no effects of the real intersubject variability could have been evaluated using these idealized models. For this reason, the need to develop patient-specific models with realistic morphology emerged.

The first published patient-specific model was developed by the research group from the Politecnico di Milano (Votta *et al.* 2008a). The MV model was created through a semi-automatic procedure from TTE image data and included realistic geometry of the leaflets at end-diastole with transversely isotropic material properties, described using strain energy function proposed by May-Newman and Yin (1998). The movement of the annulus and PMs was also derived from echocardiographic data. However, the anatomical information acquired from TTE image data was not fully exploited. The profile of the leaflets was simplified and described by a sinusoidal function, and the movement of the PMs was defined by integrating image data since the PM tips are not always entirely visible in TTE images. Furthermore, the chordae tendineae was defined according to data from the literature, as they are not visible in echocardiographic images.

In the later study by the researchers from the Politecnico di Milano, a new approach to the MV modeling was taken (Conti *et al.* 2010). The geometry of the MV was reconstructed from cMRI data, characterized by the superior image clarity compared to echocardiographic data. The valvular structures were segmented manually at the end-diastole frame of image data, whereas the positions of the

annulus and the PMs were traced in all frames of the cardiac cycle. The chordae tendineae were represented in a more complete way than in previous studies, including basal and strut chordae. Their insertion points into the PMs were no longer represented by a single point, but by a circumference of points, each representing the insertion place of a different chorda. This new approach was used to simulate the systolic function of healthy and pathological MV models.

Similar modeling strategy was adopted by the research group from the University of Texas Health Science Center at Houston (United States) to investigate patient-specific annular motion effect on the MV function (Rim *et al.* 2013). The main difference is that in this study the geometry of the MV (Fig. 1.9) was reconstructed through a semi-automatic procedure from echocardiographic images instead of cMRI data.

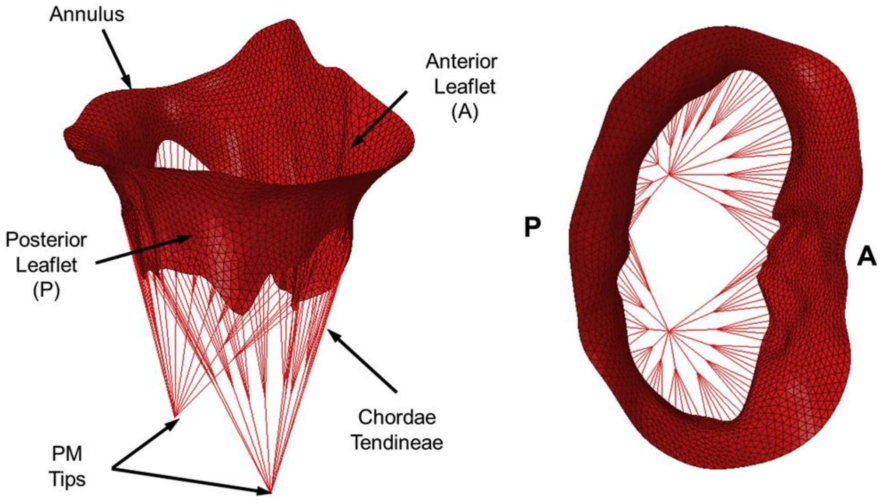

Fig. 1.9. Patient-specific mitral valve model used to investigate annular motion effect on the valve function by Rim *et al.* (2013)

The automatization of the geometry creation process was proposed by Mansi *et al.* (2012) from the Research and Technology center at Siemens Corporation (United States). Their model, created from TEE image data, included realistic geometry of the mitral annulus, leaflets and PMs. However, the purpose of the study was to obtain a model capable to predict valve behavior given the specific images of a subject, rather than to investigate valve behavior in terms of strains and deformations. For this reason, the MV leaflets were modeled as linear, transversely isotropic elastic tissue, and simulation results were analyzed only in terms of the geometry.

All previously described patient-specific modeling approaches have in common the aspect of being discretized with shell elements. The first FE model of the patient-specific MV described by solid elements was developed in the University of Connecticut (United States) by Wang and Sun (2013). Their FE model of a healthy MV was created from micro-computed tomography (micro-CT) image data with detailed leaflets thickness, chordae tendineae insertion points and PMs location. The mechanical behavior of the leaflets tissue was described using constitutive hyperelastic anisotropic material model (see paragraph 1.2.4).

The usage of micro-CT can increase the level of anatomical detail of valvular structures, but, contrary to echocardiography or cMRI, usually only in vitro imaging is performed (Gao *et al.* 2017), as visualization of moving objects, such as heart valves, using micro-CT is challenging (Badea *et al.* 2008) and requires additional techniques to minimize imaging artifacts caused by cardiac motion (Desjardins and Kazerooni 2004). Moreover, the simulation of models described by solid elements involves a relatively high computational cost compared to shell elements. Up to 12 hours can be needed to simulate function of the detailed MV model discretized by solid elements (Toma *et al.* 2017), whereas for the model described by shell elements, depending on the mesh size, about half of this time (Sturla *et al.* 2015a), and usually even less (Pappalardo *et al.* 2017), is required.

1.2.2. Fluid-Structure Interaction Models of Mitral Valve and Blood

FSI models combine the structural modeling of a solid body with the fluid dynamics modeling of fluid by coupling FE model with computational fluid dynamics (CFD) model. In this particular case, FSI models aim to investigate the interaction between the MV and the blood flow (Mansi *et al.* 2012). This method is more sophisticated than FEM, in which the action of fluid is usually approximated and imposed as boundary condition by applying pressure load on the surface of the leaflets. The challenge of FSI method is that the fluid mechanics is normally described using the Eulerian formulation, while the equations for the tissue are described in the Lagrangian form (Gao *et al.* 2017).

The first FSI model of the MV was developed by Kunzelman *et al.* (2007) to simulate normal and pathological valve functions (Fig. 1.10). The leaflets were modeled as membranes and the chordae tendineae as tension-only cables, both described as the nonlinear materials. The MV was positioned in a tubular fluid volume, thus approximating the LV domain and neglecting the cardiac wall motion as well as its effect on the blood flow. Only valve closure was simulated, and the comparison with the structural model was made, comparing stress distribution across the leaflets in a closed valve configuration.

Lau *et al.* from the University College London (United Kingdom) compared MV dynamics with and without fluid, based on linear material models (2010). In this study, the effect of the fluid on valve dynamics was quantified in both tubular and ventricular-shaped fluid volumes. Full cardiac cycle including valve opening and closing was simulated, calculating stress values on the leaflets, blood flow rate and fluid velocity in the LV.

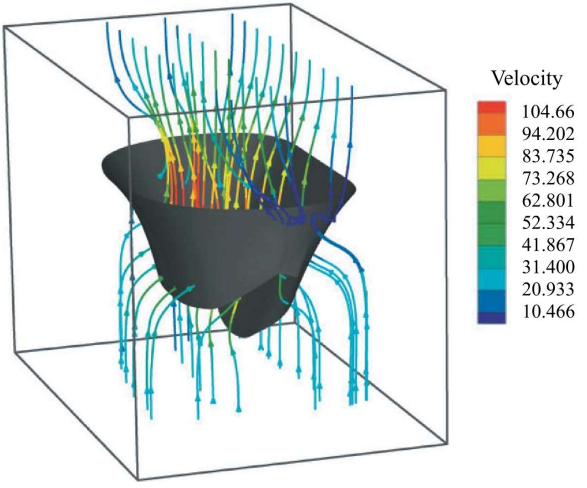

Fig. 1.10. Stream traces of blood velocity in the fluid-structure interaction model by Kunzelman *et al.* (2007)

The first anatomically realistic MV model based on in vivo cMRI data was created in the University of Glasgow (United Kingdom) by Ma *et al.* (2013). The leaflets and the chordae tendineae were treated as elastic structures immersed in the semi-rigid tubular fluid volume under physiological transvalvular pressure load. The simulation of a full cardiac cycle was performed and the influence of patient-specific geometry on fluid dynamic parameters was investigated. The simulation results were compared to clinical measurements, thus achieving the initial validation of the model.

A more detailed geometrical model was introduced by the researchers from the Georgia Institute of Technology (United States) (Toma *et al.* 2016). The geometric data was acquired during a micro-CT scan of ex vivo ovine valve. The MV model was described by solid elements and the importance of individual chordae on MV closure dynamics was investigated by simulating rupture of each and every chordal branch. However, some simplifications were done. A rigid tube was used as an approximation of the LV domain and the computed severity of MR was

approximated by calculating the regurgitant area with no hemodynamic variables included in the calculations.

While including blood flow patterns inside the LV, FSI approach can be used for comprehensive analysis of MV physiology (Gao *et al.* 2017). However, blood flow boundary conditions for the FSI simulation are required, which could be difficult to obtain during clinical measurements. For this reason, the standard modeling approach is to immerse the MV into an idealized fluid domain, which, however, may not reflect the actual condition of the patient (Mansi *et al.* 2012). Moreover, FSI modeling involves much longer calculation time, and simulating full cardiac cycle can take up to 240 hours (Caballero *et al.* 2018). For these reasons, the FSI method is often excluded from the field of surgical planning and training, and its application is generally limited to the study of MV within simplified fluid domains.

1.2.3. Computational Models for Mitral Valve Repair

Computational models of the MV, though are not used for the direct clinical analysis, can be an important support tool for the clinical action, such as evaluation of the novel MV repair methods. They can provide information on the biomechanics of the valvular structure that would otherwise be impossible to obtain. Different methods of the MV repair was investigated using models with both idealized and patient-specific geometries.

The first computational model concerning MV repair was developed by the research group from the University of Washington (Reimink *et al.* 1995). The model was used to evaluate the behavior of the MV following the replacement of the AL broken chordae with ePTFE neochordae. The geometry was created from measurements of ex vivo porcine valves (Kunzelman *et al.* 1993) and included a complete valve system with the annulus, leaflets, marginal and basal chordae, and PMs. The MV leaflets were described as linear anisotropic material, while the chordae tendineae were assigned linear isotropic mechanical properties.

Several chordae were removed from the AL and replaced with ePTFE sutures, thus simulating rupture of the chordae tendineae and MV repair with neochordae implantation. The simulation of systolic function indicated that ePTFE sutures restore MV function and stresses to normal range. Therefore, it has been shown that implantation of the neochordae, which have a high stiffness value, does not restrict the physiological functions of the MV.

Different MV repair method was investigated by Votta *et al.* (2002). The MV leaflets profile and the chordae tendineae were created in accordance with data found in the literature. The MV prolapse was simulated applying pressure on the atrial surface of the leaflets while in closed valve configuration. Edge-to-edge repair technique was used to restore the valve competence by suturing middle

portions of the free margins of the leaflets. Stress analysis was performed to investigate the outcomes of such surgical procedure.

However, due to their idealized geometry, these early models could not have been evaluated against clinical data. The first patient-specific MV model for the simulation of surgical procedure was created by the research group from the Politecnico di Milano (Stevanella *et al.* 2011). The same approach as in the earlier mentioned study by Conti *et al.* (2010) was used to reconstruct the geometry of the MV from echocardiographic data. The effects of annuloplasty surgical procedure were investigated, calculating stress distribution across the leaflets and reaction forces acting on the PMs.

Researchers from the Politecnico di Milano also made a big contribution while simulating MV repair with neochordae implantation. Several studies were published (Sturla *et al.* 2014; 2015b; 2015c), investigating and quantifying different neochordae implantation techniques in terms of both chordal and neochordal tension, and leaflet stress distribution.

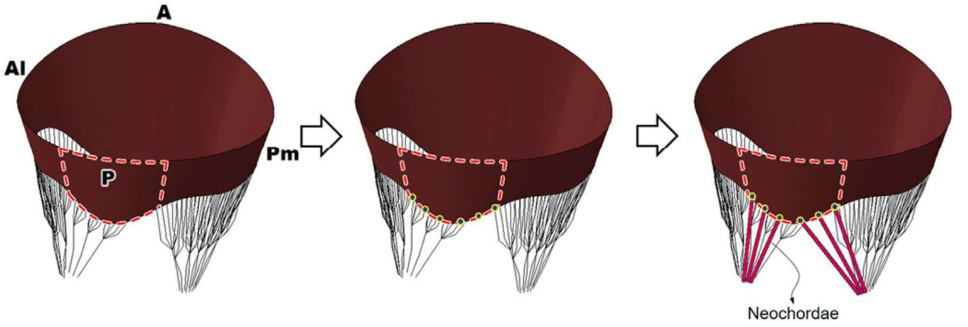

Fig. 1.11. Patient-specific model used for the simulation of mitral valve repair with neochordae implantation (Choi *et al.* 2017)

While the majority of models for investigating MV repair are decoupled from the blood flow, Lau *et al.* (2011) used the FSI approach with nonlinear MV material description to investigate edge-to-edge surgical repair technique. Similar modeling strategy as in their previous and already mentioned work (Lau *et al.* 2010) was used to calculate parameters emerging from the interaction between the MV and the blood flow.

More studies considering MV repair using patient-specific data and numerical simulation were published during the last decade. Different repair methods were investigated:

- leaflet resection (Rim *et al.* 2015; Morgan *et al.* 2016; Choi *et al.* 2017);

- edge-to-edge repair (Avanzini *et al.* 2011; Zhong *et al.* 2014; Sturla *et al.* 2015a);
- annuloplasty procedure (Choi *et al.* 2014; Baillargeon *et al.* 2015; Kong *et al.* 2018);
- MV repair with neochordae implantation (Rim *et al.* 2014; Morgan *et al.* 2016; Choi *et al.* 2017 (Fig. 1.11)).

1.2.4. Material Models for Mitral Valve Leaflets and Chordae Tendineae

Material characterization of the MV tissue is essential in understanding and investigating the valve function and evaluating novel MV surgical repair techniques (Krishnamurthy *et al.* 2008). The mechanical properties of the different valvular components vary due to their structural differences.

Structurally, the tissue of the MV leaflets is composed of collagen, elastin and muscle fibers. When subjected to traction, individual collagen fibers are straightened and stiffened up at different levels. Once all collagen fibers are straightened, further elongation of the material causes the elongation of the fibers themselves. For this reason, MV leaflets tissue has a mechanical response that can be defined as nonlinear.

Tissue abundant in collagen fibers demonstrates higher stiffness along the fiber direction compared with the cross-fiber one. Since in the MV leaflets collagen fibers are oriented along the longitudinal direction (parallel to the annulus), the mechanical response in this direction is stiffer than in the transversal one (perpendicular to the annulus). The response of the MV leaflets tissue is, therefore, nonlinear and transversely isotropic (Lee *et al.* 2015).

Early attempts to describe valve tissue relied on the linear elastic material models following the generalized Hooke's law (Sun *et al.* 2014). Kunzelman and Cochran (1992) performed the uniaxial tensile test on the specimens of porcine valve tissue, applying the force in two different directions: parallel and orthogonal to the fiber alignment. The mechanical response of the leaflets was described as the relationship between stresses σ and deformations ε using fourth order polynomial model:

$$\sigma = c_0 + c_1\varepsilon + c_2\varepsilon^2 + c_3\varepsilon^3 + c_4\varepsilon^4, \tag{1.1}$$

where c_0, c_1 c_2, c_3 and c_4 are the material parameters derived from the experimental data of the uniaxial test.

The first constitutive model, which represented nonlinear transversely isotropic behavior of the MV leaflets due to the presence of collagen fibers, was proposed by May-Newman and Yin (1998). The biaxial test was performed on

both the AL and the PL of the porcine valve. Both leaflets proved to be less extensible in the circumferential direction compared to the axial. Moreover, different stiffness values for leaflets were observed, showing greater extensibility of the PL. The constitutive model based on the strain energy function Ψ that depends on two invariants of strain I_1 and I_4 was suggested:

$$\Psi(I_1, I_4) = c_0\left[e^{c_1(I_1-3)^2+c_2\left(\sqrt{I_4}-1\right)^2}-1\right], \tag{1.2}$$

where the term $(I_1-3)^2$ is related to the isotropic response of the elastin fibers, while the term $\left(\sqrt{I_4}-1\right)^2$ describes the collagen fibers response and is activated only if $I_4 \geq 1$, and c_0, c_1, c_2 are the material parameters.

The subsequent constitutive model was developed by Wang and Sun (2013). Their model was based on the fiber-reinforced hyperelastic material model proposed by Holzapfel *et al.* (2005). The leaflets tissue was assumed to be composed of a matrix material with embedded collagen and elastin fibers, each of which has a preferred direction. The strain energy function was expressed as:

$$\begin{aligned}\Psi(I_1, I_4) &= c_0\left[e^{c_1(I_1-3)^2+c_2\left(\sqrt{I_4}-1\right)^2}-1\right]+\\ &\frac{k_1}{2k_2}\sum_{i=1}^{2}\left[e^{k_2\left[\kappa I_1+I_{4i}(1-3\kappa)-1\right]^2}-1\right]+\frac{1}{D}(J-1)^2,\end{aligned} \tag{1.3}$$

where c_0, c_1, k_1, k_2 and D are the material parameters, J is the elastic volume ratio, and κ is a dispersion parameter used to describe the distribution of fiber orientation. The strain invariant I_1 is used to describe the matrix material, and the invariants I_{4i} are used to characterize the properties of the collagen and elastin fibers.

Another study concerning the mechanical behavior of the MV leaflets was done by Lee *et al.* (2013) from the University of Texas at Austin (United States). In this study, the effects of material anisotropy at the tissue level was considered. A computational MV model with the incorporated detailed architecture of the collagen fibers was developed using micro-CT image data of ovine valve. The invariant-based constitutive model for the stress-strain behavior of the MV leaflets was implemented:

$$\Psi(I_1, I_4) = c_0(I_1-3)+c_1\left((1-\beta)e^{\left[c_2(I_2-3)^2\right]}+\beta e^{\left[c_3(I_4-1)^2\right]}-1\right), \tag{1.4}$$

where β is a constitutive material parameter ranging from 0 to 1 and related to the level of material anisotropy, and c_0, c_1, c_2, c_3 are the remaining material parameters.

The proposed constitutive model enables the investigation of how the material anisotropy at the tissue level affects the MV functional response at the organ level.

The chordae tendineae are mainly composed of collagen fibers aligned along the longitude of these tendons, thus making them both stiff and robust. Due to the presence of collagen fibers, the mechanical response of the chordae tendineae can be defined as nonlinear (Ritchie *et al.* 2005).

Since the chordae undergo only small or moderately large strains (<100%) during the cardiac cycle (Casado *et al.* 2012), their mechanical behavior can be described using polynomial hyperelastic model (Dassault Systèmes 2010). The basic strain energy density form of the polynomial model is:

$$\Psi(I_1, I_2) = \sum_{i+j=1}^{N} c_{ij} (I_1 - 3)^i (I_2 - 3)^j + \sum_{i=1}^{N} \frac{i}{D_i} (J - 1)^{2i}, \tag{1.5}$$

where $I_1 = \lambda_1^2 + \lambda_2^2 + \lambda_3^2$ and $I_2 = \lambda_1^{-2} + \lambda_2^{-2} + \lambda_3^{-2}$ are the invariants of the right Cauchy-Green strain tensor, λ_1, λ_2, λ_3 are the stretch ratios in different directions, D_i are the constitutive material parameters that control bulk compressibility of the material and can be estimated from volumetric test data, and c_{ij} are the material parameters that control the shear behavior.

The uniaxial tensile test on porcine chordae tendineae was performed by Kunzelman and Cochran (1990) to identify the mechanical properties of the marginal and basal chordae. It was noticed that with increasing strain a notable increase in stiffness appears and the stress-strain behavior of the chordae becomes almost linear. Moreover, there is a difference in mechanical behavior between different chordae: stiffness of the marginal chordae is higher than that of the basal, meaning that under the same degree of deformation marginal chordae will carry a greater stress load.

However, no significant differences in terms of elastic and failure properties of the chordae tendineae were distinguished by the research group from the University of Connecticut (Zuo *et al.* 2016). In general, while the size of marginal, basal and strut chordae varies, the layer of fibrous tissue surrounding the central core of the chordae do not contribute to their overall strength. For example, the thinner marginal chordae are stiffer than the basal, and the strut chordae are the weakest. Similarly, the anterior chordae are stiffer than the posterior at lower load but weaker and more compliant at higher load.

1.3. Conclusions of Chapter 1 and Formulation of the Thesis Tasks

After considering the problem of MV prolapse from a medical perspective and reviewing the studies describing different MV computational models, the following conclusions are done:

1. According to medical literature, MV repair over replacement is generally preferred for several important reasons. Repairing the valve preserves the natural geometry and functionality of the LV, reduces the risk of valve-related complications and improves the long-term survival rate of a patient.
2. Early clinical studies on transapical MV repair proves the efficiency of such surgical technique in terms of survival rate and MR reduction. However, some aspects of this surgical technique, such as positioning of the neochordae or adjustment of neochordal length, are still currently unknown and require additional studies. Therefore, the use of numerical simulation to clarify such aspects should be considered.
3. The computational MV models found in the literature can be divided into two categories: structural models, which use FEM to simulate the MV function without directly considering the blood flow, and FSI models, which combine the structural modeling of the MV with the fluid dynamics modeling of blood. Due to simplifications made in the reviewed FSI modeling studies and the demand for particularly high computational cost and time, FSI method is often excluded from the field of surgical planning and training. Structural modeling, on the other hand, is less time consuming and can be suitable for the investigation of both physiological and pathological behavior of the MV, and for the analysis of specific surgical treatment.
4. The literature review showed that during the last three decades, a significant number of computational models for MV repair simulations were introduced. However, only several studies on the modeling of MV repair with neochordae implantation were published to this date. Moreover, none of them had addressed the problem of transapical MV repair.

Based on the conclusions, the following tasks have to be performed to achieve the aim of the thesis:

1. To develop modeling strategy applied for the numerical simulation of virtual transapical MV repair procedure.
2. To reconstruct the geometry of patient-specific MV using echocardiographic image data and kinematic parameters of MV motion, and to create

structural FE model of the MV with prolapse based on the reconstructed geometry.

3. To apply the created model for the implementation of virtual transapical MV repair followed by the simulation of MV systolic function, and to investigate the effect of neochordal length on post-repair MV functioning.
4. To evaluate the outcomes of virtual transapical MV repair and to consider the eligibility of the developed numerical modeling strategy.

2

Formulation of Mitral Valve Modeling Problem

In the present chapter, the modeling strategy applied for virtual transapical MV repair is introduced. Firstly, a mathematical formulation of the MV modeling problem is presented and the material models used to describe the mechanical behavior of the MV structure are depicted. The stages for the development of patient-specific FE model of the MV with imposed mechanical properties and boundary conditions are then described. Virtual transapical MV repair technique is presented, followed by a dynamic FE simulation of MV systolic function before and after virtual repair.

Parts of this chapter are published in Gaidulis *et al.* (2018a; 2018b; 2019) and Romashov *et al.* (2016).

2.1. Modeling Strategy for Transapical Mitral Valve Repair Simulation

Numerical simulation of the MV structure based on patient-specific data has proven to be useful to evaluate the effects of the MV surgical repair techniques (Drach *et al.* 2018). Studies regarding MV repair with neochordae implantation

were previously published by several authors (Reimink *et al.* 1995; Rim *et al.* 2014; Sturla *et al.* 2014; 2015b; 2015c; Morgan *et al.* 2016; Choi *et al.* 2017), however, none of them had addressed the problem of transapical MV repair.

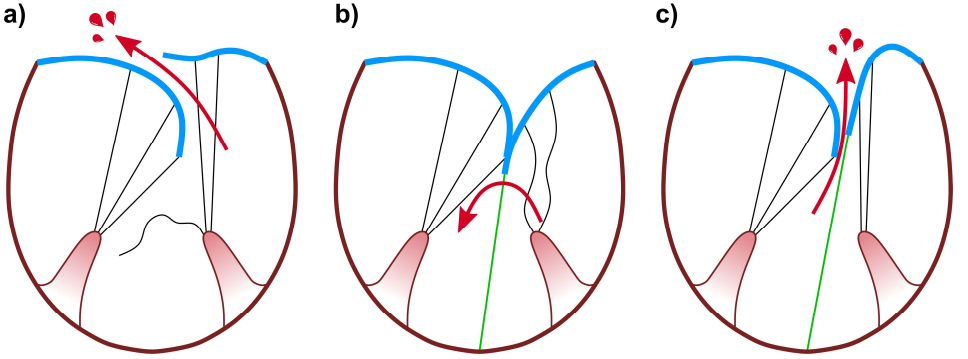

Fig. 2.1. Influence of the neochordal length on the function of mitral valve: a) prolapsing mitral valve; b) mitral valve after the implantation of too short neochordae; c) mitral valve after the implantation of too long neochordae

Transapical MV repair with neochordae implantation is a novel surgical technique, allowing beating-heart correction of MV prolapse with MR through a minimally-invasive approach using NeoChord DS1000 device (see paragraph 1.1.6). While transapical implantation of neochordae shows promising clinical results (Rucinskas *et al.* 2014; Lancellotti *et al.* 2016; Colli *et al.* 2016; Colli *et al.* 2018; Kiefer *et al.* 2018), there are some problematic aspects regarding this surgical technique. The main challenge that emerges in case of transapical MV repair is the correct length adjustment of the neochordae. During the cardiac cycle, the length between the free margin and the LV apex varies at systole and at diastole due to the lack of mutual interaction between the implantation points. This variation is about 10 times larger than the one between the free margin and the PMs, as the simultaneous contraction of the LV myocardium and the PMs allows the PMs to stay in place with reference to the MV. Therefore, there is a higher risk of residual prolapse or tearing of the repaired leaflet after transapical implantation, if either too short or too long neochordae are formed (Fig. 2.1) (Weber *et al.* 2012).

In the present study, FE modeling is used to analyze transapical MV repair considering the challenges associated with the execution of such a procedure. For this reason, structural model of the MV based on patient-specific imaging data is created (Fig. 2.2) and nonlinear dynamic analysis in FE software Abaqus is performed to simulate the systolic function of the MV before and after virtual

transapical repair procedure, and to analyze its outcomes in terms of deformations, acting forces and stress distribution.

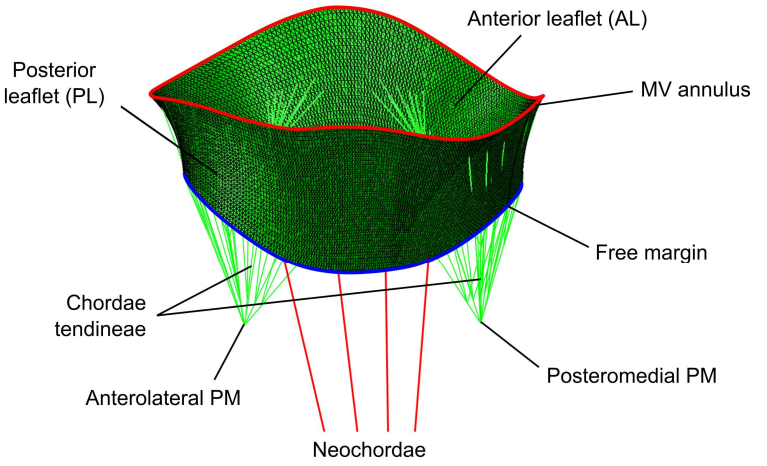

Fig. 2.2. Computational model of the mitral valve structure based on patient-specific imaging data

For the implementation of such workflow, the modeling strategy used for virtual transapical MV repair application is developed (Fig. 2.3). During this procedure, the echocardiographic image data is converted to a structural FE model followed by virtual repair and dynamic simulation in Abaqus. This strategy consists of the following steps:

1. 3D TEE image data acquisition of the whole LV during the cardiac cycle.
2. Segmentation of patient-specific image data.
3. Reconstruction of 3D MV geometry.
4. Mesh generation and implementation of mechanical properties, initial and boundary conditions.
5. Virtual transapical MV repair with adjusted neochordal length.
6. Dynamic FE simulation in Abaqus.

The following paragraphs present the mathematical formulation of the MV modeling problem and describe in detail the steps of the developed strategy used for the creation of structural MV model and simulation of its systolic function before and after virtual repair.

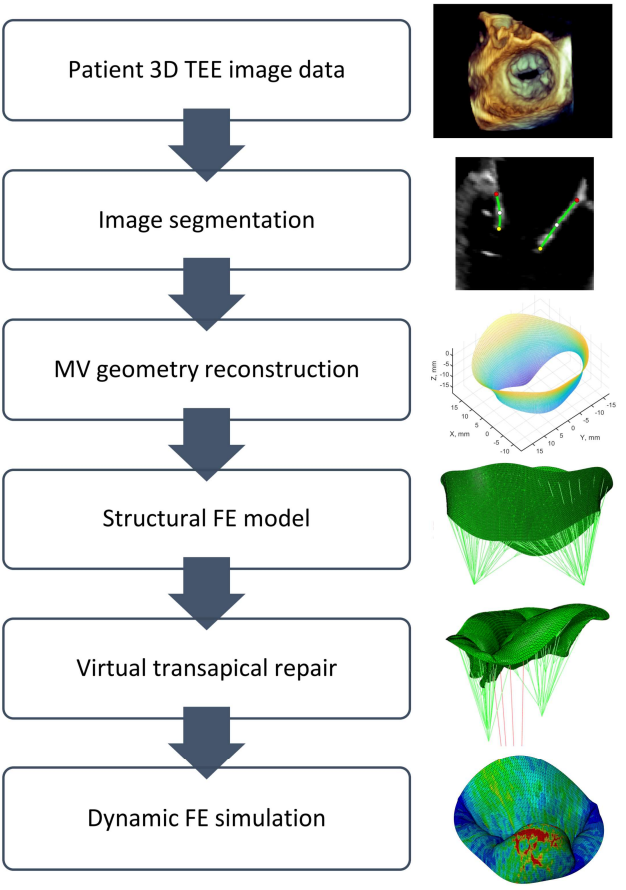

Fig. 2.3. Modeling strategy applied for virtual transapical mitral valve repair

2.2. Mathematical Formulation of Modeling Problem

A general nonlinear equilibrium equation for the *i*th node of the structural physical system in FEM can be written as (Mansi *et al.* 2012):

$$\mathbf{M}\ddot{\mathbf{u}}_i + \mathbf{C}\dot{\mathbf{u}}_i + \mathbf{K}\mathbf{u}_i = \mathbf{P}_i, \tag{2.1}$$

where $\mathbf{M}$ is the mass matrix, $\ddot{\mathbf{u}}_i$ is the acceleration vector, $\mathbf{C}$ is the damping matrix, $\dot{\mathbf{u}}_i$ is the velocity vector, $\mathbf{K}$ is the stiffness matrix, $\mathbf{u}_i$ is the displacement vector, and $\mathbf{P}_i$ is the applied load vector.

In Abaqus, there are two analysis methods, used for solving structural problems, namely Abaqus/Standard and Abaqus/Explicit. Abaqus/Standard employs static and dynamic implicit integration schemes and is suitable for solving only smooth nonlinear problems. However, the presence of the contact or material complexities can cause a large number of iterations, which needs many sets of linear equations to be solved, thus making such simulations particularly expensive in terms of used memory and disk space. Meanwhile, Abaqus/Explicit employs explicit integration scheme to solve nonlinear systems with complex contacts without iterating and requires much less memory and disk space, therefore, is more suitable for solving complex dynamic problems for nonlinear materials. For this reason, Abaqus/Explicit is chosen to perform the simulations of the MV systolic function.

The explicit dynamic analysis in Abaqus is based upon the implementation of an explicit integration rule together with the use of diagonal element mass matrices. Therefore, the accelerations of the *i*th node of the MV structure at the beginning of each increment are computed by:

$$\ddot{\mathbf{u}}_i^{(n)} = \left(\mathbf{M}\right)^{-1}\left(\mathbf{P}_i^{(n)} - \mathbf{I}_i^{(n)}\right), \tag{2.2}$$

where $\mathbf{M}$ is the diagonal mass matrix, $\mathbf{I}_i$ is the internal force vector, and the superscript (n) refers to the increment number. To calculate the internal forces at the *i*th node, the internal forces for all elements attached to that node (see equation 2.9) are simply summed up, therefore, the explicit procedure requires no tangent stiffness matrix and no iterations to update accelerations, velocities and displacements.

The body motion equations are integrated using the explicit central-difference integration rule:

$$\dot{\mathbf{u}}_i^{(n+1/2)} = \dot{\mathbf{u}}_i^{(n-1/2)} + \frac{\Delta t^{(n+1)} + \Delta t^{(n)}}{2}\ddot{\mathbf{u}}_i^{(n)}; \tag{2.3}$$

$$\mathbf{u}_i^{(n+1)} = \mathbf{u}_i^{(n)} + \Delta t^{(n+1)}\dot{\mathbf{u}}_i^{(n+1/2)}, \tag{2.4}$$

where the superscripts $(n - 1/2)$ and $(n + 1/2)$ refer to mid-increment values in the explicit dynamics step. The central-difference integration operator is explicit in the sense that the kinematic state is advanced using known values of $\dot{\mathbf{u}}_i^{(n-1/2)}$ and $\ddot{\mathbf{u}}_i^{(n)}$ from the previous increment.

The central-difference operator, however, is not self-starting because the value of the mid-increment velocity $\dot{\mathbf{u}}_i^{(n-1/2)}$ needs to be defined:

$$\dot{\mathbf{u}}_i^{(n-1/2)} = \dot{\mathbf{u}}_i^{(n)} + \frac{\Delta t^{(n)}}{2} \ddot{\mathbf{u}}_i^{(n)}. \tag{2.5}$$

In this particular case, the initial values (at time $t = 0$) of velocity and acceleration are set to zero, thus giving:

$$\dot{\mathbf{u}}_i^{(n-1/2)} = 0.$$

The explicit procedure integrates through time by using many small time increments Δt. If the time increment is too large, the central-difference operator becomes unstable and diverges rapidly. The solution is stable when the following condition is met:

$$\Delta t \le \frac{2}{\omega_{max}}, \tag{2.6}$$

where ω_{max} is the highest eigenvalue in the system.

Abaqus/Explicit contains a global estimation algorithm, which automatically determines the highest eigenvalue of the entire model.

Once the displacement vector $\mathbf{u}_i$ is calculated, the computation of the internal force at the ith node can be done in such a manner:

$$\boldsymbol{\varepsilon}^{(n)} = \mathbf{B}\mathbf{u}_i^{(n)}; \tag{2.7}$$

$$\boldsymbol{\sigma}^{(n)} = \boldsymbol{\sigma}\left(\boldsymbol{\varepsilon}^{(n)}\right); \tag{2.8}$$

$$\mathbf{I}_i^{(n)} = \int_V \mathbf{B}^T \boldsymbol{\sigma}^{(n)} dV, \tag{2.9}$$

where $\boldsymbol{\varepsilon}$ is the deformation of the element attached to the ith node, $\boldsymbol{\sigma}$ is the stress in the element, $\mathbf{B}$ is the strain-displacement matrix, and V is the volume of the model.

The external force vector at the ith node accounts for all volume loads $\mathbf{P}^V$ and surface loads $\mathbf{P}^S$ and can be expressed as:

$$\mathbf{P}_i^{(n)} = \int_V \mathbf{N}^T \mathbf{P}^V dV + \int_S \mathbf{N}^T \mathbf{P}^S dS, \tag{2.10}$$

where $\mathbf{N}$ is the shape function, and S is the surface area of the model.

After calculating the internal and external forces, computation of acceleration can be done. Besides, since only the mid-increment value of the velocity was previously computed, for the presentation of the results, velocity is stored as a linear interpolation of the mean velocities:

$$\dot{\mathbf{u}}_i^{(n+1)} = \dot{\mathbf{u}}_i^{(n+1/2)} + \frac{1}{2}\Delta t^{(n+1)}\ddot{\mathbf{u}}_i^{(n+1)}. \tag{2.11}$$

The geometry of the MV is then updated by adding the displacement increments to the initial geometry:

$$\mathbf{x}_i^{(n+1)} = \mathbf{x}_i^{(n)} + \dot{\mathbf{u}}_i^{(n+1)}, \tag{2.12}$$

where $\mathbf{x}_i$ is the position vector of the ith node.

To enable the presented workflow, the physical equation (2.8) needs to be implemented within Abaqus through material model description either as a user-defined VUMAT (Vectorized User-defined MATerial) subroutine or by choosing the material model from Abaqus material model library (Dassault Systèmes 2010).

2.3. Material Models for Mitral Valve Structure

2.3.1. Mechanical Behavior of Mitral Valve Leaflets

Structurally, the MV leaflets present a membrane of soft tissue abundant in collagen fibers oriented parallel to the annulus, thus increasing stiffness in this direction. Therefore, the following assumptions are made:

1. Because of the high content of collagen fibers, the mechanical behavior of the leaflets is assumed nonlinear.
2. Since a tissue with collagen fibers demonstrates higher stiffness along the fiber direction, the anisotropic mechanical response is included.
3. As the MV model is described by thin shell elements (see paragraph 2.5), plane stress assumption is made, meaning that all stresses are applied in a single plane while stress in the thickness direction is disregarded from calculations, thus allowing a two-dimensional stress analysis.

The stress-strain behavior of the leaflets is described using hyperelastic strain energy density function, proposed by Lee *et al.* (2013), which considers the effects of material anisotropy at the tissue level, as it enables the investigation of how the material anisotropy at this level affects the mitral valve functional response at the organ level. In the equation (1.4), the strain invariants I_1 and I_4 are defined in accordance with the right Cauchy-Green strain tensor:

$$I_1 = tr(\mathbf{C}); \tag{2.13}$$

$$I_4 = \mathbf{NCN}, \tag{2.14}$$

where $\mathbf{C} = \mathbf{F}^T\mathbf{F}$ is the right Cauchy-Green strain tensor, $\mathbf{N}$ is the unit vector identifying the direction of collagen fibers in the unloaded configuration, $\mathbf{F} = \partial\mathbf{x}/\partial\mathbf{X}$ is the deformation gradient tensor, defined as the derivative of the position in the deformed configuration $\mathbf{x}$ with respect to the position in the original (undeformed) configuration $\mathbf{X}$.

The components of the right Cauchy-Green strain tensor $\mathbf{C}$ can be calculated as:

$$C_{11} = \lambda_{11}^2 + \lambda_{12}^2; \tag{2.15}$$

$$C_{12} = \lambda_{12}\left(\lambda_{11} + \lambda_{22}\right); \tag{2.16}$$

$$C_{22} = \lambda_{22}^2 + \lambda_{12}^2; \tag{2.17}$$

$$C_{33} = \left(\lambda_{11}\lambda_{22} - \lambda_{12}^2\right)^{-2}, \tag{2.18}$$

where λ_{11} is the stretch ratio in the direction parallel to the MV annulus, λ_{12} is the shear stretch ratio, and λ_{22} is the stretch ratio in the direction perpendicular to the MV annulus.

The strain energy density function is implemented in a user-defined VUMAT subroutine within Abaqus, in which the derivatives of strain energy Ψ with respect to the invariants I_1 and I_4 are evaluated:

$$\frac{\partial\Psi}{\partial I_1} = c_0 + 2c_1c_2\left(1-\beta\right)\left(I_1 - 3\right)e^{\left[c_2\left(I_1-3\right)^2\right]}; \tag{2.19}$$

$$\frac{\partial\Psi}{\partial I_4} = 2c_1c_3\beta\left(I_4 - 1\right)e^{\left[c_3\left(I_4-1\right)^2\right]}, \tag{2.20}$$

and the components of the Cauchy stress tensor $\boldsymbol{\sigma}$ are returned as an output:

$$\sigma_{11} = 2\left(\frac{\partial\Psi}{\partial I_1}C_{11} + \frac{\partial\Psi}{\partial I_4}\lambda_{11}^2\right) - 2\frac{\partial\Psi}{\partial I_1}C_{33}; \tag{2.21}$$

$$\sigma_{12} = 2\frac{\partial\Psi}{\partial I_1}C_{12}; \tag{2.22}$$

$$\sigma_{22} = 2\frac{\partial\Psi}{\partial I_1}C_{22} - 2\frac{\partial\Psi}{\partial I_1}C_{33}. \tag{2.23}$$

As the plane stress assumption is implied, the Cauchy stress tensor component σ_{33} is equal to zero.

2.3.2. Mechanical Behavior of Chordae Tendineae

The following assumptions are made while modeling the branched network of the chordae tendineae:

1. Because the chordae tendineae are mainly composed of collagen fibers, their mechanical behavior is assumed nonlinear.
2. Since the chordae are modeled as truss elements (see paragraph 2.5), the isotropic mechanical response is considered.
3. The chordae undergo only uniaxial tension, meaning that the normal tensile stress σ_{11} is the only nonzero component of the Cauchy stress tensor.
4. The incompressible behavior of the chordae tendineae is assumed since no volumetric data is defined.

For the mechanical behavior of the chordae tendineae, as described in 1.2.4 paragraph, 2nd order polynomial hyperelastic model ($N = 2$) is chosen, since the chordae undergo only small or moderately large strains (<100%) during the cardiac cycle. The basic strain energy density form of the polynomial model was presented in equation (1.5). Since no volumetric behavior of the chordae tendineae is defined, the second half of the equation can be disregarded, and the function for the chordae that depends on two invariants of strain I_1 and I_2 can be written as:

$$\Psi = c_{10}(I_1 - 3) + c_{01}(I_2 - 3) + c_{11}(I_1 - 3)(I_2 - 3) + c_{20}(I_1 - 3)^2 + c_{02}(I_2 - 3)^2. \tag{2.24}$$

For the uniaxial tension, the principal stretch is:

$$\lambda = \lambda_1 = \frac{1}{\lambda_2^2} = \frac{1}{\lambda_3^2}, \tag{2.25}$$

and the invariants of the right Cauchy-Green strain tensor become:

$$I_1 = \lambda^2 + 2\lambda^{-1}; \tag{2.26}$$

$$I_2 = \lambda^{-2} + 2\lambda. \tag{2.27}$$

From the principle of virtual work, it follows that:

$$\delta\Psi = \sigma\delta\lambda, \tag{2.28}$$

and the stress can be represented as:

$$\sigma = \frac{\partial \Psi}{\partial \lambda} = \frac{\partial \Psi}{\partial I_1}\frac{\partial I_1}{\partial \lambda} + \frac{\partial \Psi}{\partial I_2}\frac{\partial I_2}{\partial \lambda} = 2\left(1-\lambda^{-3}\right)\left(\lambda\frac{\partial \Psi}{\partial I_1} + \frac{\partial \Psi}{\partial I_2}\right) = 2\left(1-\lambda^{-3}\right)\begin{bmatrix} c_{10}\lambda + c_{01} + c_{11}\left(I_1 - 3 + \lambda\left(I_2 - 3\right)\right) \\ +2c_{20}\lambda\left(I_1 - 3\right) + 2c_{02}\left(I_2 - 3\right) \end{bmatrix}. \tag{2.29}$$

2.4. Patient-Specific Mitral Valve Geometry

2.4.1. Echocardiographic Data Acquisition

To create the patient-specific MV model, image data of the whole LV throughout the cardiac cycle is obtained using TEE, during which the ultrasound transducer is placed into the esophagus of the subject. TEE over TTE is chosen because of the better image quality and the relevant viewing field since the whole LV needs to be seen in the echocardiographic images in order to capture the movement of the MV, PMs and LV apex. The acquired data is stored as a volumetric medical image (VolDICOM) and exported for further processing.

2.4.2. Echocardiographic Image Segmentation

The segmentation of the echocardiographic images is performed using the custom platform developed in MATLAB (MathWorks, Inc.) by Biomechanics Research Group of Politecnico di Milano (Conti *et al.* 2010). The acquired image data is imported into this dedicated software, which allows to navigate and visualize volumetric images plane-by-plane and frame-by-frame.

The reference system is positioned within the imported image data such that the z-axis would go through the LV apex and the MV centroid, while x- and y-axes would be perpendicular to the MV annular plane, thus creating two long-axis planes and one short-axis plane, which is oriented parallel to the annular plane. The 3D data is cropped into 18 radial planes, distributed uniformly around the z-axis by rotating long-axis plane by every 10°.

On each radial plane, the following points of the MV surface are manually identified (Fig. 2.4):

- two points indicating the position of the mitral annulus;
- two points on the free margin of each leaflet;
- multiple points to describe the profile of the MV leaflets.

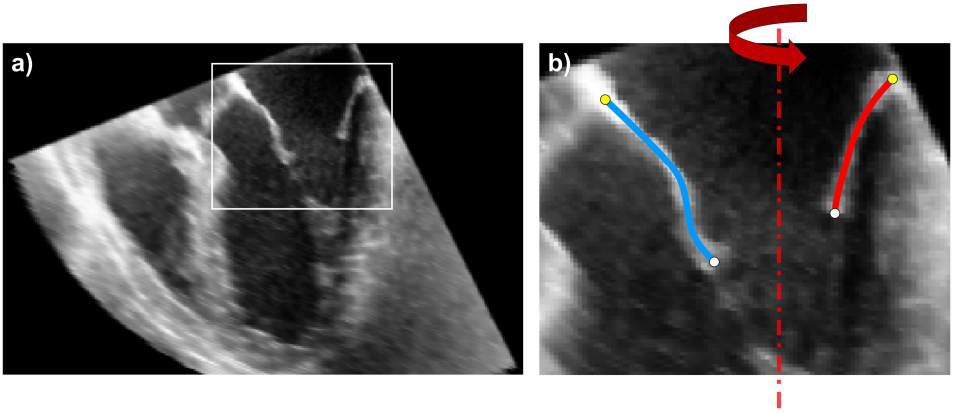

Fig. 2.4. Segmentation of the mitral valve structure from echocardiographic images: a) extraction of the region of interest; b) manual tracing of anterior (blue line) and posterior (red line) leaflets, mitral annulus (yellow dots) and free margin (white dots)

Moreover, to complete the valvular system, the positions of the PMs are also estimated. Image segmentation is performed on the end-diastole frame of the echocardiographic image data, chosen as the last frame before the MV starts to close, with a hypothesis that at this point in time the MV is approximately unloaded, as suggested by other authors (Kunzelman *et al.* 1993, Votta *et al.* 2009). The collected data is subsequently processed to reconstruct the 3D geometry of the MV (see paragraph 2.4.3).

In addition, the LV apex position is manually defined. The apex is located at the bottom of the LV, inferior to the MV, and is an entry site into the heart for transapical MV repair. During surgery, LV apex is used as the anchoring region for the implanted neochordae, therefore, obtaining its position is necessary for performing virtual transapical MV repair.

For the following image data frames, up to peak systole, the positions of the annulus, PMs and LV apex are identified on each radial plane. This data is further processed to reconstruct the field of time-varying displacements to be imposed on the annulus and the PMs in the form of kinematic boundary conditions (see paragraph 2.7).

2.4.3. Patient-Specific Geometry Reconstruction

The reconstruction of the MV geometry is started with the definition of the mitral annulus. The coordinates of the points on the annulus, identified during image segmentation on radial planes, are transformed into three-dimensional Cartesian

space, with the origin in the centroid of the MV annulus, and the z-axis normal to the least-square plane of the annular points. In this frame of reference, a local cylindrical coordinate system is set. The coordinates of the annulus points are then transformed from Cartesian to cylindrical. To avoid artifacts due to manual tracing, Fourier approximation is used. The continuous profile of the annulus is obtained approximating radial (ρ) and axial (z) positions of every annular point through 4th order Fourier functions of the angular position (φ):

$$\rho(\varphi) = a_0 + \sum_{k=1}^{4}\left[a_k \cos(k\varphi) + b_k \sin(k\varphi)\right]; \tag{2.30}$$

$$z(\varphi) = c_0 + \sum_{k=1}^{4}\left[c_k \cos(k\varphi) + d_k \sin(k\varphi)\right], \tag{2.31}$$

where a_0, a_k, b_k, c_0, c_k, d_k are the coefficients of the resulting Fourier function. These coefficients are calculated in MATLAB by fitting the coordinates of the annulus points using a built-in *fit* function with (2.30) and (2.31) assigned as custom *fitType* equations.

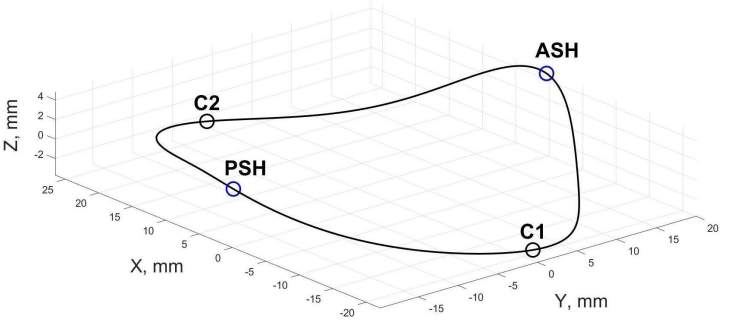

Fig. 2.5. Positions of saddle horns (ASH, PSH) and commissures (C1, C2) on the reconstructed annular profile

On the continuous annular profile, four notable points are identified (Fig. 2.5):

- anterior saddle horn (ASH), defined as an absolute maximum point of the annular profile;
- posterior saddle horn (PSH), situated in the opposite side and determined as the point that divides the posterior annular section into two portions of equal length;

- two commissures (C1 and C2) facing each other and identified as the minimum points of the annular profile.

Fourier approximation is also used to create a continuous profile of the free margin in the same cylindrical reference system.

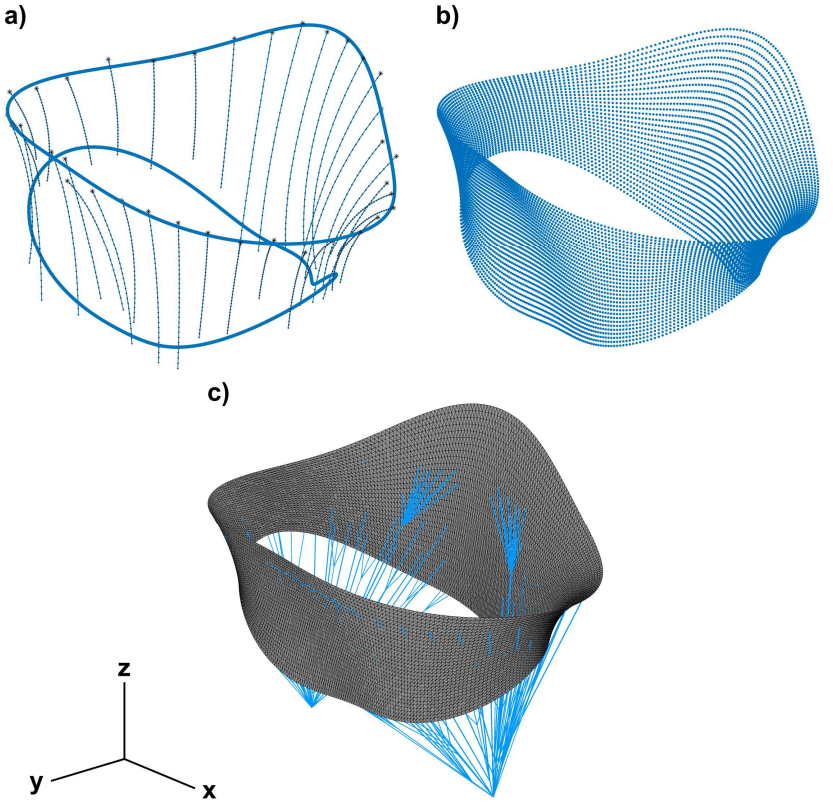

Fig. 2.6. Reconstruction of mitral valve geometry: a) profile of the leaflets defined by manually traced points interpolated with cubic splines; b) point cloud created after Fourier approximation; c) complete model of the mitral valve and the chordae tendineae after mesh generation

Regarding the leaflets, each set of points selected to define leaflets profile in 18 radial planes are approximated with a cubic spline (Fig. 2.6 a). In this way, $2 \times 18 = 36$ splines are obtained with the points of the annulus and the free margin set as extremes. Each spline is resampled to 32 points, uniformly distributed along the length of the leaflet in the direction annulus-free margin, thus gaining a 3D

point cloud of $2 \times 18 \times 32 = 1152$ points that can be organized in 32 parallels, each with 36 points.

For each parallel, the coordinates of 36 points are approximated with Fourier function, as done for the annular points, to filter the noise due to manual tracing. The approximating Fourier functions are then upsampled to 200 points, and a 3D point cloud of $32 \times 200 = 6400$ points is generated, consisting of 32 parallels running from the annulus to the free margin, each with 200 points, uniformly distributed along the circumference of the MV (Fig. 2.6 b).

To evaluate the reconstructed geometry of the MV, the following geometrical parameters of the mitral annulus are measured (Fig. 2.7) and compared with the data from the literature:

- commissural diameter (Al-Pm), measured between anterolateral and posteromedial commissures C1 and C2;
- anteroposterior diameter (A-P), as a distance between anterior (ASH) and posterior (PSH) saddle horns;
- annular height (AH), identified as a vertical distance between the lowest and the highest points on the annulus;
- mitral annular 3D circumference (C3D), i.e. a perimeter of the mitral annulus;
- mitral annular 2D area (A2D), which is defined as the area of the annulus in the projection plane.

In addition, for a more complete evaluation of the reconstructed geometry, the surface area and the midline length of the MV leaflets are measured and compared with the values found in the literature.

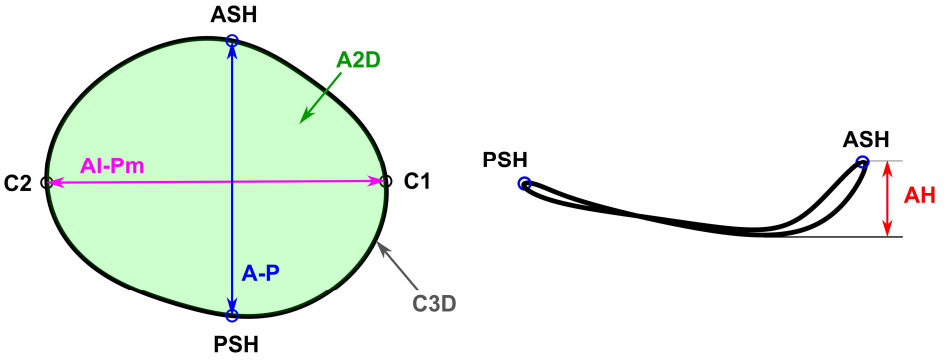

Fig. 2.7. Geometrical parameters of the mitral annulus shown on the top and side views of the annular profile: commissural diameter Al-Pm, anteroposterior diameter A-P, annular height AH, perimeter of the annulus C3D and annular area A2D

The reconstruction of the geometry is completed by adding the positions of the PMs and the chordal attachment points on the leaflets. The positions of the PMs are defined as two single nodes, neglecting the presence of multiple heads in the same PM. Since the chordae tendineae are barely seen in the echocardiographic images, their insertion sites on the leaflets are determined in accordance with ex vivo findings (Lam *et al.* 1970, Degandt *et al.* 2007) and indications by clinicians (Stevanella *et al.* 2011).

Finally, the coordinates of all identified points are transformed back into a Cartesian reference system with the origin and the z-axis coinciding with those of the cylindrical reference system.

2.5. Finite Element Mesh of Mitral Valve Model

The MV leaflets are modeled as a thin membrane described by shell elements. 3D point cloud, generated during geometry reconstruction, is connected into a mesh of S3R shell elements in Abaqus (Fig. 2.6 c).

The structural element S3R in Abaqus (Fig. 2.8) is a 3-node general-purpose conventional shell element, which can be used for the stress-strain analysis of both thick and thin shells. A thin shell has a thickness, which is small compared to its other dimensions, and deformations in such shell are not large compared to thickness. Thick shells are needed where transverse shear flexibility is important. This occurs when the shell thickness is more than 1/15 of a characteristic length on the mid-surface of the shell (Dassault Systèmes 2010). In the present study, the MV is assumed to be described by thin shell elements, as the length of the leaflets significantly exceeds the shell thickness.

S3R shell element has six degrees of freedom at each node: translations in x-, y- and z-directions (u_x, u_y, u_z) and rotations about x-, y- and z-axes (θ_x, θ_y, θ_z). Therefore, the displacement vector for shell element at each node i can be written as:

$$\mathbf{u}_i = \left\{ u_{xi}, u_{yi}, u_{zi}, \theta_{xi}, \theta_{yi}, \theta_{zi} \right\}. \tag{2.32}$$

For the prediction of the element behavior, reduced numerical integration is used, meaning that there is only a single integration point located at the centroid of the element. Hence, S3R elements use lower order integration to form the element stiffness matrix. This allows to significantly reduce the computational time, while providing accurate computational results, as the mass matrix and distributed loads are still fully integrated (Laulusa *et al.* 2006).

General-purpose conventional shell elements allow to evaluate transverse shear deformation. While the shell thickness increases, Mindlin-Reissner shell

theory is used that takes into account shear deformations through the thickness of the shell (Liu and Quek 2014). As the thickness decreases, S3R elements are discretized by Kirchhoff-Love thin shell theory, and the transverse shear deformation becomes small enough to be neglected (Kiendl *et al.* 2015).

Conventional shell elements account for finite membrane strains and arbitrary large rotations, therefore, they are suitable for geometrically nonlinear finite-strain analysis. For elastic materials, the Poisson's ratio as a part of the shell section definition needs to be specified, allowing the shell thickness change to be described as a function of strain. However, for hyperelastic materials, the thickness change should be based on the element material definition (Dassault Systèmes 2010).

Regionally varying thickness is assigned to the leaflets, as suggested by Kunzelman *et al.* (2007), with an average value of 1.32 mm for the anterior and 1.26 mm for the posterior leaflet. Density for the MV leaflets was assumed to be 10.4 g/cm³, which is ten times higher than the real density (Xu *et al.* 2010), thus taking into account the inertial effects of the blood volume spanned and moved by the MV during its closure. Such volume is about ten times larger than the volume of the MV leaflets (Reimink *et al.* 1995, Sturla *et al.* 2014).

To complete the MV model, a branched network of marginal, basal and strut chordae is created, connecting the PM tips with the earlier identified attachment points on the leaflets (Fig. 2.6 c). The marginal chordae are inserted into the free margin, the basal are attached to the ventricular surface of the leaflets closer to the annulus, while two of the strut chordae are connected to the AL and two to the PL.

The chordae tendineae are modeled as structural T3D2 truss elements in Abaqus (Fig. 2.8) and assigned constant cross-sectional area values of 0.40, 0.79 and 1.15 mm² for marginal, basal and strut chordae, respectively (Votta *et al.* 2008b). Generally, truss elements are used to characterize long, slender structural elements that are connected at their ends, thus all external actions and support reactions consist of forces applied at the truss nodes. Such elements use linear interpolation for position and displacement, and have a constant stress value (Ranzi and Gilbert 2014).

T3D2 element in Abaqus is a three-dimensional 2-node truss element that can transmit only axial force because it has no initial stiffness to resist loading acting perpendicular to its axis. The nodes in a truss element are assumed pinned, meaning that they possess no rotational rigidity and cannot transmit moments, therefore, T3D2 element has only three translational degrees of freedom at each node (u_x, u_y, u_z) and the displacement vector at node i can be written as:

$$\mathbf{u}_i = \left\{ u_{xi}, u_{yi}, u_{zi} \right\}. \tag{2.33}$$

By default, T3D2 element is linear, however, nonlinearity can be assigned by making truss stiffness to be ignored if a tension-only element is subjected to compressive forces or if a compression-only element is subjected to tensile forces (Dassault Systèmes 2010). Since in the present study only the closure of the MV is considered, the chordae are discretized with tension-only truss elements, thus making their resistance to axial compressive loads negligible.

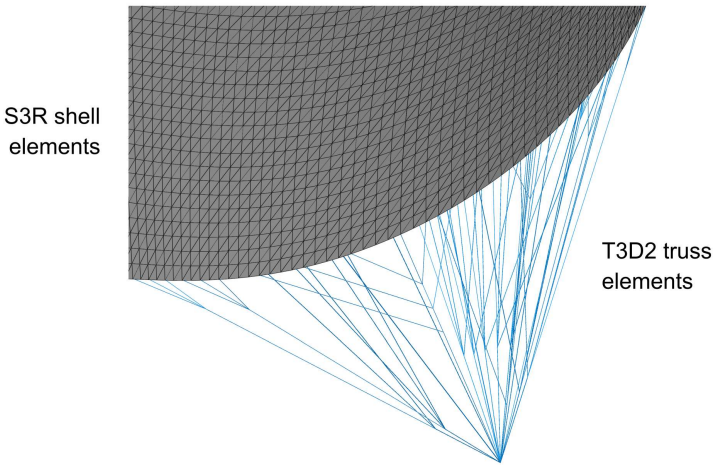

Fig. 2.8. A closer look to the mesh created in Abaqus showing S3R and T3D2 elements

Density for the chordae tendineae is assumed the same as for the MV leaflets and equal to 10.4 g/cm³.

2.6. Mechanical Properties of Mitral Valve Leaflets and Chordae Tendineae

The mechanical properties of the MV leaflets and chordae tendineae are implemented using previously described material models (see paragraph 2.3). For the leaflets, the constitutive parameters of the hyperelastic strain energy density function are identified according to the experimental data by May-Newman and Yin (1998) of biaxial tensile test on the porcine MV leaflets (Fig. 2.9). Since the only available tensile test data of human MV was obtained using aged and calcified specimens with altered mechanical properties (Pham and Sun 2014), healthy porcine data was chosen in the present study, as it can be held the most physiologically and clinically relevant to the human heart.

Table 2.1. Material parameters of the mitral valve leaflets tissue

Mitral valve leaflet	c_0, MPa	c_1, MPa	c_2	c_3	β
Anterior leaflet	$0.826 \cdot 10^{-3}$	$0.048 \cdot 10^{-3}$	25.5	32.5	0.195
Posterior leaflet	$0.248 \cdot 10^{-3}$	$0.145 \cdot 10^{-3}$	10.15	17.973	0.044

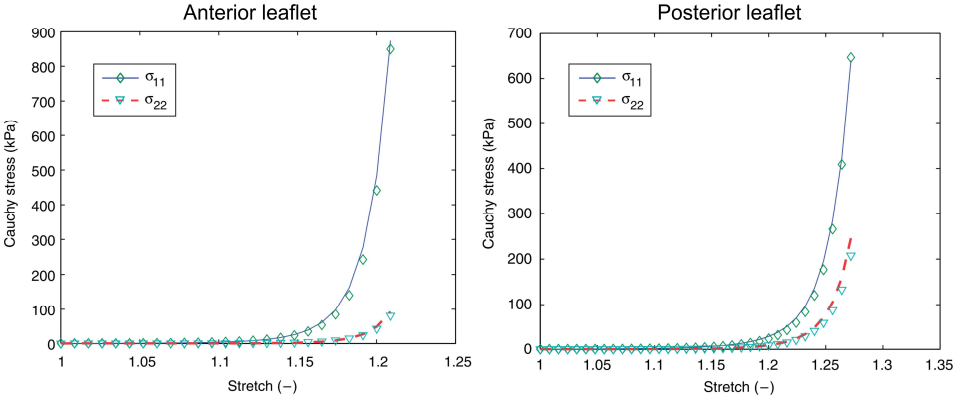

Fig. 2.9. Mechanical response of the mitral valve leaflets in the direction parallel (σ_{11}) and perpendicular (σ_{22}) to the annulus (May-Newman and Yin 1998)

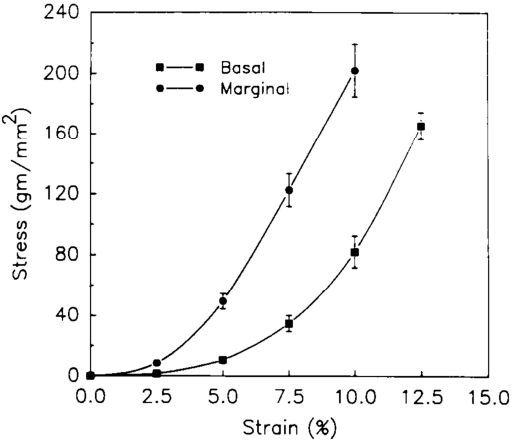

Fig. 2.10. Stress-strain behavior of marginal and basal chordae (Kunzelman and Cochran 1990)

Stress-stretch curve fitting to the reported experimental data using a nonlinear least square method is performed in MATLAB, and the parameters of the strain energy density function are calculated. The values of these parameters are presented in Table 2.1.

Mechanical properties of the chordae tendineae are implemented into the model by choosing 2nd order polynomial strain energy density function from Abaqus material model library. The constitutive material parameters c_{ij} for the chordae tendineae are automatically computed by Abaqus by fitting uniaxial test data on porcine chordae (Fig. 2.10) reported by Kunzelman and Cochran (1990).

PM tips and LV apex are treated as single nodes without any physical or mechanical properties.

2.7. Initial and Boundary Conditions for Transapical Mitral Valve Repair Simulation

The structural model of MV decoupled from the blood flow is prepared for the nonlinear dynamic FE analysis. The following initial conditions are applied:

1. End-diastole is chosen as the initial state, identified as the last frame of echocardiographic image data before the MV starts to close. No initial structural displacements or velocities are considered, assuming the MV to be at rest:

$$\mathbf{u}\left(\mathbf{x}_i, 0\right) = 0; \tag{2.34}$$

$$\dot{\mathbf{u}}\left(\mathbf{x}_i, 0\right) = 0, \tag{2.35}$$

where $\mathbf{u}$ is the displacement vector, $\dot{\mathbf{u}}$ is the velocity vector, and $\mathbf{x}_i$ is the position vector of the ith node of the MV annulus, the PMs and the LV apex, which define the initial unloaded configuration of the MV model to be the one identified during image segmentation and geometry reconstruction.

2. During end-diastole, the MV can be assumed as approximately unloaded, since at this point in time the transvalvular pressure p acting on the leaflets can be considered equal to zero:

$$p\left(\mathbf{x}_j, 0\right) = 0, \tag{2.36}$$

where $\mathbf{x}_j$ is the position vector of the jth node on the ventricular surface of the MV leaflets.

3. Since the MV at the initial state is assumed to be at rest, no prestress is applied to the model.

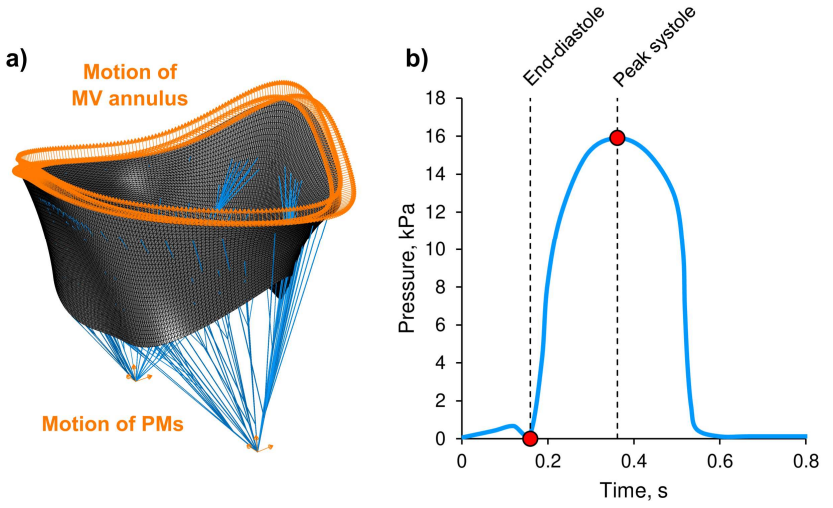

Fig. 2.11. Boundary conditions applied to the finite element model: a) arrows highlight the nodes on the mitral valve annulus and the papillary muscles with applied nodal displacements according to patient-specific motion data; b) time-dependent physiologic transvalvular pressure between end-diastole and peak systole applied on the ventricular surface of the leaflets is highlighted on the transvalvular pressure curve of the whole cardiac cycle at the heart rate of 74 bpm

Both MV models, created at the end-diastole image frame, are associated with the following boundary conditions:

1. Patient-specific kinematic boundary conditions expressed in terms of time-varying nodal displacements are applied (Fig. 2.11 a). The motion of the MV annulus and the PMs are traced during image segmentation procedure up to the peak systole frame of TEE image data. At peak systole, ventricular volume decreases to the lowest level, and ventricular pressure reaches its maximum while the MV remains closed. The annular contraction and the movement of the PMs are modeled by applying nodal displacements to the points of the annulus and the PM tips. Moreover, the patient-specific displacement is also applied to the LV apex node. The displacement of the *i*th node of the MV structure can be expressed as:

$$\mathbf{u}_i = \mathbf{u}\left(\mathbf{x}_i, t\right), \tag{2.37}$$

where the position vector of the corresponding point $\mathbf{x}_i$ at a given time is calculated in terms of velocity:

$$\mathbf{x}_i\left(t+\Delta t\right)=\mathbf{x}_i\left(t\right)+\dot{\mathbf{u}}_{\mathbf{x}_i}\left(t\right)\Delta t, \tag{2.38}$$

and the velocity vector is acquired by differentiating the displacement data:

$$\dot{\mathbf{u}}_{\mathbf{x}_i}=\frac{\mathrm{d}\mathbf{x}_i}{\mathrm{d}t}. \tag{2.39}$$

2. Decoupled behavior of blood is specified by applying time-dependent physiologic transvalvular pressure ranging between 0 and 16 kPa on every node of the ventricular surface of the leaflets (Fig. 2.11 b):

$$p_j=p\left(\mathbf{x}_j,t\right). \tag{2.40}$$

3. To capture the contact of the leaflets, a general contact algorithm available in Abaqus with a scale penalty method and a friction coefficient of 0.05 is set between the atrial sides of the leaflets.

2.8. Virtual Transapical Mitral Valve Repair and Simulation Setup

MV model with implemented material properties and boundary conditions is prepared for virtual transapical MV repair. The chordae tendineae inserted into the prolapsing segment of the leaflet are removed and model with MV prolapse is created.

Virtual transapical MV repair is performed by inserting one side of the neochordae into the free margin of the leaflet and anchoring the other side to the LV apex. In general, implantation of more than two neochordae is desired to balance a load per suture and to provide structural support as needed. Early clinical results show that three to six ePTFE CV-4 type sutures with a diameter of 0.307 mm are usually implanted (Colli *et al.* 2018), however, it all depends on the level of MV prolapse and the severity of MR.

The neochordae are modeled as truss elements (type T3D2 in Abaqus) and assigned constant cross-sectional area value of 0.074 mm², which corresponds to the cross-sectional area of ePTFE CV-4 type suture, typically used for transapical MV repair. Density for the neochordae is assumed to be ten times higher than the real density and equal 22.0 g/cm³, thus taking into account the inertial effects of the blood. Mechanical properties of the sutures are described as nonlinear and

isotropic using 2nd order polynomial hyperelastic model. The constitutive material parameters c_{ij} are computed from uniaxial test data reported by Dang *et al.* (1990).

Virtual transapical MV repair procedure is evaluated during dynamic FE simulation. The systolic function simulations of two FE models, representing MV before and after virtual repair, are used. For both models, input files for the dynamic analysis in Abaqus/Explicit are prepared, and simulations of the MV function in the time frame between end-diastole and peak systole are run.

2.9. Conclusions of Chapter 2

1. As transapical MV repair surgical technique relies solely on the echocardiographic determination of proper neochordal length, the main challenge related to this approach is the correct length adjustment of the implanted neochordae. The implantation of either too long or too short neochordae can result in inadequate post-repair MV function and increase the risk of residual prolapse or tearing of the repaired leaflet.
2. The modeling strategy applied for virtual transapical MV repair was introduced. This strategy allows to create patient-specific computational models of prolapsing MV based on echocardiographic image data and to perform virtual transapical MV repair followed by dynamic FE simulation.
3. Explicit dynamic analysis using central-difference integration rule was chosen to simulate the systolic function of pre- and post-operative MV. Such analysis allows to solve nonlinear systems with complex contacts and calculate stress, strains and internal forces, as well as update accelerations, velocities and displacements without creating the tangent stiffness matrix or iterating.

3

Modeling of Transapical Mitral Valve Repair

In the present chapter, the simulations of transapical MV repair are performed using two sets of patient-specific data: the healthy one, used to test the procedure and to investigate the effect of neochordal length on post-repair MV function, and the pathological one, used to evaluate the suggested method of neochordal length determination and to compare the systolic function simulation results with the real-life surgical procedure outcomes. The parameters calculated during MV systolic function simulations before and after virtual repair for both MV models are presented and evaluated, comparing them with computational results and critical values found in the literature, as well as with post-operative echocardiographic images.

Parts of this chapter are published in Gaidulis *et al.* (2018a; 2018b; 2019) and Romashov *et al.* (2016).

3.1. Patient-Specific Mitral Valve Models

In the present study, two patients were considered: the first one without any MV pathology, whereas the second one affected by PL prolapse with MR due to the rupture of the chordae tendineae.

The image data of the healthy MV movement at the heart rate of 66 bpm was obtained during TEE at Leiden University Medical Center (The Netherlands) using GE Vivid E95 ultrasound machine. The full cardiac cycle consisted of 20 image frames with a resolution of 0.69 mm/px.

The data of the pathological MV (Fig. 3.1) was acquired during transapical MV repair surgery performed using NeoChord DS1000 device at Vilnius University Hospital Santaros Klinikos (Lithuania). The patient was diagnosed with MV prolapse of the P2L segment and moderate to severe MR (grade 3) due to the rupture of marginal chordae of the PL. During the surgery, a total of three neochordae were implanted into the PL and secured to the LV apex: two neochordae were inserted into the P2L segment and one into the P2M segment for better support. ePTFE CV-4 type sutures with a diameter of 0.307 mm were used to form the neochordae.

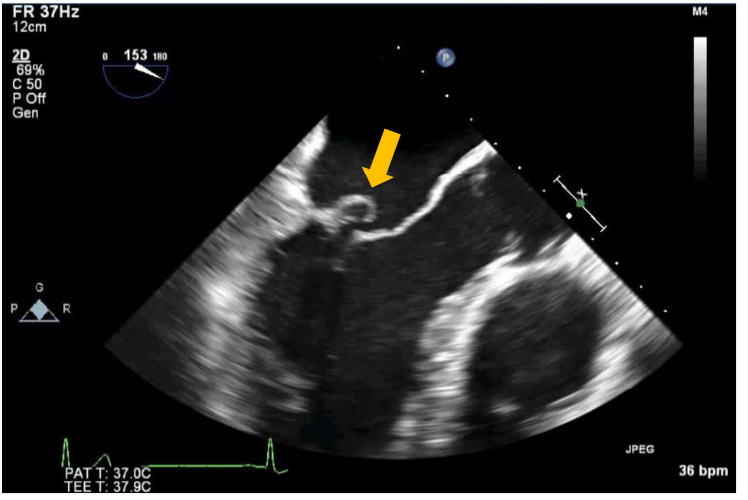

Fig. 3.1. Echocardiographic image of pathological mitral valve during peak systole. The arrow indicates the prolapsing segment of the posterior leaflet

Unfortunately, soon after the implantation, criss-crossing between the neochordae and the native chordae of the AL was noticed, and in a few minutes rupture of native chordae occurred causing prolapse of the A2L segment. For this reason, three more neochordae were implanted into the AL. The implantation of the neochordae has ensured decent support for both PL and AL, as well as reduced MR to mild (grade 1).

During the surgery, two image data sets were obtained using Philips EPIQ 7C ultrasound machine:

- Pre-operative image data at the heart rate of 52 bpm, showing the movement of the prolapsing MV before the neochordae implantation. A total of 17 image frames with a resolution of 0.63 mm/px for a full cardiac cycle were acquired.
- Post-operative image data at the heart rate of 74 bpm, obtained after the implantation of the neochordae into both PL and AL. The full cardiac cycle consisted of 19 images with a resolution of 0.68 mm/px.

The acquired data sets were stored as volumetric medical images for further processing. For the MV modeling, only the data of healthy and pre-operative valves were selected, and post-operative echocardiographic images were put aside for the later evaluation of morphological compliance between the virtually repaired MV and the real-life surgical procedure outcomes.

For each acquired data set, image segmentation was performed, tracing the positions of the MV leaflets, PMs and LV apex in the time frame between end-diastole and peak systole, as described in paragraph 2.4.2. Geometry reconstruction was then carried out, describing the profile of the MV leaflets with a 3D point cloud, generated after approximating the coordinates of the leaflet points with Fourier functions. The MV geometry was completed after including the positions of the PMs and the chordal attachment points on the leaflets.

The MV annular dimensions, described in paragraph 2.4.3, were measured after geometry reconstruction in healthy and pathological MV models at end-diastole. The estimated values in both MV models are presented in Table 3.1.

Table 3.1. Geometrical parameters of mitral annulus at end-diastole

Mitral valve model	Al-Pm, mm	A-P, mm	AH, mm	C3D, mm	A2D, mm²
Healthy	37.1	33.1	6.4	114.8	978.1
Pathological	43.6	41.7	7.2	134.4	1354.0

Al-Pm, commissural diameter; A-P, anteroposterior diameter; AH, annular height; C3D, three-dimensional circumference of mitral annulus; A2D, mitral annular two-dimensional area.

For the healthy case, the annular dimensions had a good agreement with the data defining healthy MV geometrical parameters, which was found in the literature (Sonne *et al.* 2009; Mihăilă *et al.* 2014). Regarding the pathological MV model, the mitral annulus enlargement was noticed, which can be related to the enlargement of the whole LV, typical to MR (Nishimura *et al.* 2016).

Moreover, the surface area and the midline length of the leaflets were measured in both models. The obtained data is presented in Table 3.2.

Table 3.2. Geometrical parameters of mitral valve leaflets

Mitral valve model	Length, mm	Surface area, mm²
Healthy		
Anterior leaflet	24.2	784.9
Posterior leaflet	14.6	407.3
Pathological		
Anterior leaflet	25.7	903.1
Posterior leaflet	17.9	502.5

Again, the measurements in the healthy MV model showed a good agreement with the data from the literature (Mihăilă *et al.* 2014; Munín *et al.* 2014), while in the pathological model a slight elongation of the PL was observed, which can be associated with the presence of MR (Saito *et al.* 2012).

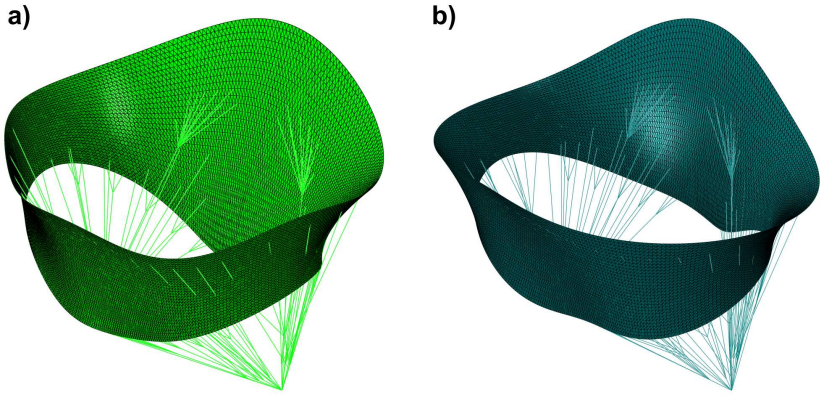

Fig. 3.2. Computational models created using patient-specific echocardiographic image data: a) healthy mitral valve model; b) pathological model

Healthy and pathological computational MV models were created (Fig. 3.2), connecting generated point clouds into meshes of finite elements. Since the same reconstruction approach for both valves was used, a total of 18 900 shell elements describing MV leaflets were generated for each model. However, as the amount of the chordae depends on the geometrical parameters of the MV model, a different number of chordae were created for healthy and pathological valves (Table 3.3).

Because of the different amount of the chordae and their branches, a total of 226 elements for healthy and 247 elements for pathological MV were created, as in the latter case the prolapsing valve is a bit larger in size.

Table 3.3. Number of chordae tendineae in healthy and pathological mitral valve models

Mitral valve model	Marginal chordae	Basal chordae	Strut chordae	**Total**
Healthy	22	53	4	**79**
Pathological	24	55	4	**83**

Mechanical behavior of the MV leaflets and chordae tendineae was characterized using material models, described in paragraph 2.3. Initial and patient-specific boundary conditions were applied for both models, depicting the motion of the MV up to the peak systole frame of TEE image data.

Because of the different heart rate in the echocardiographic image data sets, the time interval between end-diastole and peak systole in the healthy model was larger (t_H = 0.25 s) than in the pathological model (t_P = 0.20 s). However, for the simplification of the analysis time incrementation and processing of the results, these time frames were scaled to t = 1 s each.

3.2. Computational Analysis of Prolapsing Mitral Valve Model

3.2.1. Virtual Repair with Different Neochordal Length

The prolapsing MV model was prepared using echocardiographic images of the healthy subject to investigate the outcomes of the virtual repair approach and to determine the effect of the neochordal length on the function of the prolapsing MV. Since the most common segment involved in MV prolapse is the middle segment (P2) of the PL (Suzuki *et al.* 2012), the chordae tendineae inserted into the P2 segment of the healthy MV model were ruptured and computational model with MV prolapse (referred to as MVP model) was prepared for the simulation of the systolic function.

In general, three to six ePTFE CV-4 type sutures are usually implanted during transapical MV repair, and the implantation of four neochordae is the most common case (Colli *et al.* 2018). Therefore, virtual transapical repair using four neochordae, evenly distributed along the free margin of the P2 segment, was planned, connecting the prolapsing segment of the leaflet and the LV apex. In order to evaluate the effect of the neochordal length on post-repair MV function, a total of four virtual repair procedures using sutures of different length were performed.

The neochordal length used for every virtual repair procedure was determined in the following manner. In the first case, this length was set to be equal to the distance between the LV apex and the neochordal insertion points during

diastole, creating the model named VR0. In the next three cases, the sutures were elongated by 5%, 10% and 15% of their own length, thus creating VR5, VR10 and VR15 models. The 5% elongation step was chosen, which falls into the range of 2.5–3.5 mm for the average neochordal length of 50–70 mm, and could be manageable in the real-life surgery procedure. All neochordae were modeled with truss elements, as described in 2.8 paragraph. The mean length values of the implanted neochordae in every model were equal 55.7±1.0, 58.4±1.2, 61.0±1.2 and 63.6±1.2 mm, respectively.

To model the relaxation and bending of these elongated neochordae, which occurs during diastole due to the opening of the MV, each suture was composed of two equal size elements, with their junction point moved along the y-axis in such way that the calculated total neochordal length would be ensured (Fig. 3.3).

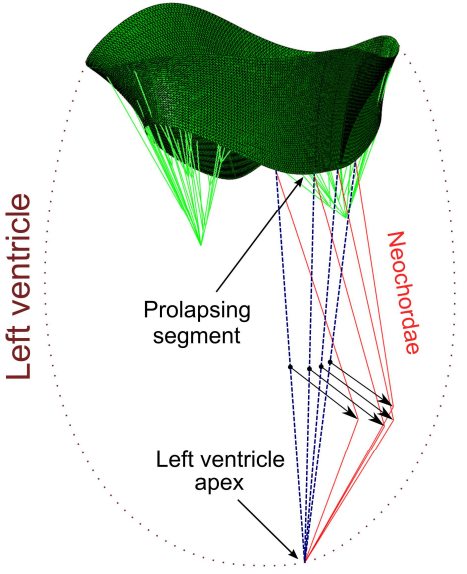

Fig. 3.3. Virtual transapical repair of prolapsing mitral valve model using four neochordae during end-diastole

The effect of the neochordal length on post-repair MV function was evaluated during dynamic FE simulations. The systolic function simulations of the prolapsing model and four models representing MV after virtual repair were used. For all models, input files for the dynamic analysis in Abaqus/Explicit were prepared.

The created input files were imported into Abaqus/Explicit, and simulations of the MV function in the time frame between end-diastole and peak systole were

run. The largest time increment Δt for the integration procedure to remain stable was calculated to be $1.8 \cdot 10^{-6}$ s. However, this estimated Δt is only approximate, and in most cases actual stable time increment should be less than this (Dassault Systèmes 2010). For this reason, automatic time incrementation with the maximum allowed time increment of $0.5 \cdot 10^{-6}$ s was specified for all simulations.

3.2.2. Computational Results of Prolapsing Model

Firstly, the systolic function of the prolapsing MV model with the ruptured chordae tendineae was simulated. At peak systole, the model demonstrated MV prolapse with a flail of the PL middle segment (P2). The region of prolapse is highlighted in Fig. 3.4, which is characterized by a rise of the leaflet towards the LA. This results in a reduction of the coaptation area of the leaflets, defined as the area of each MV leaflet in contact with the opposite leaflet, and a loss of the coaptation length, which can be described as the length of the leaflets apposition measured on the midline of the prolapsing region. While only the P2 segment was prolapsing, the loss of coaptation was extended to the other segments of the PL as well, resulting in the appearance of a noticeable gap between the leaflets, which in real-life would lead to MR.

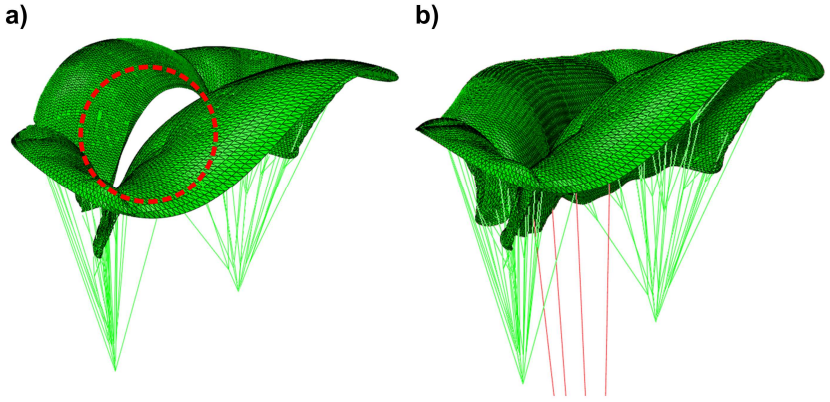

Fig. 3.4. Prolapsing mitral valve model at peak systole: a) model before virtual transapical mitral valve repair with region of prolapse circled; b) model after virtual repair with four neochordae implanted

Following virtual transapical MV repair with the implantation of four neochordae, post-repair MV functions were compared with the functions of the MV prior to virtual repair and evaluated in terms of several aspects:

1. Maximum displacement along the z-axis of the MV free margin ($u_{z,max}$).

2. Coaptation area (CoA) and coaptation length (CoL) of the leaflets.
3. Reaction forces on the PMs (F_{PM}) and LV apex (F_{LVA}).
4. Tension forces in native chordae (F_{CT}) and neochordae (F_{NC}).
5. Peak value of the maximum principal stress acting on the leaflets ($S_{1,peak}$).

The values of the computed parameters are shown in Table 3.4.

All virtual repair procedures repositioned the prolapsing segment of the PL below the annular plane, resulting in the elimination of MV prolapse. In the model prior to virtual repair, the maximum z-axis displacement of 14.1 mm appeared on the free margin of the prolapsing P2 segment. Following virtual repair, prolapse of the PL was eliminated and the maximum z-axis displacement was reduced to values ranging from 1.9 mm in VR0 model to 7.6 mm in VR15 model.

As the MV prior to virtual repair was prolapsing, almost no contact between the AL and the PL was present. All virtual repair procedures restored a contact between the leaflets and significantly increased the CoA. The smallest increase of this area by 85.5% was obtained after the implantation of the longest neochordae (VR15 model), while the largest increase by 134.1% was acquired in VR5 model (Fig. 3.5 c).

Since in the prolapsing model the leaflets on anteroposterior diameter were not in a contact, there was no actual CoL either (Fig 3.6 a). All virtual repair procedures restored the different level of the CoL, ranging from 3.9 mm (VR0 model) to 7 mm (VR10 model) (Fig. 3.6 c).

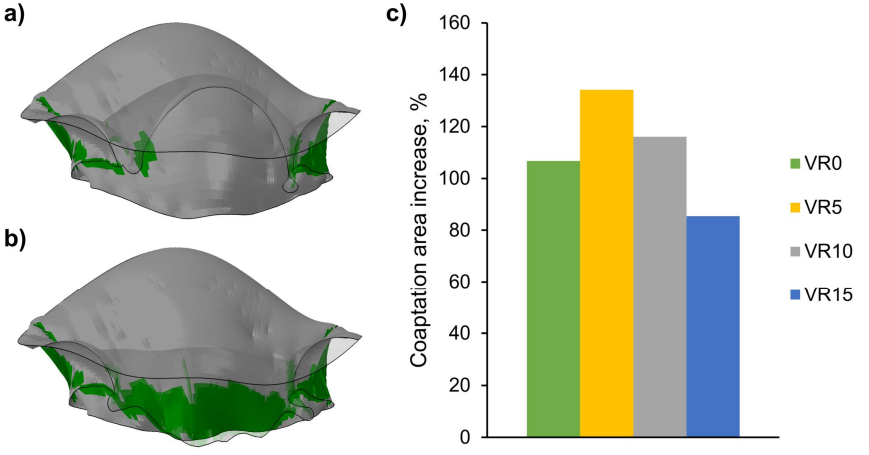

Fig. 3.5. Calculated coaptation area in prolapsing model before and after virtual transapical repair: a) coaptation area prior to virtual repair; b) coaptation area after implantation of neochordae in VR5 model; c) increase of coaptation area after every virtual repair procedure

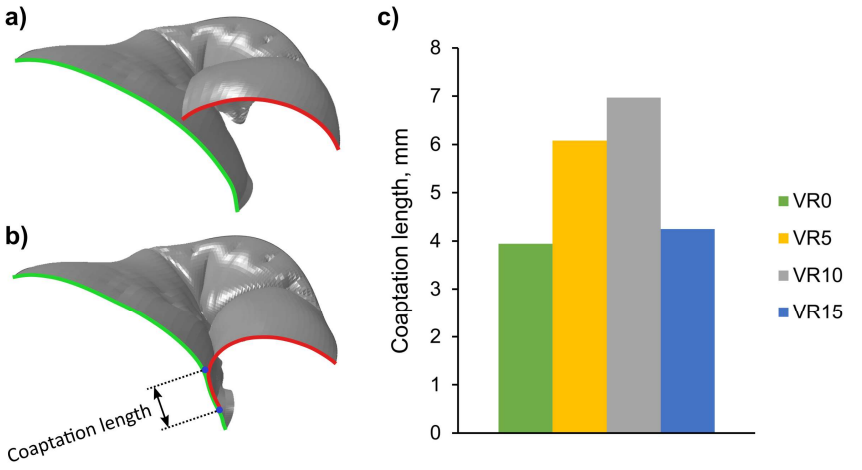

Fig. 3.6. Coaptation length in prolapsing mitral valve model: a) no leaflet contact on anteroposterior diameter in the mitral valve model before virtual repair; b) coaptation length after virtual repair (VR10 model); c) values of coaptation length for each simulation at peak systole

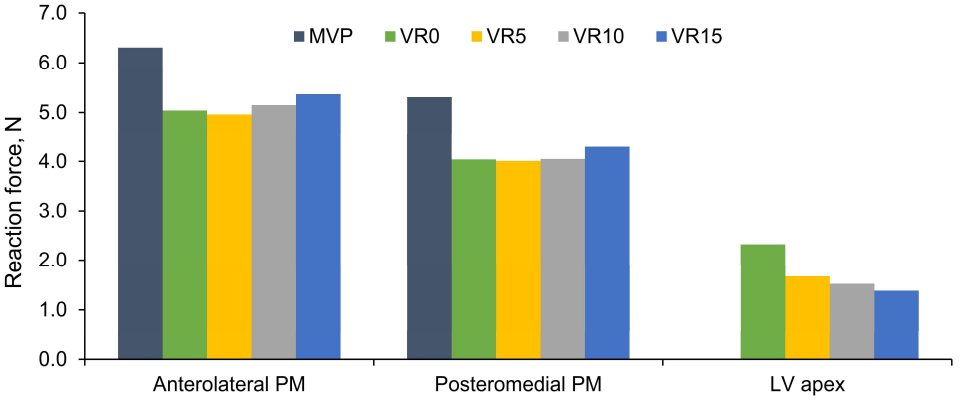

Fig. 3.7. Comparison of reaction forces on left ventricle apex, anterolateral and posteromedial papillary muscles at peak systole

The measurement of the reaction forces in the PMs provides information on the tension forces acting in the chordae tendineae as a whole. In the initial model, the reaction forces acting on the anterolateral and posteromedial PMs were 6.31 and 5.31 N, respectively. After the implantation of the neochordae, these forces

were reduced (Fig 3.7), since the tension forces were partially transferred from the native chordae to the neochordae.

Table 3.4. Computational results of prolapsing model at peak systole

Parameter	MVP	VR0	VR5	VR10	VR15
$u_{z,max}$, mm	14.1	1.9	2.7	5.1	7.6
CoA, mm²	132.7	274.3	310.7	286.7	246.1
CoL, mm	–	3.9	6.1	7.0	4.3
F_{PM}, N					
Anterolateral PM	6.31	5.04	4.96	5.15	5.37
Posteromedial PM	5.31	4.05	4.01	4.05	4.30
F_{LVA}, N	–	2.32	1.67	1.52	1.38
F_{CT}, N	1.08	0.72	0.74	0.74	0.72
F_{NC}, N	–	0.63	0.45	0.48	0.57
$S_{1,peak}$, MPa	1.67	0.96	0.70	0.65	0.91

MVP, mitral valve model with prolapse; VR0, VR5, VR10, VR15, mitral valve models with different neochordal length; $u_{z,max}$, maximum displacement along the z-axis of the free margin of the MV; CoA, coaptation area; CoL, coaptation length; F_{PM}, reaction force on the papillary muscle; F_{LVA}, reaction force on the left ventricle apex; F_{CT}, maximum tension force in the native chordae; F_{NC}, maximum tension force in the neochordae; $S_{1,peak}$, peak value of the maximum principal stress acting on the leaflets.

Moreover, after the implantation of the neochordae, the reaction force appeared on the LV apex. This force in each post-repair MV depended inversely on the length of the neochordae: the longer the sutures were used, the smaller the reaction force value was, and vice versa.

The implantation of the neochordae allowed to reduce forces acting in the native chordae. The highest value of the tension forces in the chordae tendineae occurred in the native marginal chorda neighboring the prolapsing P2 segment of the MV prior to virtual repair, with a peak value of 1.08 N. After each virtual repair procedure, the tension was partially transferred to neochordae and the maximum tension force in the chordae tendineae of each model was reduced to almost identical values ranging from 0.72 to 0.74 N.

Regarding neochordal tension, the maximum force after every virtual repair occurred in the neochorda closest to anterolateral PM, with the highest value of 0.63 N in VR0 model and the lowest value of 0.45 N in VR5 model.

While the virtual repair procedure hasn't influenced stress distribution across the non-prolapsing segments of the MV much, stresses on the prolapsing segment as well as in its neighboring regions changed considerably compared to the MV prior to virtual repair.

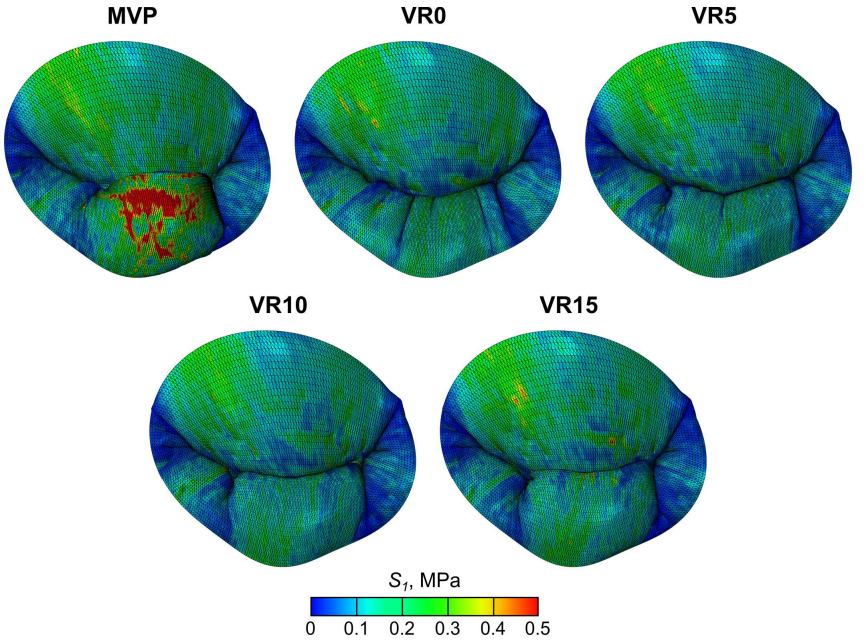

Fig. 3.8. Stress distribution across the leaflets after the implantation of neochordae of different length at peak systole

In the initial model, the peak stress value of 1.67 MPa was noticed in the region neighboring the prolapsing P2 segment. Moreover, high stress concentration area appeared in the middle of the bulging segment of the leaflet (Fig. 3.8). After virtual repair, these stress concentrations were reduced in every post-repair model, although stresses slightly increased along the free margin of the P2 segment near the attachment points of the neochordae.

3.2.3. Evaluation of Prolapsing Model

To this date, only several studies on the modeling of different neochordae implantation techniques were published (Reimink *et al.* 1995; Rim *et al.* 2014; Sturla *et al.* 2014; 2015b; 2015c; Morgan *et al.* 2016; Choi *et al.* 2017). However, none of them had addressed the problem of transapical MV repair. For this reason, parameters calculated during dynamic FE simulations of the prolapsing model were compared with the ones published in the studies quantitatively investigating different neochordal implantation techniques, but not the transapical approach.

While all virtual repair procedures considerably increased the coaptation area, the coaptation length on anteroposterior diameter was insufficient after the

implantation of the shortest (VR0 model) and the longest (VR15 model) neochordae. Minimum coaptation length to ensure adequate MV function is considered to be 5 mm (David 2007), and in both mentioned cases, this length was below the limit (3.9 and 4.3 mm, respectively). Meanwhile, the coaptation length calculated in VR5 and VR10 models were 6.1 and 7.0 mm, showing the sufficient leaflet closure at peak systole.

These results show that after the implantation of the shortest neochordae the movement of the PL was partially restricted, thus preventing adequate leaflet apposition. On the other hand, the implantation of the longest neochordae caused the opposite effect, the movement of the PL was not restricted enough and some bulging remained, therefore, the coaptation length stayed insufficient. Meanwhile, neochordae in VR5 and VR10 models ensured proper coaptation length of the post-repair MV.

While evaluating the coaptation of the leaflets, it should be noticed that the coaptation area and length are the parameters strongly dependent on the geometry of the MV. Therefore, these parameters are hardly comparable with the ones found in the literature. Still, the post-repair coaptation area recovery values are similar to the ones reported by Rim *et al.* (2014).

Stress analysis of the prolapsing MV showed large maximum principal stress concentration on the bulging section of the P2 segment and in the regions neighboring this segment. These computed stress patterns are similar to those reported by the other authors (Rim *et al.* 2014; Sturla *et al.* 2014; Choi *et al.* 2017). Such excessive stresses over a longer period of time can cause an additional chordal rupture (Rim *et al.* 2014).

All virtual repair procedures reduced these excessive stresses. After the implantation of the neochordae in VR5 and VR10 models, the bulging of the PL was eliminated, and maximum stress value on the leaflet was reduced from 1.67 MPa to 0.70 and 0.65 MPa, respectively. However, virtual repair in VR0 and VR15 models provided the smallest stress reduction to 0.96 and 0.91 MPa, as in these cases the PL was partially restricted (VR0 model) or some bulging of the prolapsing segment remained (VR15 model).

Regarding the tension forces in the native chordae, in all cases the reduction was quite similar, maximum force decreased from 1.08 N to values ranging between 0.72 and 0.74 N. This reduction occurred as a result of partial stress transfer from native chordae to neochordae.

The computed values of tension forces in the native chordae were slightly higher than the ones published by Rim *et al.* (2014), though they did not exceed the chordal failure tension values reported in the literature (Sedransk *et al.* 2002). This difference could be due to the higher systolic pressure used in the present study with a peak value of 16 kPa compared to 12 kPa used by Rim and colleagues.

The comparison of the obtained results with the existing ones showed that all calculated parameters had a good agreement with those reported by other authors and did not exceed any critical values found in the literature. Moreover, the evaluation of the effect of the neochordal length on post-repair MV function demonstrated that the length of the implanted neochordae has a significant impact on the correction of MR caused by chordae tendineae rupture. Therefore, special consideration on the length of the sutures should be given, as implantation of either too short or too long neochordae can result in inadequate post-repair MV function.

3.3. Computational Analysis of Pathological Mitral Valve Model

3.3.1. Virtual Repair with Calculated Neochordal Length

For the pathological model, the chordae tendineae were removed from the edge of the P2L segment to replicate MV prolapse seen on pre-operative TEE images.

As shown during the analysis of the prolapsing model, the length of the implanted neochordae has a significant impact on the correction of MR caused by chordae tendineae rupture. Therefore, special consideration on the length of the sutures should be given. For this reason, the method to determine the required neochordal length is suggested (Fig. 3.9).

Firstly, the bulging height of the prolapsing segment from the annular plane at peak systole was identified. For this, the physiological MV model with complete and intact chordal apparatus, referred to as pre-model, was created. The simulations of the systolic function of pre-model and earlier created pathological model were then performed, and the positions of the investigated segment in both models at peak systole were determined. The bulging height of this segment was calculated by subtracting the coordinates of corresponding nodes on the free margin in the pre-model from the ones in the pathological model. For this, the prolapsing MV model in the systolic configuration was used. The neochordal length L_{AC*} for the virtual repair was then determined:

$$L_{AC*} = L_{AC} - L_{CC*}, \tag{3.1}$$

where L_{AC} is the distance between LV apex and the neochordal insertion point on the prolapsing segment of the leaflet, and L_{CC*} is the bulging height of the leaflet.

The length of each required suture was calculated by subtracting the earlier determined bulging height from a distance between the nodes of the LV apex and the free margin of the prolapsing segment. Each neochorda was composed of two equal size elements, with their junction point moved along the y-axis to ensure the calculated neochordal length.

Following the real-life surgery, three virtual neochordae with a mean length of 66.6±1.4 mm were implanted into the PL, connecting the LV apex and the free margin of the leaflet.

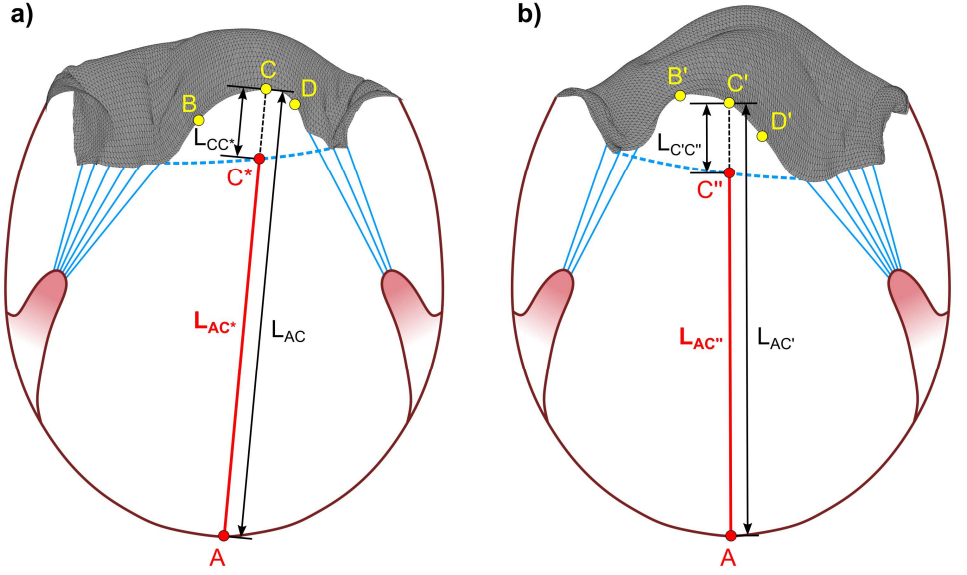

Fig. 3.9. Determination of the neochordal length: a) neochordal insertion sites on the posterior leaflet are marked with points B, C, D; b) insertion sites of the neochordae on the anterior leaflet are marked B', C', D'. For the point C, the neochordal length L_{AC^*} was determined by subtracting the bulging height of the leaflet L_{CC^*} from a distance between the left ventricle apex (point A) and the free margin L_{AC}. The procedure was repeated for every insertion point to determine all neochordal lengths

After the implantation of the neochordae into the PL, the same procedure was repeated with the A2L segment thus allowing to recreate prolapse of the AL, which occurred during the surgery due to the rupture of the native chordae. Three neochordae with a mean length of 65.2±0.2 mm were implanted.

A total of four FE models were prepared for the dynamic simulation in Abaqus/Explicit representing:

- prolapse of the posterior leaflet (PLP);
- virtual repair with neochordae implantation into the posterior leaflet (PLVR);
- prolapse of the anterior leaflet, which occurred during the surgery (ALP);

- virtual repair with neochordae implantation into the anterior leaflet (ALVR).

For each model, the input file for the dynamic analysis in Abaqus/Explicit was prepared. All simulations were carried out one by one, thus allowing to recreate the real-life surgery process.

3.3.2. Computational Results of Pathological Model

Regarding the pathological model, a rare bi-leaflet transapical MV repair, which occurs in less than 5% of the cases (Colli *et al.* 2018), was investigated. At first, the simulation of the systolic function of the initial prolapsing model (PLP) revealed prolapse of only P2L segment, characterized by a bulging of the PL. No leaflet contact in the midline of the prolapsing region was noticed and a gap between the leaflets was present. Following the surgical procedure executed by surgeons, virtual repair with the implantation of three neochordae (PLVR) was performed and MV prolapse was eliminated.

However, the rupture of the chordae tendineae inserted into the AL caused prolapse of the A2L segment (ALP), and eversion of the AL towards the LA was observed. A good contact between the leaflets was restored after another virtual repair procedure (ALVR), during which three neochordae were implanted into the AL, as in the real-life surgical procedure.

After each simulation (i.e. prolapsing PL followed by virtual repair and prolapsing AL followed by virtual repair), the parameters described in 3.2.2 paragraph were identified at peak systole, and the effect of virtual transapical MV repair were evaluated. In addition, the morphological comparison between the virtual models and the TEE image data was performed. The values of the calculated parameters are shown in Table 3.5.

Since the prolapsing model was reconstructed from the echocardiographic data of the healthy MV, the morphological comparison with the real-life surgery outcomes could not have been done. However, in case of the pathological model, the simulation results could have been used to evaluate morphological compliance between virtual models and TEE image data. This was done by visually comparing the computed systolic leaflet configurations of virtual PLP and ALVR models with the pre- and post-operative echocardiographic images. Fig. 3.10 shows a good agreement in deformed leaflet morphology between the simulation results and the echocardiographic data.

In both PLVR and ALVR models, the neochordae used during virtual transapical repair securely repositioned the prolapsing regions of the leaflets under the annular plane, resulting in the disappearance of MV prolapse. In PLP model, the maximum displacement along the z-axis was found on the free margin of the prolapsing P2L segment and was equal to 18.6 mm. After virtual repair, prolapse of

the PL was eliminated, and this value was reduced to 13.5 mm. In ALP model, prolapse of the anterior leaflet occurred and the maximum z-axis displacement of 19.1 mm was noticed on the free margin of the A2L segment. ALVR eliminated prolapse and reduced the maximum displacement value to 12.9 mm.

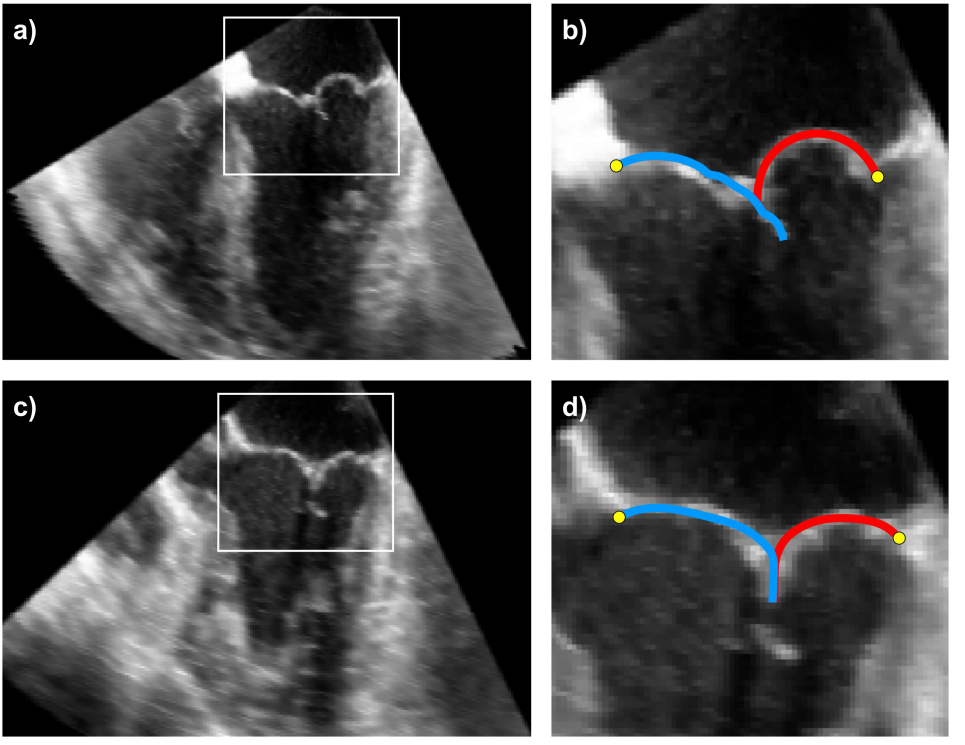

Fig. 3.10. Morphological comparison of computed systolic leaflet configuration in pathological model with echocardiographic images: a) region of interest in pre-operative image; b) cross-sectional view of computational model after virtual repair with neochordae implantation into the posterior leaflet superimposed to pre-operative echocardiographic image; c) region of interest in post-operative echocardiographic image; d) cross-sectional view of computational model after virtual repair with neochordae implantation into the anterior leaflet superimposed to post-operative echocardiographic image

In the initial model, a lack of contact between A2L and P2L segments due to the prolapsing PL was present. After PLVR, a contact between the segments was recovered, restoring the coaptation length of 5.8 mm and increasing the coaptation area by 27.5%. However, after the rupture of the A2L native chordae, the bulging

of the anterior leaflet occurred, resulting in a decrease of the coaptation area by 13.7%. A good contact between the leaflets was restored after ALVR, increasing the coaptation length from none to 6.4 mm. Compared to the PLP model, a total increase of the coaptation area by 72.2% was achieved during both virtual repair procedures.

Both virtual repair procedures reduced the tension forces acting in the chordae tendineae since these forces were partially transferred from the native chordae to the implanted neochordae. In the PLP model, reaction forces acting on the anterolateral and posteromedial PMs were almost equal, with values of 7.77 and 7.85 N, respectively. After PLVR, these values were reduced to 6.23 and 6.44 N. However, after the rupture of the chordae tendineae inserted into the AL, the reaction force on the posteromedial PM increased to 7.18 N, while the one on the anteromedial PM decreased even more to 5.21 N. This decrease can be explained by the reduced number of the chordae tendineae inserted into this PM. Finally, after ALVR, the reaction forces once again were reduced to 4.18 and 6.53 N for the anteromedial and posterolateral PMs, respectively (Fig 3.11).

The maximum tension forces in the chordae tendineae were found in the marginal chordae neighboring the prolapsing segment. In PLP model, the peak value of tension force in the marginal chorda inserted into the border of P1-P2L segments was 1.10 N, whereas in ALP model the maximum tension force of 1.08 N occurred in the marginal chorda inserted into the edge of A1-A2L segments. After each virtual repair procedure, these values were reduced to 0.65 and 0.50 N, respectively.

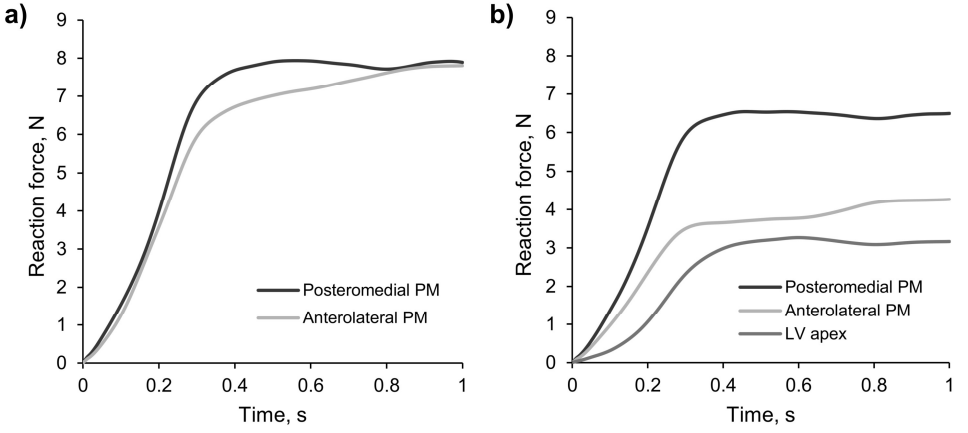

Fig. 3.11. Reaction forces on the papillary muscles and left ventricle apex: a) before virtual transapical mitral valve repair; (b) after virtual repair procedure

Table 3.5. Computational results of pathological model at peak systole

Parameter	PLP	PLVR	ALP	ALVR
$u_{z,max}$, mm				
Anterior leaflet	14.0	14.1	19.1	12.9
Posterior leaflet	18.6	13.5	13.6	12.8
CoA, mm²				
Anterior leaflet Posterior leaflet	287.3	366.2	316.0	494.7
CoL, mm				
Anterior leaflet Posterior leaflet	–	5.8	–	6.4
F_{PM}, N				
Anterolateral PM	7.77	6.23	5.21	4.18
Posteromedial PM	7.85	6.44	7.18	6.53
F_{LVA}, N	–	2.15	1.94	3.15
F_{CT}, N				
Anterior leaflet	0.49	0.29	1.08	0.50
Posterior leaflet	1.10	0.65	0.60	0.61
F_{NC}, N				
Anterior leaflet	–	–	–	0.88
Posterior leaflet	–	0.96	1.04	0.86
$S_{1,peak}$, MPa				
Anterior leaflet	0.59	0.63	0.85	0.79
Posterior leaflet	1.09	0.71	0.76	0.77

PLP, prolapse of the posterior leaflet; PLVR, virtual repair with neochordae implantation into the posterior leaflet; ALP, prolapse of the anterior leaflet; ALVR, virtual repair with neochordae implantation into the anterior leaflet; $u_{z,max}$, maximum displacement along the z-axis of the free margin of the MV; CoA, coaptation area; CoL, coaptation length; F_{PM}, reaction force on the papillary muscle; F_{LVA}, reaction force on the left ventricle apex; F_{CT}, maximum tension force in the native chordae; F_{NC}, maximum tension force in the neochordae; $S_{1,peak}$, peak value of the maximum principal stress acting on the leaflets.

Tension forces in the neochordae were calculated after PLVR and ALVR. Following PLVR, the maximum value of the force exerted by the neochordae implanted into the PL was 0.96 N. This value was decreased to 0.86 N after ALVR, whereas the maximum tension force in the neochordae implanted into the AL was calculated to be 0.88 N.

The change of tension in the native chordae and neochordae as a whole can be represented as an alteration of reaction forces acting on the PMs and LV apex during dynamic FE analysis. Fig. 3.11 shows that virtual repair procedures reduced reaction forces on the PMs since tension in the native chordae was partially

transferred to the neochordae, resulting in the appearance of reaction force on the LV apex.

Stress distribution across the leaflets of the prolapsing and virtually repaired MV models are shown in Fig. 3.12. All simulations specified the peak value of the maximum principal stress to be on the MV free margin. In PLP model, the high stress concentration area occurred near the prolapsing P2L segment with a maximum value of 1.09 MPa. Following virtual repair, this high stress concentration was significantly reduced. However, the increase of the stress near the attachment points of the neochordae was noticed with a peak value of 0.71 MPa.

After the rupture of the A2L chordae, new high stress concentration areas appeared on the AL. As previously, the highest stress values occurred near the prolapsing segment along the free margin of the leaflet with a maximum value of 0.85 MPa. In addition, stress increase was noticed in the middle of the bulging region of the leaflet. Following ALVR, these stress values were reduced, still, as before, the increase of the stress appeared near the neochordal attachment points with a peak value of 0.79 MPa.

3.3.3. Evaluation of Pathological Model

The pathological model was used to recreate the real-life transapical repair surgery of rare bi-leaflet MV prolapse, which occurred due to the chordae tendineae rupture during the surgical procedure while repairing a common prolapse of the PL. The modeling strategy, tried out earlier while simulating the systolic function of the prolapsing model, with the implemented neochordal length determination method was used. To recreate the surgery process, a total of four simulations were run one by one, indicating the prolapsing PL followed by virtual repair, and the appearance of the AL prolapse, also followed by virtual repair.

The maximum displacement along the z-axis of the MV free margin and the coaptation area of the leaflets are the parameters strongly dependent on the geometry of the MV. Therefore, these parameters are hardly comparable with the ones published by other authors. Still, the post-repair maximum z-axis displacement and coaptation area recovery values are similar to the ones reported by Sturla *et al.* (2014). In addition, both virtual repair procedures restored a sufficient coaptation length larger than 5 mm, which is considered to be a minimum coaptation length required to ensure adequate MV function (David 2007).

In terms of tension forces in the native chordae, the calculated values were slightly higher than the ones reported by Rim *et al.* (2014). The reason for this was already explained during the evaluation of the prolapsing model (see paragraph 3.2.3). Regarding the tension forces in the neochordae, the calculated values are comparable with the ones measured in vitro (Bajona *et al.* 2008) and in vivo

(Bajona *et al.* 2009; Jensen *et al.* 2014) by other authors. Tension forces, estimated in the current study, fall into the reported range between 0.5 and 1.05 N.

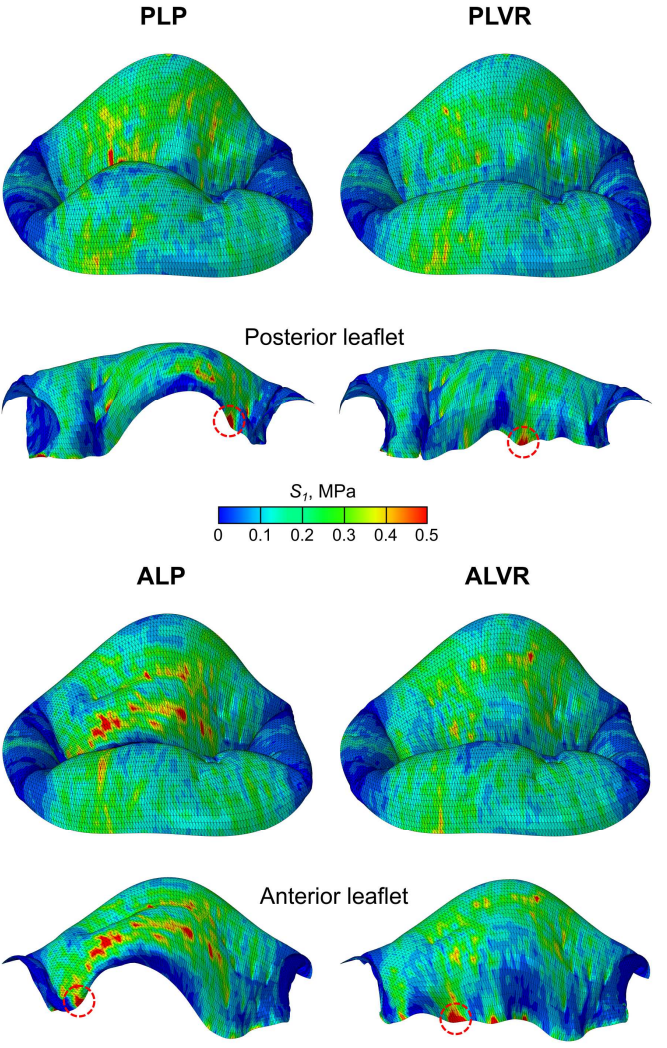

Fig. 3.12. Maximum principal stress distribution across the mitral valve leaflets at peak systole following each simulation of pathological models. High stress concentration areas with stress peak values are circled in red

The computed stress patterns, as in the prolapsing model, were similar to the ones reported by other authors (Rim *et al.* 2014; Sturla *et al.* 2014; Choi *et al.*

2017). In both models with MV prolapse, the highest stress concentration areas occurred near the prolapsing segments, whereas following virtual repair procedures these values were reduced but the increase of the stress near the attachment points of the neochordae appeared. However, the calculated peak values of the maximum principal stress did not exceed the failure stress limit reported by Grande-Allen *et al.* (2005).

Moreover, in this particular case, the comparison between pre- and post-operative virtual models and real-life TEE image data in terms of morphological compliance was done. This comparison showed a good agreement in leaflet deformation between the MV simulation data and the echocardiographic images, supporting the eligibility of the used modeling strategy.

3.4. Limitations of the Study

The presented modeling strategy provided a detailed quantification of MV biomechanics, showing a potential to be used for the comprehensive analysis of transapical MV repair in scenarios of clinical relevance. However, some limitations of the present study should be highlighted.

Firstly, it should be noted that although the reconstruction of the MV geometry was based on realistic echocardiographic images, the thickness of the leaflets was assigned according to the measurements on healthy MV reported by Kunzelman *et al.* (2007). This assumption was made due to the impossibility to measure leaflets thickness directly from clinical images.

Also, the chordae tendineae, which cannot be seen in the echocardiographic images, were modeled through a scheme created in accordance with ex vivo findings (Lam *et al.* 1970; Degandt *et al.* 2007) and indications by clinicians (Stevanella *et al.* 2011). The configuration of the chordae tendineae has a significant impact on the function of the whole valvular structure (Siefert *et al.* 2014), therefore, a patient-specific implementation of the chordae positioning may lead to a better consistency with in vivo data.

Furthermore, in the present study, mechanical properties of the MV leaflets and the chordae tendineae were described using available stress-strain curves obtained from ex vivo testing on the healthy porcine valve (May-Newman and Yin 1998; Kunzelman and Cochran 1990). The properties of the human valvular structure, especially for the diseased one, are likely to be different from the ones assumed in the present study.

One last consideration, which is worth paying attention to, is the time needed for such simulations. On a standard personal computer with a quad-core processor, one simulation lasted for about 4 hours. The time for geometry reconstruction and FE model creation, which took at least several hours for every model, should

also be considered. Therefore, while the simulation results seem to be reliable, the whole process needs to become faster in order for the described approach to be used as a clinical analysis tool.

3.5. Conclusions of Chapter 3

1. Evaluation of the effect of the neochordal length on post-repair MV function showed that the length of the implanted neochordae has a significant impact on the correction of MR caused by chordae tendineae rupture. After the implantation of the shortest (VR0 model) and the longest (VR15 model) neochordae, the coaptation length on anteroposterior diameter was insufficient (3.9 ir 4.3 mm), while in VR5 and VR10 models coaptation length was calculated to be adequate (6.1 and 7.0 mm). Regarding pathological model, both virtual repair procedures (PLVR and ALVR) with calculated neochordal length restored proper coaptation (5.8 and 6.4 mm).
2. Computed parameters, including coaptation area and length, reaction forces, tension forces and stress distribution across the MV leaflets, for both prolapsing and pathological models coincided well with the ones found in the literature, thus supporting the eligibility of the used modeling strategy for virtual transapical MV repair procedure and the validity of the suggested method for the neochordal length determination.
3. Morphological comparison between computed leaflet deformation in pathological model and TEE images was performed, as an additional way to assess the reliability of the used modeling strategy. A resembling configuration in terms of shape and bulging of the deformed leaflets was determined after the visual comparison between the simulation results and the echocardiographic data.
4. Limitations of the presented modeling strategy were highlighted: theoretical MV leaflets thickness, idealized configuration of the chordae tendineae, mechanical properties based on ex vivo porcine data, and the high computational cost for the simulation of MV systolic function. Elimination of such limitations should be considered for a more complete research study in the future.

General Conclusions

1. After reviewing the scientific literature related to computational modeling of mitral valve structure and function, it has been determined that numerical simulation can provide insights into the relationships between mitral valve components and allow to analyze the outcomes of various surgical techniques used for the repair of the valve affected by the disease.
2. Patient-specific prolapsing finite element model of the mitral valve was created and used for the investigation of the neochordal length influence on the function of the mitral valve after virtual transapical repair. The systolic function simulations of the mitral valve models with different neochordal length showed that the length of the implanted sutures has a significant impact on the correction of mitral regurgitation caused by chordae tendineae rupture. While all virtual repair procedures eliminated mitral valve prolapse and considerably increased the coaptation area by 109.8±24.3%, the coaptation length on anteroposterior diameter was insufficient (<5 mm) after the implantation of the shortest (3.9 mm) and the longest neochordae (4.3 mm).
3. Method for neochordal length determination during virtual transapical mitral valve repair procedure based on numerical simulation results was suggested. This method allows to adjust the length of the neochordae, thus eliminating mitral valve prolapse and reducing stresses acting on the

leaflets, therefore abolishing the risk of tearing up the repaired leaflet in post-operative mitral valve model.

4. The developed method for neochordal length determination was tested on pathological finite element model created using patient-specific echocardiographic data. Simulation of the systolic function of virtually repaired mitral valve with neochordal length adjusted using the suggested method, demonstrated eliminated prolapse, improved leaflet coaptation by 72.2%, decreased chordal tension forces from 1.1 N to 0.5 N and reduced excessive leaflet stress from 1.09 MPa to 0.77 MPa, while maintaining the morphological compliance with the echocardiographic data.
5. The comparison of the obtained results, including coaptation area and length, reaction forces, tension forces and stress distribution across the mitral valve leaflets, with the ones found in the literature showed that calculated parameters had a good agreement with those reported by other authors and did not exceed any known critical values. Such evaluation proved the eligibility of the used modeling strategy and supported the validity of the suggested method for the neochordal length determination.
6. The computed parameters show the potential of the presented modeling strategy to be used as a tool for predicting post-operative mitral valve morphology and coaptation of the leaflets as the main indicators of mitral valve prolapse elimination.

References

Anderson, Y.; Wilson, N.; Nicholson, R.; Finucane, K. 2008. Fulminant mitral regurgitation due to ruptured chordae tendinae in acute rheumatic fever, *Journal of Paediatrics and Child Health* 44(3): 134–137.

Apostolakis, E. E.; Baikoussis, N. G. 2009. Methods of estimation of mitral valve regurgitation for the cardiac surgeon, *Journal of Cardiothoracic Surgery* 4: 34.

Avanzini, A.; Donzella, G.; Libretti, L. 2011. Functional and structural effects of percutaneous edge-to-edge double-orifice repair under cardiac cycle in comparison with suture repair, *Proceedings of the Institution of Mechanical Engineers, Part H: Journal of Engineering in Medicine* 225(10): 959–971.

Badea, C. T.; Drangova, M.; Holdsworth, D. W.; Johnson, G.A. 2008. In vivo small animal imaging using micro-CT and digital subtraction angiography, *Physics in Medicine & Biology* 53(19): R319–R350.

Baillargeon, B.; Costa, I.; Leach, J. R.; Lee, L. C.; Genet, M.; Toutain, A.; Wenk, J. F.; Rausch, M. K.; Rebelo, N.; Acevedo-Bolton, G.; Kuhl, E.; Navia, J. L.; Guccione, J. M. 2015. Human cardiac function simulator for the optimal design of a novel annuloplasty ring with a sub-valvular element for correction of ischemic mitral regurgitation, *Cardiovascular Engineering and Technology* 6(2): 105–116.

Bajona, P.; Zehr, K. J.; Liao, J.; Speziali, G. 2008. Tension measurement of artificial chordae tendinae implanted between the anterior mitral valve leaflet and the left

ventricular apex: an in vitro study, *Innovations: Technology and Techniques in Cardiothoracic and Vascular Surgery* 3(1): 33–37.

Bajona, P.; Katz, W. E.; Daly, R. C.; Zehr, K. J.; Speziali, G. 2009. Beating-heart, off-pump mitral valve repair by implantation of artificial chordae tendineae: an acute in vivo animal study, *Journal of Thoracic and Cardiovascular Surgery* 137(1): 188–193.

Barber, J. E.; Kasper, F. K.; Ratliff, N. B.; Cosgrove, D. M.; Griffin, B. P.; Vesely, I. 2001. Mechanical properties of myxomatous mitral valves, *Journal of Thoracic and Cardiovascular Surgery* 122(5): 955–962.

Caballero, A.; Mao, W.; McKay, R.; Primiano, C.; Hashim, S.; Sun, W. 2018. New insights into mitral heart valve prolapse after chordae rupture through fluid-structure interaction computational modeling, *Scientific Reports* 8: 17306.

Camacho, P.; Fan, H.; Liu, Z.; He, J.-Q. 2016. Large mammalian animal models of heart disease, *Journal of Cardiovascular Development and Disease* 3(4): 30.

Carpentier, A. 1983. Cardiac valve surgery – the "French correction", *Journal of Thoracic and Cardiovascular Surgery* 86(3): 323–337.

Carpentier, A.; Adams, D. H.; Filsoufi, F. 2010. *Carpentier's Reconstructive Valve Surgery*. Philadelphia: Saunders.

Casado, J. A.; Diego, S.; Ferreño, D.; Ruiz, E.; Carrascal, I.; Méndez, D.; Revuelta, J. M.; Pontón, A.; Icardo, J. M.; Gutiérrez-Solana, F. 2012. Determination of the mechanical properties of normal and calcified human mitral chordae tendineae, *Journal of the Mechanical Behavior of Biomedical Materials* 13: 1–13.

Choi, A.; Rim, Y.; Mun, J. S.; Kim, H. 2014. A novel finite element-based patient-specific mitral valve repair: virtual ring annuloplasty, *Bio-Medical Materials and Engineering* 24(1): 341–347.

Choi, A.; McPherson, D. D.; Kim, H. 2017. Neochordoplasty versus leaflet resection for ruptured mitral chordae treatment: virtual mitral valve repair, *Computers in Biology and Medicine* 90: 50–58.

Colli, A.; Manzan, E.; Zucchetta, F.; Bizzotto, E.; Besola, L.; Bagozzi, L.; Bellu, R.; Sarais, C.; Pittarello, D.; Gerosa, G. 2016. Transapical off-pump mitral valve repair with neochord implantation: early clinical results, *International Journal of Cardiology* 204: 23–28.

Colli, A.; Manzan, E.; Aidietis, A.; Rucinskas, K.; Bizzotto, E.; Besola, L.; Pradegan, N.; Pittarello, D.; Janusauskas, V.; Zakarkaite, D.; Drasutiene, A.; Lipnevicius, A.; Danner, B. C.; Sievert, H.; Vaskelyte, L.; Schnelle, N.; Salizzoni, S.; Marro, M.; Rinaldi, M.; Kurnicka, K.; Wrobel, K.; Ceffarelli, M.; Savini, C.; Pacini, D.; Gerosa, G. 2018. An early European experience with transapical off-pump mitral valve repair with NeoChord implantation, *European Journal of Cardio-Thoracic Surgery* 54(3): 460–466.

Conti, C. A.; Stevanella, M.; Maffessanti, F.; Trunfio, S.; Votta, E.; Roghi, A.; Parodi, O.; Caiani, E. G.; Redaelli, A. 2010. Mitral valve modelling in ischemic patients: finite

element analysis from cardiac magnetic resonance imaging, *Computing in Cardiology* 37: 1059–1062.

Dal Pan, F.; Donzella, G.; Fucci, C.; Schreiber, M. 2005. Structural effects of an innovative surgical technique to repair heart valve defects, *Journal of Biomechanics* 38(12): 2460–2471.

Dal-Bianco, J. P.; Beaudoin, J.; Handschumacher, M. D.; Levine, R. A. 2014. Basic mechanisms of mitral regurgitation, *Canadian Journal of Cardiology* 30(9): 971–981.

Dang, M. C.; Thacker, J. G.; Hwang, J. C.; Rodeheaver, G. T.; Melton, S. M.; Edlich, R. F. 1990. Some biomechanical considerations of polytetrafluoroethylene sutures, *Archives of Surgery* 125(5): 647–650.

Dassault Systèmes. 2010. *Abaqus Analysis User's Manual*. Providence: Dassault Systèmes.

David, T. E. 2007. Outcomes of mitral valve repair for mitral regurgitation due to degenerative disease, *Seminars in Thoracic and Cardiovascular Surgery* 19(2): 116–120.

Degandt, A. A.; Weber, P. A.; Saber, H. A.; Duran, C. M. 2007. Mitral valve basal chordae: comparative anatomy and terminology, *Annals of Thoracic Surgery* 84(4): 1250–1255.

Demetrio, P.; Andrea, C.; Gianclaudio, F.; Antonio, M.; Gino, G.; Carlo, O. 2015. Transesophageal echocardiography in NeoChord procedure, *Annals of Cardiac Anaesthesia* 18(2): 191–197.

Desjardins, B.; Kazerooni, E. A. 2004. ECG-gated cardiac CT, *American Journal of Roentgenology* 182(4): 993–1010.

Drach, A.; Khalighi, A. H.; Sacks, M. S. 2018. A comprehensive pipeline for multi-resolution modeling of the mitral valve: Validation, computational efficiency, and predictive capability, *International Journal for Numerical Methods in Biomedical Engineering* 34(2): e2921.

Durst, R.; Gilon, D. 2015. Imaging of mitral valve prolapse: what can we learn from imaging about the mechanism of the disease, Journal of Cardiovascular Development and Disease 2(3): 165–175.

El Sabbagh, A.; Reddy, Y. N. V.; Nishimura, R. A. 2018. Mitral valve regurgitation in the contemporary era: insights into diagnosis, management, and future directions, *JACC: Cardiovascular Imaging* 11(4): 628–643.

Enriquez-Saranom, M.; Nkomo, V. T.; Michelena, H. I. 2009. Mitral regurgitation, in *Valvular Heart Disease. Contemporary Cardiology*. New York: Humana Press, 221–246.

Fukuta, H.; Little, W. C. 2008. The cardiac cycle and the physiologic basis of left ventricular contraction, ejection, relaxation, and filling, *Heart Failure Clinics* 4(1): 1–11.

Gabbay, U.; Yosefy, C. 2010. The underlying causes of chordae tendinae rupture: a systematic review, *International Journal of Cardiology* 143(2): 113–118.

Gao, H.; Qi, N.; Feng, L.; Ma, X.; Danton, M.; Berry, C.; Luo, X. 2017. Modelling mitral valvular dynamics – current trend and future directions, *International Journal of Numerical Methods in Biomedical Engineering* 33(10): e2858.

Grande-Allen, K. J.; Barber, J. E.; Klatka, K. M.; Houghtaling, P. L.; Vesely, I.; Moravec, C. S.; McCarthy, P. M. 2005. Mitral valve stiffening in end-stage heart failure: evidence of an organic contribution to functional mitral regurgitation, *Journal of Thoracic and Cardiovascular Surgery* 130(3): 783–790.

Gunnal, S. A.; Wabale, R. N.; Farooqui, M. S. 2015. Morphological study of chordae tendinae in human cadaveric hearts, *Heart Views* 16(1): 1–12.

Hall, J. E. 2015. *Guyton and Hall Textbook of Medical Physiology* (13th ed.). Philadelphia: Saunders.

Han, H. C.; Ha, F. J.; Teh, A. W.; Calafiore, P.; Jones, E. F.; Johns, J.; Koshy, A. N.; O'Donnell, D.; Hare, D. L.; Farouque, O.; Lim, H. S. 2018. Mitral valve prolapse and sudden cardiac death: a systematic review, *Journal of the American Heart Association* 7(23): e010584.

Holzapfel, G. A.; Sommer, G.; Gasser, C. T.; Regitnig, P. 2005. Determination of layer-specific mechanical properties of human coronary arteries with nonatherosclerotic intimal thickening and related constitutive modeling, *American Journal of Physiology – Heart and Circulatory Physiology* 289(5): H2048–H2058.

Hysi, I.; Rebet, O.; Gautier, L.; Fabre, O. 2017. A standardized loop technique for mitral valve repair, *Annals of Thoracic Surgery* 103(1): e105–e106.

Ibrahim, M.; Rao, C.; Athanasiou, T. 2012. Artificial chordae for degenerative mitral valve disease: critical analysis of current techniques, *Interactive CardioVascular and Thoracic Surgery* 15(6): 1019–1032.

Ibrahim, M.; Rao, C.; Savvopoulou, M.; Casula, R.; Athanasiou, T. 2014. Outcomes of mitral valve repair using artificial chordae, *European Journal of Cardio-Thoracic Surgery* 45(4): 593–601.

Jensen, H.; Jensen, M. O.; Waziri, F.; Honge, J. L.; Sloth, E.; Fenger-Gron, M.; Nielsen, S. L. 2014. Transapical neochord implantation: is tension of artificial chordae tendineae dependent on the insertion site, *Journal of Thoracic and Cardiovascular Surgery* 148(1): 138–143.

Jimenez, J. H.; Soerensen, D. D.; He, Z.; He, S.; Yoganathan, A. P. 2003. Effects of a saddle shaped annulus on mitral valve function and chordal force distribution: an in vitro study, *Annals of Biomedical Engineering* 31(10): 1171–1181.

Kiefer, P.; Meier, S.; Noack, T.; Borger, M. A.; Ender, J.; Hoyer, A.; Mohr, F. W.; Seeburger, J. 2018. Good 5-year durability of transapical beating heart off-pump mitral valve repair with neochordae, *Annals of Thoracic Surgery* 106(2): 440–445.

Kiendl, J.; Ming-Chen, H.; Wu, M. C. H.; Reali, A. 2015. Isogeometric Kirchhoff–Love shell formulations for general hyperelastic materials, *Computer Methods in Applied Mechanics and Engineering* 291: 280–303.

Kong, F.; Pham, T.; Martin, C.; Elefteriades, J.; McKay, R.; Primiano, C.; Sun, W. 2018. Finite element analysis of annuloplasty and papillary muscle relocation on a patient-specific mitral regurgitation model, *PLoS One* 13(6): e0198331.

Krishnamurthy, G.; Ennis, D. B.; Itoh, A.; Bothe, W.; Swanson, J. C.; Karlsson, M.; Kuhl, E.; Miller, D. C.; Ingels Jr., N. B. 2008. Material properties of the ovine mitral valve anterior leaflet in vivo from inverse finite element analysis, *American Journal of Physiology-Heart and Circulatory Physiology* 295(3): H1141–H1149.

Kunzelman, K. S.; Cochran, R. P. 1990. Mechanical properties of basal and marginal mitral valve chordae tendineae, *ASAIO transactions* 36(3): M405–M408.

Kunzelman, K. S.; Cochran, R. P. 1992. Stress/strain characteristics of porcine mitral valve tissue: parallel versus perpendicular collagen orientation, *Journal of Cardiac Surgery* 7(1): 71–78.

Kunzelman, K. S.; Cochran, R. P.; Chuong, C.; Ring, W. S.; Verrier, E. D.; Eberhart, R. D. 1993. Finite element analysis of the mitral valve, *Journal of Heart Valve Disease* 2(3): 326–340.

Kunzelman, K. S.; Cochran, R. P.; Verrier, E. D.; Eberhart, R. C. 1994. Anatomic basis for mitral valve modelling, *Journal of Heart Valve Disease* 3(5): 491–496.

Kunzelman, K.; Reimink, M. S.; Verrier, E. D.; Cochran, R. P. 1996. Replacement of mitral valve posterior chordae tendineae with expanded polytetrafluoroethylene suture: a finite element study, *Journal of Cardiac Surgery* 11(2): 136–145.

Kunzelman, K. S.; Reimink, M. S.; Cochran, R. P. 1997. Annular dilatation increases stress in the mitral valve and delays coaptation: a finite element computer model, *Cardiovascular Surgery* 5(4): 427–434.

Kunzelman, K. S.; Quick, D. W.; Cochran, R. P. 1998. Altered collagen concentration in mitral valve leaflets: biochemical and finite element analysis, *Annals of Thoracic Surgery* 66(6): S198–S205.

Kunzelman, K. S.; Einstein, D. R.; Cochran, R. P. 2007. Fluid-structure interaction models of the mitral valve: function in normal and pathological states, *Philosophical Transactions of the Royal Society B: Biological Sciences* 362(1484): 1393–1406.

Lam, J. H.; Ranganathan, N.; Wigle, E. D.; Silver, M. D. 1970. Morphology of the human mitral valve. I. Chordae tendineae: a new classification, *Circulation* 41(3): 449–458.

Lancellotti, P.; Radermecker, M.; Durieux, R.; Modine, T.; Oury, C.; Fattouch, K. 2016. Transapical beating-heart chordae implantation in mitral regurgitation: a new horizon for repairing mitral valve prolapse, *Journal of Thoracic Disease* 8(12): E1665–E1671.

Lau, K. D.; Diaz, V.; Scambler, P.; Burriesci, G. 2010. Mitral valve dynamics in structural and fluid-structure interaction models, *Medical Engineering & Physics* 32(9): 1057–1064.

Lau, K. D.; Díaz-Zuccarini, V.; Scambler, P.; Burriesci, G. 2011. Fluid-structure interaction study of the edge-to-edge repair technique on the mitral valve, *Journal of Biomechanics* 44(13): 2409–2417.

Laulusa, A.; Bauchau, O. A.; Choi, J.-Y.; Tan, V. B. C.; Li, L. 2006. Evaluation of some shear deformable shell elements, *International Journal of Solids and Structures* 43(17): 5033–5054.

Lee, C. H.; Oomen, P. J. A.; Rabbah, J. P.; Yoganathan, A.; Gorman, R. C.; Gorman 3rd, J. H.; Amini, R.; Sacks, M. S. 2013. A high-fidelity and micro-anatomically accurate 3D finite element model for simulations of functional mitral valve, in *Functional Imaging and Modeling of the Heart. Lecture Notes in Computer Science (vol. 7945)*. Berlin Heidelberg: Springer-Verlag, 416–424.

Lee, C. H.; Rabbah, J. P.; Yoganathan, A. P.; Gorman, R. C.; Gorman 3rd, J. H.; Sacks M. S. 2015. On the effects of leaflet microstructure and constitutive model on the closing behavior of the mitral valve, *Biomechanics and Modeling in Mechanobiology* 14(6): 1281–1302.

Levine, R. A.; Triulzi, M. O.; Harrigan, P.; Weyman, A. E. 1987. The relationship of mitral annular shape to the diagnosis of mitral valve prolapse, *Circulation* 75(4): 756–767.

Liao, J.; Vesely, I. 2003. A structural basis for the size-related mechanical properties of mitral valve chordae tendineae, *Journal of Biomechanics* 36(8): 1125–1133.

Lim, K. H.; Yeo, J. H.; Duran, C. M. 2005. Three-dimensional asymmetrical modeling of the mitral valve: a finite element study with dynamic boundaries, *Journal of Heart Valve Disease* 14(3): 386–392.

Liu, G. R.; Quek, S. S. 2014. *The Finite Element Method: A Practical Course* (2nd ed.). Oxford: Butterworth-Heinemann.

Ma, X.; Gao, H.; Griffith, B. E.; Berry, C.; Luo, X. 2013. Image-based fluid-structure interaction model of the human mitral valve, *Computers & Fluids* 71: 417–425.

Madu, E. C.; D'Cruz, I. A. 1997. The vital role of papillary muscles in mitral and ventricular function: echocardiographic insights, *Clinical Cardiology* 20(2): 93–98.

Mansi, T.; Voigt, I.; Georgescu, B.; Zheng, X.; Mengue, E. A.; Hackl, M.; Ionasec, R. I.; Noack, T.; Seeburger, J.; Comaniciu, D. 2012. An integrated framework for finite-element modeling of mitral valve biomechanics from medical images: application to MitralClip intervention planning, *Medical Image Analysis* 16(7): 1330–1346.

May-Newman, K.; Yin, F. C. 1998. A constitutive law for mitral valve tissue, *Journal of Biomechanical Engineering* 120(1): 38–47.

Merk, D. R.; Aidietis, A.; Seeburger, J. 2015. Off-pump transapical neo-chordae implantation, *Annals of Cardiothoracic Surgery* 4(3): 293–294.

Mick, S. L.; Keshavamurthy, S.; Gillinov, A. M. 2015. Mitral valve repair versus replacement, *Annals of Cardiothoracic Surgery* 4(3): 230–237.

Mihăilă, S.; Muraru, D.; Piasentini, E.; Miglioranza, M. H.; Peluso, D.; Cucchini, U.; Iliceto, S.; Vinereanu, D.; Badano, L. P. 2014. Quantitative analysis of mitral annular geometry and function in healthy volunteers using transthoracic three-dimensional echocardiography, *Journal of the American Society of Echocardiography* 27(8): 846–857.

Morgan, A. E.; Pantoja, J. L.; Grossi, E. A.; Ge, L.; Weinsaft, J.W.; Ratcliffe, M.B. 2016. Neochord placement versus triangular resection in mitral valve repair: a finite element model, *Journal of Surgical Research* 206(1): 98–105.

Munín, M.; Thierer, J.; Raggio, I. M.; Goerner, M. S.; Lombardero, M.; Godia, J.; Sánchez, G. A.; Spernanzoni, F.; Ortega, J.; Torres, V. 2014. Three-dimensional echocardiographic analysis of mitral valve characteristics, *Argentine Journal of Cardiology* 82(4): 279–284.

NeoChord. 2016. *NeoChord Artificial Chordae Delivery System Model DS1000: Instructions for Use*. Minnesota: NeoChord.

Nishimura, R. A.; Vahanian, A.; Eleid, M. F.; Mack, M. J. 2016. Mitral valve disease – current management and future challenges, *Lancet* 387(10025): 1324–1334.

Obadia, J. F.; Casali, C.; Chassignolle, J. F.; Janier, M. 1997. Mitral subvalvular apparatus: different functions of primary and secondary chordae, *Circulation* 96(9): 3124–3128.

Pappalardo, O. A.; Sturla, F.; Onorati, F.; Puppini, G.; Selmi, M.; Luciani, G. B.; Faggian, G.; Redaelli, A.; Votta, E. 2017. Mass-spring models for the simulation of mitral valve function: looking for a trade-off between reliability and time-efficiency, *Medical Engineering & Physics* 47: 93–104.

Pham, T.; Sun, W. 2014. Material properties of aged human mitral valve leaflets, *Journal of Biomedical Materials Research* 102(8): 2692–2703.

Pozzoli, A.; De Bonis, M.; Alfieri, O. 2016. Mitral valve repair, *F1000Research* 5: 1326.

Prot, V.; Skallerud, B.; Holzapfel, G. A. 2007. Transversely isotropic membrane shells with application to mitral valve mechanics. Constitutive modelling and finite element implementation, *International Journal for Numerical Methods in Engineering* 71(8): 987–1008.

Prot, V.; Skallerud, B.; Haaverstad, R. 2009a. Finite element analysis of the mitral apparatus: annulus shape effect and chordal force distribution, *Biomechanics and Modeling in Mechanobiology* 8(1): 43–55.

Prot, V.; Skallerud, B. 2009b. Nonlinear solid finite element analysis of mitral valves with heterogeneous leaflet layers, *Computational Mechanics* 43(3): 353–368.

Prot, V.; Skallerud, B.; Sommer, G.; Holzapfel, G. A. 2010. On modelling and analysis of healthy and pathological human mitral valves: two case studies, *Journal of the Mechanical Behavior of Biomedical Materials* 3(2): 167–177.

Ranzi, G.; Gilbert, R. I. 2014. *Structural Analysis: Principles, Methods and Modelling*. Boca Raton: CRC Press.

Reimink, M. S.; Kunzelman, K. S.; Verrier, E. D.; Cochran, R. P. 1995. The effect of anterior chordal replacement on mitral valve function and stresses. A finite element study, *ASAIO Journal* 41(3): M754–M762.

Rim, Y.; McPherson, D. D.; Chandran, K. B.; Kim, H. 2013. The effect of patient-specific annular motion on dynamic simulation of mitral valve function, *Journal of Biomechanics* 46(4): 1104–1112.

Rim, Y.; Laing, S. T.; McPherson, D. D.; Kim, H. 2014. Mitral valve repair using ePTFE sutures for ruptured mitral chordae tendineae: a computational simulation study, *Annals of Biomedical Engineering* 42(1): 139–148.

Rim, Y.; Choi, A.; McPherson, D. D.; Kim, H. 2015. Personalized computational modeling of mitral valve prolapse: virtual leaflet resection, *PLoS One* 10(6): e0130906.

Ritchie, J.; Warnock, J. N.; Yoganathan, A. P. 2005. Structural characterization of the chordae tendineae in native porcine mitral valves, *Annals of Thoracic Surgery* 80(1): 189–197.

Rucinskas, K.; Janusauskas, V.; Zakarkaite, D.; Aidietiene, S.; Samalavicius, R.; Speziali, G.; Aidietis, A. 2014. Off-pump transapical implantation of artificial chordae to correct mitral regurgitation: early results of a single-center experience, *Journal of Thoracic and Cardiovascular Surgery* 147(1): 95–99.

Saito, K.; Okura, H.; Watanabe, N.; Obase, K.; Tamada, T.; Koyama, T.; Hayashida, A.; Neishi, Y.; Kawamoto, T.; Yoshida, K. 2012. Influence of chronic tethering of the mitral valve on mitral leaflet size and coaptation in functional mitral regurgitation, *JACC: Cardiovascular Imaging* 5(4): 337–345.

Salvador, L.; Mirone, S.; Bianchini, R.; Regesta, T.; Patelli, F.; Minniti, G.; Masat, M.; Cavarretta, E.; Valfrè, C. 2008. A 20-year experience with mitral valve repair with artificial chordae in 608 patients, *Journal of Thoracic and Cardiovascular Surgery* 135(6): 1280–1287.

Sedransk, K. L.; Grande-Allen, K. J.; Vesely, I. 2002. Failure mechanics of mitral valve chordae tendineae, *Journal of Heart Valve Disease* 11(5): 644–650.

Seeburger, J.; Borger, M. A.; Tschernich, H.; Leontjev, S.; Holzhey, D.; Noack, T.; Ender, J.; Mohr, F. W. 2010. Transapical beating heart mitral valve repair, *Circulation: Cardiovascular Interventions* 3(6): 611–612.

Seeburger, J.; Leontjev, S.; Neumuth, M.; Noack, T.; Höbartner, M.; Misfeld, M.; Borger, M. A.; Mohr, F. W. 2012. Trans-apical beating-heart implantation of neo-chordae to mitral valve leaflets: results of an acute animal study, *European Journal of Cardio-Thoracic Surgery* 41(1): 173–176.

Shah, P. M. 2010. Current concepts in mitral valve prolapse – diagnosis and management, *Journal of Cardiology* 56(2): 125–133.

Shibata, T.; Kato, Y.; Motoki, M.; Takahashi, Y.; Morisaki, A.; Nishimura, S.; Hattori, K. 2015. Mitral valve repair with loop technique via median sternotomy in 180 patients, *European Journal of Cardio-Thoracic Surgery* 47(3): 491–496.

Siefert, A. W.; Rabbah, J. P.; Pierce, E. L.; Kunzelman, K. S.; Yoganathan, A. P. 2014. Quantitative evaluation of annuloplasty on mitral valve chordae tendineae forces to

supplement surgical planning model development, *Cardiovascular Engineering and Technology* 5(1): 35–43.

Sonne, C.; Sugeng, L.; Watanabe, N.; Weinert, L.; Saito, K.; Tsukiji, M.; Yoshida, K.; Takeuchi, M.; Mor-Avi, V.; Lang, R. M. 2009. Age and body surface area dependency of mitral valve and papillary apparatus parameters: assessment by real-time three-dimensional echocardiography, *European Journal of Echocardiography* 10(2): 287–294.

Stevanella, M.; Maffessanti, F.; Conti, C. A.; Votta, E.; Arnoldi, A.; Lombardi, M.; Parodi, O.; Caiani, E. G.; Redaelli, A. 2011. Mitral valve patient-specific finite element modeling from cardiac MRI: application to an annuloplasty procedure, *Cardiovascular Engineering and Technology* 2(2): 66–76.

Sturla, F.; Onorati, F.; Votta, E.; Pechlivanidis, K.; Stevanella, M.; Milano, A. D.; Puppini, G.; Mazzucco, A.; Redaelli, A.; Faggian, G. 2014. Is it possible to assess the best mitral valve repair in the individual patient? Preliminary results of a finite element study from magnetic resonance imaging data, *Journal of Thoracic and Cardiovascular Surgery* 148(3): 1025–1034.

Sturla, F.; Redaelli, A.; Puppini, G.; Onorati, F.; Faggian, G.; Votta, E. 2015a. Functional and biomechanical effects of the edge-to-edge repair in the setting of mitral regurgitation: consolidated knowledge and novel tools to gain insight into its percutaneous implementation, *Cardiovascular Engineering and Technology* 6(2): 117–140.

Sturla, F.; Votta, E.; Onorati, F.; Pechlivanidis, K.; Pappalardo, O. A.; Gottin, L.; Milano, A. D.; Puppini, G.; Redaelli, A.; Faggian, G. 2015b. Biomechanical drawbacks of different techniques of mitral neochordal implantation: When an apparently optimal repair can fail, *Journal of Thoracic and Cardiovascular Surgery* 150(5): 1303–1312.

Sturla, F.; Onorati, F.; Votta, E.; Stevanella, M.; Milano, A. D.; Pechlivanidis, K.; Puppini, G.; Redaelli, A.; Faggian, G. 2015c. Repair of mitral valve prolapse through ePTFE neochordae: a finite element approach from CMR, in *Biomedical Technology. Lecture Notes in Applied and Computational Mechanics (vol. 74).* Cham: Springer, 117–128.

Sun, W.; Martin, C.; Pham, T. 2014. Computational modeling of cardiac valve function and intervention, *Annual Review of Biomedical Engineering* 16: 53–76.

Suzuki, K.; Murata, M.; Yasuda, R.; Tsuruta, H.; Tomotsugu, N.; Abe, T.; Iwanaga, S.; Akaishi, M.; Fukuda, K. 2012. Effect of lesional differences in prolapsed leaflets on clinical outcomes in patients with mitral valve prolapse, *American Journal of Cardiovascular Disease* 2(3): 152–159.

Toma, M.; Jensen, M. Ø.; Einstein, D. R.; Yoganathan, A. P.; Cochran, R. P.; Kunzelman, K. S. 2016. Fluid-structure interaction analysis of papillary muscle forces using a comprehensive mitral valve model with 3D chordal structure, *Annals of Biomedical Engineering* 44(4): 942–953.

Toma, M.; Einstein, D. R.; Bloodworth 4th, C. H.; Cochran, R. P.; Yoganathan, A. P.; Kunzelman, K. S. 2017. Fluid-structure interaction and structural analyses using a comprehensive mitral valve model with 3D chordal structure, *International Journal for Numerical Methods in Biomedical Engineering* 33(4): e2815.

Uretsky, S.; Argulian, E.; Narula, J.; Wolff, S. D. 2018. Use of cardiac magnetic resonance imaging in assessing mitral regurgitation: current evidence, *Journal of the American College of Cardiology* 71(5): 547–563.

Votta, E.; Maisano, F.; Soncini, M.; Redaelli, A.; Montevecchi, F. M.; Alfieri, O. 2002. 3-D computational analysis of the stress distribution on the leaflets after edge-to-edge repair of mitral regurgitation, *Journal of Heart Valve Disease* 11(6): 810–822.

Votta, E.; Redaelli, A.; Soncini, M.; Arcobasso, L.; Maisano, F.; Alfieri, O.; Montevecchi, F. M. 2003. 3-D computational models for the simulation of mitral valve annuloplasty, in *Proceedings of the Summer Bioengineering Conference*. New York: ASME, 735–736.

Votta, E.; Maisano, F.; Bolling, S. F.; Alfieri, O.; Montevecchi, F. M.; Redaelli, A. 2007. The Geoform disease-specific annuloplasty system: a finite element study, *Annals of Thoracic Surgery* 84(1): 92–101.

Votta, E.; Caiani, E.; Veronesi, F.; Soncini, M.; Montevecchi, F. M.; Redaelli, A. 2008a. Mitral valve finite-element modelling from ultrasound data: a pilot study for a new approach to understand mitral function and clinical scenarios, *Philosophical Transactions of the Royal Society A: Mathematical, Physical and Engineering Sciences* 366(1879): 3411–3434.

Votta, E.; Arnoldi, A.; Stevanella, M.; Veronesi, F.; Tamborini, G.; Alamanni, F.; Caiani, E. G.; Redaelli, A. 2008b. From real-time 3D echocardiography to mitral valve finite element analysis: a novel modeling approach, in *Computers in Cardiology (vol. 35)*. Piscataway: IEEE, 1–4.

Votta, E.; Arnoldi, A.; Invernizzi, A.; Ponzini, R.; Veronesi, F.; Tamborini, G.; Pepi, M.; Alamanni, F.; Redaelli, A.; Caiani, E. G. 2009. Mitral valve patient-specific finite element modeling from 3-D real time echocardiography: a potential new tool for surgical planning, in *Proceedings of the Workshop on Cardiovascular Interventional Imaging and Biophysical Modelling*. London: MICCAI, 1–9.

Wang, Q.; Sun, W. 2013. Finite element modeling of mitral valve dynamic deformation using patient-specific multi-slices computed tomography scans, *Annals of Biomedical Engineering* 41(1): 142–153.

Weber, A.; Hurni, S.; Vandenberghe, S.; Wahl, A.; Aymard, T.; Vogel, R.; Carrel, T. 2012. Ideal site for ventricular anchoring of artificial chordae in mitral regurgitation, *Journal of Thoracic and Cardiovascular Surgery* 143(S4): S78–S81.

Xu, C.; Brinster, C. J.; Jassar, A. S.; Vergnat, M.; Eperjesi, T. J.; Gorman, R. C.; Gorman 3rd, J. H.; Jackson, B. M. 2010. A novel approach to in vivo mitral valve stress analysis, *American Journal of Physiology – Heart and Circulatory Physiology* 299(6): H1790–H1794.

Zeng, X.; Tan, T. C.; Dudzinski, D. M.; Hung, J. 2014. Echocardiography of the mitral valve, *Progress in Cardiovascular Diseases* 57(1): 55–73.

Zhong, Q.; Zeng, W.; Huang, X.; Zhao, X. 2014. Finite element analysis for edge-to-edge technique to treat post-mitral valve repair systolic anterior motion, *Acta of Bioengineering and Biomechanics* 16(4): 3–12.

Zhu, X. (ed.). 2015. *Surgical Atlas of Cardiac Anatomy*. Dordrecht: Springer.

Zuo, K.; Pham, T.; Li, K.; Martin, C.; He, Z.; Sun, W. 2016. Characterization of biomechanical properties of aged human and ovine mitral valve chordae tendineae, *Journal of the Mechanical Behavior of Biomedical Materials* 62: 607–618.

List of Scientific Publications by the Author on the Topic of the Dissertation

Publications in the Reviewed Scientific Journals

Gaidulis, G.; Selmi, M.; Zakarkaitė, D.; Aidietis, A.; Kačianauskas, R. 2019. Modelling and simulation of mitral valve for transapical repair applications, *Nonlinear Analysis: Modelling and Control* 24(4): 485–502. doi: 10.15388/NA.2019.4.1 (Clarivate Analytics Web of Science).

Gaidulis, G.; Votta, E.; Selmi, M.; Aidietienė, S.; Aidietis, A.; Kačianauskas, R. 2018a. Numerical simulation of transapical off-pump mitral valve repair with neochordae implantation, *Technology and Health Care* 26(S2): 635–645. doi: 10.3233/THC-182510 (Clarivate Analytics Web of Science).

Gaidulis, G.; Kačianauskas, R.; Kizilova, N.; Romashov, Y. 2018b. A mechanical model of heart valves with chordae for in silico real-time computations and cardiac surgery planning, *Engineering Transactions* 66(4): 391–412. doi: 10.24423/EngTrans.723.20180924.

Publications in Other Editions

Romashov, Y.; Kizilova, N.; Gaidulis, G. 2016. Mathematical modeling of mitral valve dynamics: nonlinear vs linear models, in *Proceedings of the 5th International Conference on Nonlinear Dynamics (ND-KhPI'2016), Kharkov, Ukraine, September 27–30, 2016*. Kharkov: National Technical University “Kharkov Polytechnical Institute”, 208–215.

Summary in Lithuanian

Įvadas

Problemos formulavimas

Skaitiniai metodai, ypač baigtinių elementų metodas (BEM), sėkmingai taikomi struktūrinei analizei, pastaruoju metu pradėti naudoti ir biologinių objektų modeliavimui. Žmogaus kūno, įskaitant širdies ir kraujotakos sistemą, funkcijų mechaniniai tyrimai vis dažniau yra atliekami taikant BEM. Tokie tyrimai padeda kiekybiškai įvertinti pažeistos ar ligos paveiktos širdies mechanikos pokyčius, ištirti jos fiziologiją ir patologiją bei naujų gydymo metodų poveikį.

Širdies ir kraujagyslių ligos yra pagrindinė mirties priežastis pasaulyje. Galima išskirti įvairias širdies ir kraujagyslių ligas, įskaitant širdies vožtuvų pažeidimus ar defektus. Mitralinio vožtuvo (MV) prolapsas su mitraline regurgitacija yra labiausiai paplitusi vožtuvų liga, kuria serga apie 2–3 % pasaulio gyventojų. Šią ligą dažniausiai sukelia vožtuvo judesius ribojančių struktūrų sutrikimai. Dažniausias iš jų – ligos paveiktų vienos ar kelių chordų nutrūkimas, kuris įvyksta, kai dėl tempimo jėgų chordose susidarę įtempiai viršija ribinę vertę.

Transapikalinė MV korekcija implantuojant neochordas per širdies viršūnę yra naujas chirurginis būdas, leidžiantis atlikti mitralinės regurgitacijos, atsiradusios dėl nutrūkusių chordų, korekciją minimaliai invaziniu būdu. Nors transapikalinės MV korekcijos klinikiniai rezultatai yra geri, kyla problemų, susijusių su pačiu chirurginiu būdu. Šiuo metu tam tikri metodo aspektai, pavyzdžiui, implantuojamos neochordos padėties ar ilgio

nustatymas, kuris užtikrintų vožtuvo nesandarumo pašalinimą, bet nesuvaržytų burių judesio, vis dar nėra pakankamai ištyrinėti. Norint ištirti šiuos transapikalinės chirurginės procedūros aspektus, šioje disertacijoje atliekamas MV struktūros ir transapikalinės jo korekcijos modeliavimas baigtinių elementų metodu.

Darbo aktualumas

Pastarųjų trijų dešimtmečių tyrimai rodo, kad skirtingų MV korekcijų skaitinio modeliavimo tyrimai yra naudingi, nes padeda kiekybiškai įvertinti tokių procedūrų biomechaninius aspektus. Visgi, iki šiol paskelbti tik keli tyrimai aprašantys MV korekcijos implantuojant neochordas modeliavimą. Be to, nei viename iš jų netiriama transapikalinės MV korekcijos problema.

Šioje disertacijoje sudaryta virtualios MV korekcijos modeliavimo strategija ir pagal ultragarsinio tyrimo metu gautus paciento duomenis sukurtas MV netiesinis baigtinių elementų modelis. Pagrindinis iššūkis, susijęs su transapikaline MV korekcija – implantuotų neochordų ilgio nustatymas ir šio ilgio įtaka pooperacinio vožtuvo funkcijai. Implantavus per trumpas arba per ilgas neochordas kyla koreguotos burės plyšimo arba liekamojo prolapso rizika. Kadangi atliekant transapikalinę MV korekciją tinkamas neochordų ilgis nustatomas remiantis vien tik ultragarsinio tyrimo metu gaunamais vaizdais, iki šiol nebuvo sukurtas metodas, leidžiantis apskaičiuoti šį ilgį skaitiniuose modeliuose. Todėl šiame darbe taikant BEM pirmiausia įvertinta neochordų ilgio įtaka nesandaraus MV funkcijos atkūrimui, o tada pasiūlytas metodas, padedantis nustatyti tinkamą neochordų ilgį virtualios transapikalinės MV korekcijos metu.

Tyrimo objektas

Šio tyrimo objektas – mitralinis vožtuvas, paveiktas prolapso ir regurgitacijos dėl chordų nutrūkimo, ir jo korekcijos implantuojant neochordas transapikaliniu būdu skaitinis modeliavimas.

Darbo tikslas

Pagrindinis darbo tikslas – nustatyti mitralinio vožtuvo biomechaninius parametrus po transapikalinės korekcijos ir įvertinti tokios operacijos poveikį pooperacinei mitralinio vožtuvo funkcijai.

Darbo uždaviniai

Siekiant įgyvendinti šio darbo tikslą, reikia spręsti šiuos uždavinius:

1. Apžvelgti tyrimus, kuriuose aprašomi skaitiniai modeliai, naudoti mitralinio vožtuvo biomechaninėms funkcijoms tirti, ir išnagrinėti jų tinkamumą naujiems mitralinio vožtuvo korekcijos chirurginiams būdams vertinti.
2. Sukurti virtualios transapikalinės korekcijos skaitinės simuliacijos modeliavimo strategiją.

3. Pagal ultragarsinio tyrimo metu gautus duomenis ir mitralinio vožtuvo judėjimo kinematinius parametrus atkurti personalizuotą mitralinio vožtuvo geometriją ir remiantis ja sudaryti nesandaraus mitralinio vožtuvo struktūrinį baigtinių elementų modelį.
4. Pritaikyti sukurtą modelį virtualios transapikalinės mitralinio vožtuvo korekcijos procedūrai ir atlikti vožtuvo sistolinės funkcijos simuliaciją bei ištirti neochordų ilgio įtaką pooperacinei mitralinio vožtuvo funkcijai.
5. Įvertinti virtualios transapikalinės mitralinio vožtuvo korekcijos rezultatus ir sukurtos skaitinio modeliavimo strategijos tinkamumą šios procedūros veiksmingumo vertinimui.

Tyrimo metodika

Siekiant išnagrinėti tiriamąjį objektą ir naujausius jo modeliavimo metodus, o taip pat atlikti gautų rezultatų įvertinimą, buvo atlikta literatūros ir lyginamoji analizės. Paciento MV struktūros ir judėjimo ankstyvosios sistolės metu duomenys gauti atlikus ultragarsinį tyrimą, o MV struktūrinės analizės ir transapikalinės korekcijos skaičiavimai atlikti kompiuterine programa „Abaqus“ taikant BEM.

Darbo mokslinis naujumas

Pristatytos šios transapikalinės MV korekcijos skaitinio modeliavimo naujovės:

1. Sukurta virtualios korekcijos modeliavimo strategija, kurios metu ultragarsiniai duomenys konvertuojami į baigtinių elementų modelį, atliekama jo virtuali transapikalinė korekcija ir MV sistolinės funkcijos dinaminė simuliacija.
2. Įvertintas neochordų ilgio poveikis MV sandarumo atkūrimui ir pasiūlytas šio ilgio nustatymo atliekant transapikalinę korekciją metodas.
3. Atlikus virtualią transapikalinę MV korekciją, apskaičiuoti biomechaniniai parametrai, aprašantys MV deformacijas, tempimo jėgas chordose ir neochordose, reakcijos jėgas papiliariniuose raumenyse ir širdies viršūnėje bei įtempių pasiskirstymą vožtuvo burėse.

Darbo rezultatų praktinė reikšmė

Šiame darbe MV transapikalinės korekcijos personalizuota skaitinio modeliavimo strategija leido nustatyti kiekybinius tokios chirurginės procedūros parametrus ir įvertinti, kokią įtaką neochordų implantacija turi pooperacinei MV funkcijai. Virtualūs modeliai tinka tirti MV deformacijas, veikiančias jėgas ir įtempių pasiskirstymą bei gali būti naudojami prognozuojant pooperacinę MV morfologiją bei burių koaptaciją kaip pagrindinius MV prolapso pašalinimo veiksnius. Kadangi pristatytoje modeliavimo strategijoje pateikiama išsami MV biomechanikos kiekybinė analizė, tokia strategija gali turėti praktinės klinikinės vertės.

Ginamieji teiginiai

1. Žvelgiant iš mechanikos mokslo perspektyvos, MV gali būti laikoma mechanine sistema, todėl šio biologinio objekto struktūrą galima modeliuoti taikant skaitinius metodus.
2. MV transapikalinės korekcijos metu pašalinamas vožtuvo prolapsas, atkuriama burių koaptacija, sumažėja tempimo jėgos chordose ir įtempiai burėse.
3. Tinkamas neochordų ilgio parinkimas sumažina liekamojo prolapso arba koreguotos burės plyšimo riziką.
4. Virtuali transapikalinė MV korekcija padeda prognozuoti pooperacinę vožtuvo morfologiją ir burių koaptaciją.

Darbo rezultatų aprobavimas

Disertacijos tema paskelbtos keturios mokslinės publikacijos: dvi – žurnaluose, įtrauktuose į „Clarivate Analytics Web of Science“ duomenų bazę (Gaidulis *et al.* 2018a; 2019), viena – žurnale, įtrauktame į kitas duomenų bazes (Gaidulis *et al.* 2018b), ir viena – tarptautinės konferencijos pranešimų medžiagoje (Romashov *et al.* 2016). Tyrimų rezultatai pristatyti septyniose tarptautinėse konferencijose:

- 40-ojoje tarptautinėje konferencijoje „SOLMECH 2016“, vykusioje Varšuvoje (Lenkija) 2016 m. rugpjūčio 29 d. – rugsėjo 2 d.
- 5-ojoje tarptautinėje konferencijoje „Nonlinear Dynamics 2016“, vykusioje Charkove (Ukraina) 2016 m. rugsėjo 27–30 d.
- 11-ojoje tarptautinėje konferencijoje „BIOMDLORE 2016“, vykusioje Druskininkuose (Lietuva) 2016 m. spalio 20–22 d.
- 13-ojoje tarptautinėje konferencijoje „Mechatronic Systems and Materials (MSM 2017)“, vykusioje Vilniuje (Lietuva) 2017 m. liepos 3–5 d.
- 12-ojoje tarptautinėje konferencijoje „BIOMDLORE 2018“, vykusioje Balstogėje (Lenkija) 2018 m. birželio 28–30 d.
- 41-ojoje tarptautinėje konferencijoje „SOLMECH 2018“, vykusioje Varšuvoje (Lenkija) 2018 m. rugpjūčio 27–31 d.
- 55-ojoje tarptautinėje konferencijoje „SES 2018“, vykusioje Madride (Ispanija) 2018 m. spalio 10–12 d.

Disertacijos struktūra

Disertaciją sudaro įvadas, trys skyriai, bendrosios išvados, literatūros sąrašas, autoriaus publikacijų sąrašas disertacijos tema ir santrauka lietuvių kalba. Darbo apimtis yra 104 puslapiai, neskaitant priedų, tekste panaudotos 46 numeruotos formulės, 34 paveikslai ir 6 lentelės. Rašant disertaciją buvo panaudoti 124 literatūros šaltiniai.

1. Mitralinio vožtuvo modeliavimo metodų literatūros apžvalga

MV prolapsas – tai būklė, kai vožtuvas širdies veiklos metu neužsidaro sandariai, todėl dalis kraujo iš kairiojo skilvelio sugrįžta atgal į kairįjį priešdrį. Dažna MV nesandarumo priežastis – vienos ar kelių plonyčių sausgyslių, kurios palaiko vožtuvą reikiamoje padėtyje ir yra vadinamos chordomis, nutrūkimas.

MV prolapso korekcija įprastai atliekama pakeičiant nutrūkusias chordas chirurginiais siūlais – tokia procedūra vadinama neochordų implantavimu. Vienas naujausių MV nesandarumo korekcijos metodų – transapikalinė MV korekcija, kai neochordos implantuojamos per širdies viršūnę, atliekant minimalų pjūvį ir nestabdant širdies veiklos. Klinikiniai tokių operacijų rezultatai yra geri (Colli *et al.* 2018), tačiau be išsamesnių tyrimų tam tikri metodo aspektai, pavyzdžiui, tikslus implantuojamos neochordos padėties nustatymas arba reikalingas jos ilgis, šiuo metu gali būti tik numanomi (Seeburger *et al.* 2012). Siekiant ištirti šiuos aspektus, šioje disertacijoje atliekamas MV struktūros ir jo transapikalinės korekcijos skaitinis modeliavimas taikant BEM.

Per pastaruosius tris dešimtmečius atliktų tyrimų taikant skaitinius metodus metu tyrinėtos MV funkcijos (Kunzelman *et al.* 1993; Votta *et al.* 2008a; Toma *et al.* 2016) ir vertinti nauji MV chirurginės korekcijos metodai (Reimink *et al.* 1995; Votta *et al.* 2007; Morgan *et al.* 2016). Galima išskirti dvi skaitinių modelių kategorijas: struktūriniai modeliai neatsižvelgia į kraujo tekėjimą ir naudoja BEM, o skysčio-struktūros sąveikos modeliai tiria sąveiką tarp MV ir kraujo tėkmės, naudodami skaičiuojamąją skysčių dinamiką.

Literatūroje aprašomi struktūriniai MV baigtinių elementų modeliai naudojami tiriant vožtuvo dinamiką, deformacijas ir struktūroje susidarančius įtempius širdies veiklos metu. Šie modeliai tinka tiek fiziologinio, tiek ir patologinio vožtuvo elgsenos tyrimui bei leidžia įvertinti naujų chirurginės korekcijos metodų poveikį vožtuvo darbui. Pirmųjų baigtinių elementų modelių geometrija nebuvo personalizuota, t. y. jie buvo kuriami remiantis anatominiais gyvūnų matavimais su kai kuriais geometriniais supaprastinimais, todėl atspindėjo tik vidutinį tam tikros būklės atvejį be tikslesnių anatominių detalių ir negalėjo būti taikomi klinikiniuose tyrimuose. Kiek vėliau pradėti kurti personalizuoti MV modeliai, kurių geometrija buvo sudaryta remiantis žmogaus širdies ultragarsinio tyrimo arba kompiuterinės tomografijos metu gaunamais vaizdais. Tokie modeliai, turintys realistišką morfologiją ir personalizuotas kraštines sąlygas, naudojami tirti MV mechaniką ir jos pokyčius esant patologijai bei prognozuoti vožtuvo elgseną atlikus patologijos chirurginę korekciją. Literatūroje pateikiami skirtingi vožtuvo korekcijos būdai, tyrinėti naudojant struktūrinius modelius: vožtuvo burės rezekcija (Choi *et al.* 2017), centrinės koaptacijos metodas (Sturla *et al.* 2015a), anuloplastija (Kong *et al.* 2018) ir neochordų implantavimas į papiliarinį raumenį (Morgan *et al.* 2016).

Priešingai nei struktūriniai modeliai, literatūroje aprašyti ir MV tyrimuose taikyti skysčio-struktūros sąveikos modeliai įvertina ne tik MV struktūrą, bet ir kraujo tėkmę bei jų tarpusavio sąveiką, naudodami skaičiuojamąją skysčių dinamiką. Tokie modeliai leidžia atlikti išsamesnę MV fiziologijos analizę, nei struktūriniai modeliai. Visgi, norint sukurti personalizuotą skysčio-struktūros sąveikos modelį, reikalingos kraujo kraštinės sąlygos, kurias nustatyti klinikiniais matavimais yra sunku. Todėl tokie modeliai dažniausiai

kuriami panardinant MV struktūrą ne į kraują, bet į idealizuotą skystį, o tai apriboja jų naudojimą klinikiniuose tyrimuose.

MV struktūros mechaninių savybių aprašymas yra būtinas siekiant atlikti skaitinius vožtuvo tyrimus. Skirtingų vožtuvo komponentų mechaninės savybės skiriasi dėl jų struktūrinių skirtumų. Vožtuvo burės yra sudarytos iš kolageno ir elastino skaidulų, todėl toks audinys yra standesnis skaidulų orientacijos kryptimi. Be to, šios skaidulos pasižymi netiesiškumu, dėl to MV burių mechaninės savybės yra apibūdinamos kaip netiesinės ir anizotropinės. Vožtuvo chordų struktūra skiriasi nuo burių, jos sudarytos daugiausia iš kolageno skaidulų, todėl yra standžios ir tvirtos, o jų mechaninės savybės apibūdinamos kaip netiesinės ir izotropinės.

2. Mitralinio vožtuvo modeliavimo uždavinio formulavimas

Pagrindinė problema, kylanti transapikalinės MV korekcijos metu, yra neochordų ilgio nustatymas. Širdies ciklo metu atstumas tarp MV laisvojo krašto, į kurį implantuojamas vienas neochordos galas, ir širdies viršūnės, prie kurio tvirtinamas kitas galas, nėra pastovus. Todėl reikalinga parinkti tinkamą neochordų ilgį, nes priešingu atveju kyla burės plyšimo rizika, jei implantuotos neochordos yra per trumpos, arba vožtuvo nesandarumas gali išlikti, jei neochordos yra per ilgos.

Šioje disertacijoje neochordų ilgio nustatymo problema sprendžiama pasitelkus BEM. Sudaroma modeliavimo strategija, kurios metu pagal ultragarsinio tyrimo duomenis sukuriamas personalizuotas nesandaraus MV baigtinių elementų modelis, atliekama jo virtuali transapikalinė korekcija ir sistolinės funkcijos dinaminė simuliacija baigtinių elementų kompiuterinėje programoje „Abaqus“.

MV baigtinių elementų modelio bet kurio mazgo *i* pagreičiai kiekvieno simuliacijos žingsnio *n* pradžioje yra apskaičiuojami pagal formulę:

$$\ddot{\mathbf{u}}_i^{(n)} = \left(\mathbf{M}\right)^{-1}\left(\mathbf{P}_i^{(n)} - \mathbf{I}_i^{(n)}\right), \tag{S2.1}$$

čia $\ddot{\mathbf{u}}_i$ – pagreičio vektorius, $\mathbf{M}$ – masių matrica, $\mathbf{P}_i$ – išorinių jėgų vektorius, $\mathbf{I}_i$ – vidinių jėgų vektorius.

Mazgų judėjimo lygtys sudaromos integruojant centrinių skirtumų metodu:

$$\dot{\mathbf{u}}_i^{(n+1/2)} = \dot{\mathbf{u}}_i^{(n-1/2)} + \frac{\Delta t^{(n+1)} + \Delta t^{(n)}}{2}\ddot{\mathbf{u}}_i^{(n)}; \tag{S2.2}$$

$$\mathbf{u}_i^{(n+1)} = \mathbf{u}_i^{(n)} + \Delta t^{(n+1)}\dot{\mathbf{u}}_i^{(n+1/2)}, \tag{S2.3}$$

čia $\dot{\mathbf{u}}_i$ – greičio vektorius, $\mathbf{u}_i$ – poslinkio vektorius, Δt – laiko pokytis.

Apskaičiavus poslinkių reikšmes, nustatomos MV modelio deformacijos $\boldsymbol{\varepsilon}$ ir jame susidarantys įtempiai $\boldsymbol{\sigma}$:

$$\boldsymbol{\varepsilon}^{(n)} = \mathbf{B}\mathbf{u}_i^{(n)}; \tag{S2.4}$$

$$\boldsymbol{\sigma}^{(n)} = \boldsymbol{\sigma}\left(\boldsymbol{\varepsilon}^{(n)}\right), \tag{S2.5}$$

čia **B** – deformacijų-poslinkių matrica.

Norint apskaičiuoti susidarančius įtempius, modeliui reikia priskirti MV struktūros komponentų mechaninių savybių įtempių-poslinkių priklausomybes (S2.5). MV chordų mechaninės savybės aprašomos naudojant 2-os eilės hyperelastinį polinominį modelį:

$$\begin{aligned}\Psi = c_{10}\left(I_1-3\right)+c_{01}\left(I_2-3\right)+c_{11}\left(I_1-3\right)\left(I_2-3\right)+\\ c_{20}\left(I_1-3\right)^2+c_{02}\left(I_2-3\right)^2.\end{aligned} \tag{S2.6}$$

Vožtuvo burių savybės aprašomos taikant hyperelastinį modelį, pasiūlytą Lee *et al.* (2013):

$$\Psi\left(I_1,I_4\right)=c_0\left(I_1-3\right)+c_1\left(\left(1-\beta\right)e^{\left[c_2\left(I_2-3\right)^2\right]}+\beta e^{\left[c_3\left(I_4-1\right)^2\right]}-1\right), \tag{S2.7}$$

čia I_1 ir I_4 – Cauchy-Green deformacijų tenzoriaus invariantai, β, c_0, c_1, c_2, c_3 – konstantos, apibūdinančios medžiagos savybes.

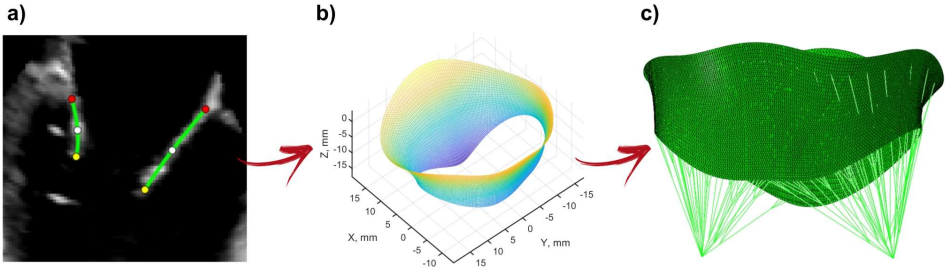

S2.1 pav. Mitralinio vožtuvo baigtinių elemento modelio kūrimas: a) ultragarsinio vaizdo segmentacija; b) vožtuvo geometrinis modelis trimatėje erdvėje; c) baigtinių elementų modelis

Siekiant įgyvendinti sudarytą modeliavimo strategiją, pagal ultragarsinio tyrimo metu gautus vaizdus kuriamas personalizuotas nesandaraus MV baigtinių elementų modelis. Pirmiausia, atliekama vaizdų segmentacija, kurios metu ultragarsiniame vaizde rankiniu būdu išskiriamos mitralinio vožtuvo burės, papiliariniai raumenys ir širdies viršūnė (S2.1 pav. a). Tada sukuriamas trimatis MV burių ir chordų geometrinis modelis (S2.1 pav. b), kuris suskirstomas baigtiniais elementais kompiuterinėje programoje „Abaqus“ (S2.1 pav. c). Vožtuvo burės modeliuojamos 3-jų mazgų netiesiniais kevalo elementais S3R, chordos – netiesiniais santvaros elementais T3D2. Baigtinių elementų modeliui priskiriamos mechaninės savybės ir personalizuotos kraštinės sąlygos, įvertinančios kraujo slėgį ir mitralinio vožtuvo kinematiką širdies ciklo metu. Atliekama virtuali transapikalinė MV korekcija implantuojant neochordas per širdies viršūnę ir vožtuvo sistolinės funkcijos simuliacija „Abaqus“ aplinkoje.

3. Transapikalinės mitralinio vožtuvo korekcijos modeliavimas

Pagal sudarytą modeliavimo strategiją, sukurti du mitralinio vožtuvo modeliai, pirmajam panaudojant sveiko paciento ultragarsinio tyrimo metu gautus duomenis, o antrajam – duomenis paciento su MV prolapsu ir mitraline regurgitacija. Abu modeliai buvo sudaryti laikantis antrajame skyriuje aprašytos modeliavimo strategijos, kai iš ultragarsinių vaizdų žingsnis po žingsnio sukuriamas nesandaraus MV baigtinių elementų modelis, atliekama jo virtuali transapikalinė korekcija ir sistolinės funkcijos simuliacija „Abaqus“ programoje.

Pirmasis MV modelis (S3.1 pav.), darbe vadinamas prolapsuojančiu, buvo skirtas modeliavimo strategijos išbandymui ir neochordų ilgio įtakos pooperacinei MV funkcijai įvertinimui. Pašalinus chordas, pritvirtintas prie užpakalinės burės vidurinio segmento, buvo imituotas MV prolapsas (modelis MVP). Tada atlikta šio nesandaraus modelio virtuali transapikalinė korekcija, naudojant keturias skirtingo ilgio neochordas. Iš viso buvo sukurti keturi pooperaciniai modeliai. Pirmuoju atveju, neochordų ilgis buvo parinktas diastolės metu išmatavus atstumą tarp širdies viršūnės ir prolapsuojančio segmento (modelis VR0). Kituose trijuose modeliuose neochordos buvo prailgintos, prie šio atstumo pridedant atitinkamai 5 %, 10 % ir 15 % ilgio (modeliai VR5, VR10, VR15). Po virtualios korekcijos atlikta kiekvieno iš šių pooperacinių modelių sistolinės funkcijos simuliacija ir įvertinta neochordų ilgio įtaka MV funkcijai.

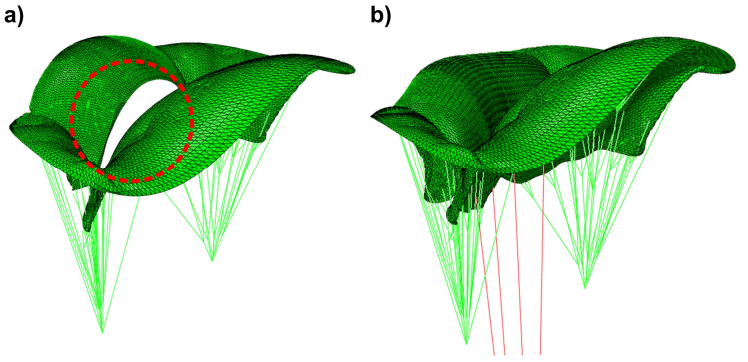

S3.1 pav. Prolapsuojantis mitralinio vožtuvo baigtinių elementų modelis sistolės piko metu: a) prieš virtualią transapikalinę korekciją; b) implantavus keturias neochordas į užpakalinę burę

Nors visos virtualios korekcijos procedūros padidino MV burių koaptacijos plotą (S3.2 pav.), po trumpiausių (modelis VR0) ir ilgiausių (modelis VR15) neochordų implantavimo atkurtos koaptacijos ilgis buvo nepakankamas (mažesnis nei 5 mm). Tai rodo, kad implantavus per trumpas neochordas burės judesys yra suvaržomas, o tai trukdo atkurti tinkamą burių koaptaciją. O implantavus per ilgas neochordas, burės judesys yra suvaržomas nepakankamai, todėl išlieka dalinis burės prolapsas ir MV nesandarumas. Be to, atlikta prolapsuojančio modelio sistolinės funkcijos simuliacija rodo, kad transapikali-

nė korekcija padeda sumažinti įtempius vožtuvo burėse (S3.3 pav.) bei tempimo jėgas chordose, nes dalį šių jėgų perima implantuotos neochordos.

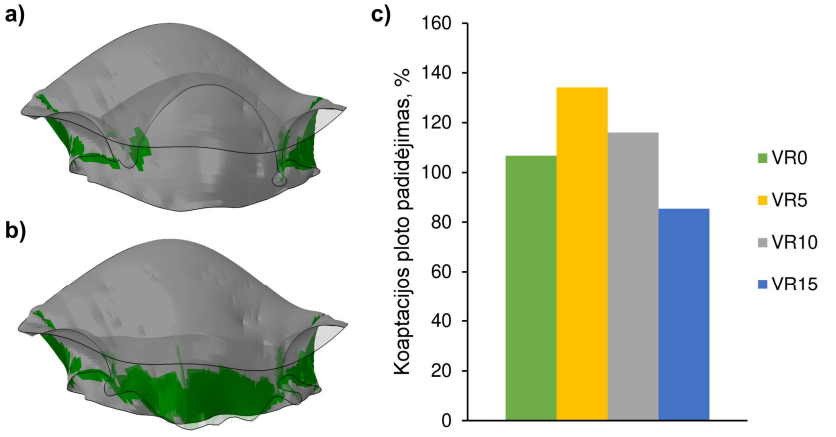

S3.2 pav. Koaptacijos ploto palyginimas prieš ir po virtualios korekcijos: a) koaptacijos plotas prieš virtualią korekciją; b) koaptacijos plotas po neochordų implantavimo (VR5 modelis); c) koaptacijos ploto padidėjimas po kiekvienos virtualios korekcijos procedūros

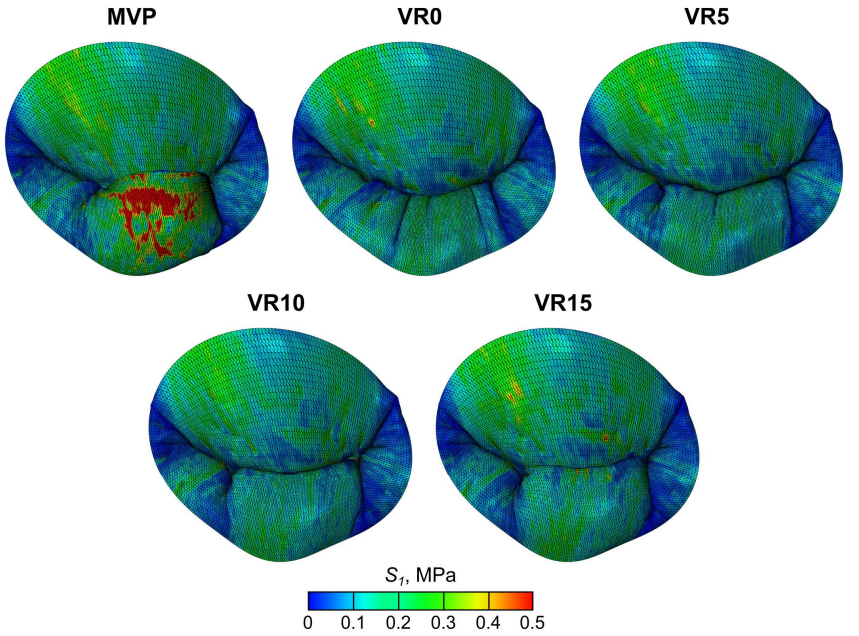

S3.3 pav. Įtempių pasiskirstymas prolapsuojančio mitralinio vožtuvo burėse sistolės piko metu

Įvertinus neochordų ilgio įtaką MV nesandarumo korekcijai, buvo pasiūlytas šio ilgio nustatymo metodas. Tam reikia išmatuoti MV segmento su nutrūkusiomis chordomis laisvojo krašto prolapsavimo aukštį ir eliminuoti šią reikšmę iš atstumo tarp širdies viršūnės ir prolapsuojančio segmento diastolės metu. Pasiūlytas metodas buvo išbandytas atliekant antrojo modelio, darbe vadinamo patologiniu, virtualią transapikalinę korekciją.

Antrasis MV modelis buvo sukurtas pagal realios chirurginės operacijos metu gautus ultragarsinius vaizdus. Šios operacijos metu neochordos buvo implantuotos ne tik į prolapsuojantį užpakalinės burės segmentą, bet ir į procedūros metu pažeistą priekinę burę. Norint pakartoti operacijos eigą, buvo sukurti keturi MV modeliai, kurių kiekvienas atspindėjo atskirą operacijos etapą: (1) modelis su prolapsuojančia užpakaline bure (PLP); (2) modelis po virtualios šios burės korekcijos (PLVR); (3) modelis su operacijos metu atsiradusiu priekinės burės prolapsu (ALP); ir (4) modelis po virtualios priekinės burės korekcijos (ALVR). Kiekvieno modelio sistolinės funkcijos simuliacijos buvo atliktos viena po kitos, taip atkuriant chirurginės operacijos procesą.

Ultragarsinio tyrimo metu buvo gauti tiek priešoperaciniai, tiek ir pooperaciniai vaizdai, todėl atlikus virtualią transapikalinę korekciją buvo galima palyginti baigtinių elementų metodu apskaičiuotą vožtuvo morfologiją su realiu vožtuvo burių išsidėstymu sistolės metu. Gauti rezultatai parodė, kad simuliacijos metu gaunama pakankamai tiksli vožtuvo morfologija, palyginus su ultragarsiniais vaizdais, gautais prieš ir po operacijos (S3.4 pav.).

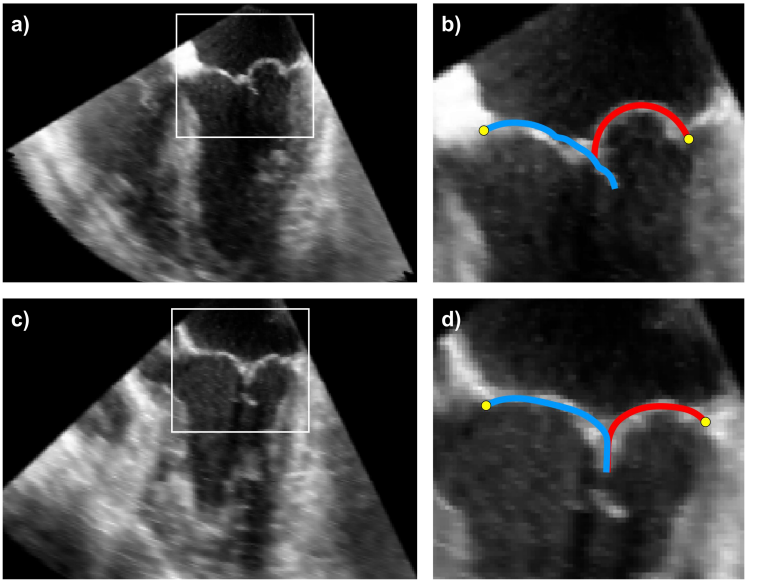

S3.4 pav. Baigtinių elementų modelio morfologijos palyginimas su ultragarsinio tyrimo metu gautais vaizdais: a) priešoperacinis ultragarsinis vaizdas; b) modelio po neochordų implantavimo į užpakalinę burę morfologijos palyginimas su priešoperaciniu ultragarsiniu vaizdu; c) pooperacinis ultragarsinis vaizdas; d) modelio po neochordų implantavimo į priekinę burę morfologijos palyginimas su pooperaciniu ultragarsiniu vaizdu

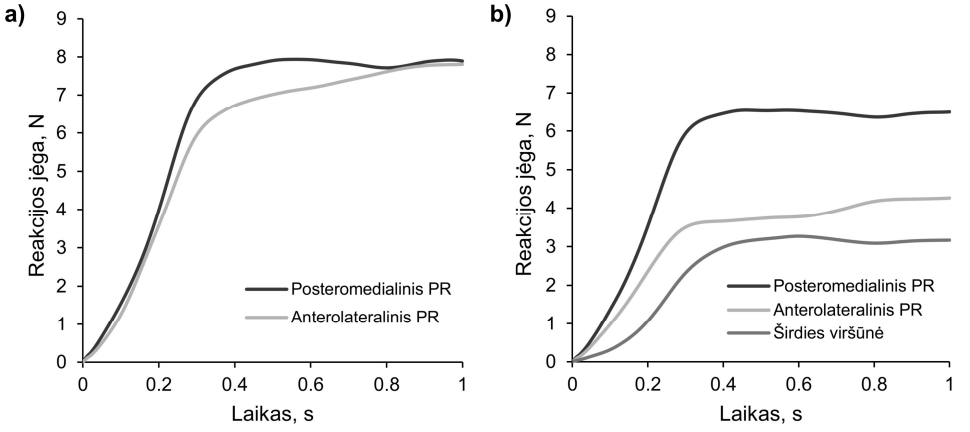

S3.5 pav. Reakcijos jėgos papiliariniuose raumenyse (PR) ir širdies viršūnėje: a) reakcijos jėgos prieš virtualią transapikalinę korekciją; b) reakcijos jėgos po virtualios korekcijos

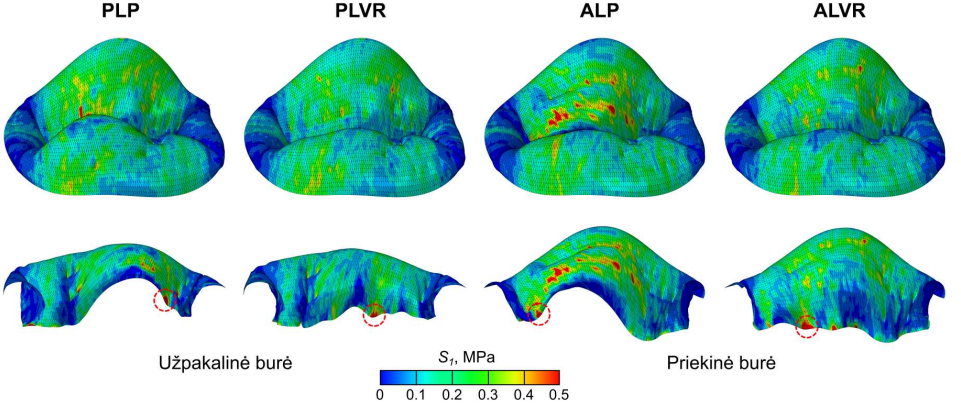

S3.6 pav. Įtempių pasiskirstymas patologinio mitralinio vožtuvo burėse sistolės piko metu. Didžiausios įtempių reikšmės apvestos raudonu apskritimu

Išnagrinėjus simuliacijos metu apskaičiuotus biomechaninius parametrus nustatyta, kad virtuali abiejų burių nesandarumo korekcija pašalino MV prolapsą, atkūrė burių koaptaciją, sumažino tempimo jėgas chordose ir reakcijos jėgas papiliariniuose raumenyse (S3.5 pav.) bei įtempius vožtuvo burėse (S3.6 pav.).

Bendrosios išvados

1. Apžvelgus mokslinę literatūrą, susijusią su mitralinio vožtuvo struktūros ir funkcijos skaitiniu modeliavimu, buvo nustatyta, kad skaitinis modeliavimas gali suteikti informacijos apie mitralinio vožtuvo struktūrinių dalių ryšį ir padėti įvertinti įvairių chirurginių būdų, naudojamų koreguoti ligos paveiktą vožtuvą, rezultatus.
2. Pagal paciento ultragarsinio tyrimo metu gautus duomenis sukurtas mitralinio vožtuvo baigtinių elementų modelis ir ištirtas neochordų ilgio, naudojamo atliekant transapikalinę mitralinio vožtuvo korekciją, poveikis pooperacinei vožtuvo funkcijai. Modelių su skirtingo ilgio neochordomis sistolinės funkcijos simuliacijos parodė, kad implantuotų neochordų ilgis turi didelę įtaką vožtuvo nesandarumo, kurį sukėlė nutrūkusios chordos, korekcijai. Nors visų virtualių procedūrų metu buvo pašalintas mitralinio vožtuvo prolapsas ir 109,8±24,3 % padidėjo koaptacijos plotas, gautas koaptacijos ilgis buvo nepakankamas (mažesnis nei 5 mm) po trumpiausios (3,9 mm) ir ilgiausios (4,3 mm) neochordų implantacijos.
3. Pasiūlytas metodas, pagal mitralinio vožtuvo skaitinio modeliavimo rezultatus leidžiantis apskaičiuoti neochordų ilgį, reikalingą atliekant virtualią transapikalinę mitralinio vožtuvo korekciją. Taikant šį metodą, nustatomas toks neochordų ilgis, kuriam esant panaikinamas mitralinio vožtuvo prolapsas ir sumažėja įtempiai vožtuvo burėse, todėl išnyksta koreguotos burės plyšimo rizika.
4. Neochordų ilgio nustatymo metodas buvo išbandytas naudojant patologinį modelį, sukurtą pagal paciento ultragarsinius duomenis. Virtualaus modelio sistolinės funkcijos simuliacija parodė, kad implantavus neochordas, kurių ilgis nustatytas taikant pasiūlytą metodą, pašalinamas mitralinio vožtuvo prolapsas, 72,2 % padidėja burių koaptacija, nuo 1,1 N iki 0,5 N sumažėja tempimo jėgos chordose, nuo 1,09 MPa iki 0,77 MPa – įtempiai burėse, ir gaunama pakankamai tiksli vožtuvo morfologija, lyginant ją su ultragarsiniais vaizdais.
5. Apskaičiavus koaptacijos plotą ir ilgį, tempimo jėgas chordose ir neochordose, reakcijos jėgas papiliariniuose raumenyse ir širdies viršūnėje, bei įtempių pasiskirstymą mitralinio vožtuvo burėse ir palyginus gautas vertes su literatūroje randamomis reikšmėmis pastebėta, kad jie atitinka kitų autorių paskelbtus dydžius ir neviršija jokių žinomų kritinių parametrų verčių. Šių parametrų įvertinimas patvirtino naudotos modeliavimo strategijos tinkamumą ir pasiūlyto neochordų ilgio nustatymo metodo pagrįstumą.
6. Gauti rezultatai rodo sudarytos modeliavimo strategijos potencialą būti naudojamai prognozuojant pooperacinę mitralinio vožtuvo morfologiją ir burių koaptaciją kaip pagrindinius vožtuvo nesandarumo korekcijos veiksmingumo rodiklius.

Annexes[1]

Annex A. Declaration of Academic Integrity

Annex B. The Co-authors' Agreements to Present Publications Material in the Doctoral Dissertation

Annex C. Copies of Scientific Publications by the Author on the Topic of the Dissertation

[1] The annexes are supplied in the enclosed compact disc

Gediminas GAIDULIS

NUMERICAL MODELING OF TRANSAPICAL MITRAL VALVE REPAIR

Doctoral Dissertation

Technological Sciences,
Mechanical Engineering (T 009)

TRANSAPIKALINĖS MITRALINIO VOŽTUVO KOREKCIJOS SKAITINIS MODELIAVIMAS

Daktaro disertacija

Technologijos mokslai,
mechanikos inžinerija (T 009)

2019 07 19. 10 sp. l. Tiražas 20 egz.
Vilniaus Gedimino technikos universiteto
leidykla „Technika“,
Saulėtekio al. 11, LT-10223 Vilnius,
http://leidykla.vgtu.lt
Spausdino UAB „BMK leidykla“,
A. Mickevičiaus g. 5, LT-08119 Vilnius